

Ph.D. Dissertation

University of West Hungary

Simonyi Károly Faculty of Engineering, Wood Sciences and Applied Arts

Cziráki József Doctoral School of Wood Sciences and Technolgoies

Bacterial cellulose thin-films for energy harvesting applications



Author: DIMITRIOS TSALAGKAS

Research Supervisor: Levente Csóka Ph.D.

Sopron

2015

Bacterial cellulose thin-films for energy harvesting applications

Értekezés doktori (PhD) fokozat elnyerése érdekében

a Nyugat-Magyarországi Egyetem Cziráki József Faanyagtudomány és Technológiák
Doktori Iskolája Rosttechnikai és nanotechnológiai tudományok programja

Írta:

DIMITRIOS TSALAGKAS

Készült a Nyugat-Magyarországi Egyetem Cziráki József Faanyagtudomány és
Technológiák Doktori Iskola Rosttechnikai és nanotechnológiai tudományok programja
keretében

Témavezető: Dr. habil. Csóka Levente

Elfogadásra javaslom (igen / nem)

(aláírás)

A jelölt a doktori szigorlaton % -ot ért el,

Sopron, 2014.12.05.

.....
a Szigorlati Bizottság elnöke

Az értekezést bírálóként elfogadásra javaslom (igen /nem)

Első bíráló (Dr.) igen /nem

(aláírás)

Második bíráló (Dr.) igen /nem

(aláírás)

(Esetleg harmadik bíráló (Dr.) igen /nem

(aláírás)

A jelölt az értekezés nyilvános vitáján.....% - ot ért el

Sopron,

.....
a Bírálóbizottság elnöke

A doktori (PhD) oklevél minősítése.....

.....
Az EDHT elnöke

I, the undersigned *Dimitrios Tsalagkas* hereby declare that this Ph.D. dissertation was made by myself, and I only used the sources given at the end. Every part that was quoted word-for-word, or was taken over with the same content, I noted explicitly by giving the reference of the source.

Sopron, April 15th, 2015

.

.....

Dimitrios Tsalagkas

Abstract

Bacterial cellulose films are gaining importance in research, since its superior properties makes bacterial cellulose suitable for several nanocomposite applications. Bacterial cellulose obtained from nata de coco, were purified under four purifications (water, one step, two step and 0.01 M NaOH) treatments. Subsequently, purified samples were submitted under ultrasonication. Two main parameters, temperature (no water, cold water and ice water bath) and distance of ultrasonic probe (1 cm and 4 cm distance), were taken under investigation. The overall aim of the work was to develop a method of obtaining homogeneous, self sustaining bacterial cellulose films exhibiting superior structural and physical properties, suitable for energy harvesting devices.

Fourier Transform Infrared Spectroscopy (FT-IR), X-ray Diffraction (XRD), Thermogravimetric Analysis (TGA), Differential Scanning Callorimetry (DSC), Field Emission Microscopy (FE-SEM) and Atomic Force Microscopy (AFM) were implemented to investigate the structural, thermal and morphological changes of treated bacterial cellulose samples.

Morphological analysis displayed that removal of bacterial cellulose impurities was depending on the purification method. Further, results indicated that purification treatments and acoustic cavitation, provoked changes in the hydrogen bonds of crystalline cellulose but did not cause any other changes in the native cellulose. In addition, depending on purification and ultrasound parameters we could obtain higher crystalline and more thermodynamically stable films. Based on the results, the most favourable process to achieve bacterial cellulose films was under 0.01 M NaOH purification, in cold water bath ultrasonication. The distance of the ultrasonic probe was 1 cm from the bottom of the container.

Table of contents

1. Introduction and problem statement	14
1.1. Introduction – bacterial cellulose.....	14
1.2. Bacterial cellulose biosynthesis.....	14
1.3. Acetobacter xylinum.....	17
1.4. Bacterial cellulose fabrication.....	18
1.5. Bacterial cellulose structure.....	19
1.6. Bacterial cellulose properties.....	21
1.7. Applications of bacterial cellulose.....	22
1.7.1. Biological / health care applications	23
1.7.2. Electronic applications.....	23
1.7.3. Polymer reinforcements.....	24
1.7.4. Nata de coco.....	24
1.8. Acoustic cavitation as a method used for cellulose fiber isolation.....	24
1.9. Piezoelectricity.....	25
1.10. Problem statement.....	27
2. Materials and methods	30
2.1. Materials.....	30
2.2. Experimental details.....	30
2.2.1. Purification of Nata de coco.....	30
2.2.2. Ultrasonication of bacterial cellulose films.....	31
2.2.3. Preparation of bacterial cellulose films	31
2.3. Bacterial cellulose films characterization techniques	33
2.3.1. Structural analysis of bacterial cellulose films	33

2.3.2.	Thermal analysis of bacterial cellulose films	37
2.3.3.	Morphological analysis of bacterial cellulose films.....	38
3.	Results	40
3.1.	Structural analysis.....	40
3.1.1.	Fourier Transform Infrared (FT-IR) spectroscopy	40
3.1.2.	X-ray diffraction analysis (XRD)	61
3.2.	Thermal analysis	68
3.2.1.	Thermo Gravimetric Aanalysis	68
3.2.2.	Differential scanning calorimetry.....	75
3.3.	Morphological	78
4.	Discussion.....	85
5.	References	93

List of Figures

Figure 1: Biochemical process for cellulose synthesis by <i>A. xylinum</i> . CS cellulose synthase, GK glucokinase, FBP fructose-1,6-bi-phosphate phosphatase, FK fructocinase, 1FPk fructose-1-phosphate kinase, PGI phosphoglucoisomerase, PGM phosphoglucomutase, PTS system of phosphotransferases, UGP pyrophosphorylase uridine diphosphoglucose, UDPGlc uridine diphosphoglucose, G6PDH glucose-6-phosphate dehydrogenase, NAD nicotinamide adenine dinucleotide, NADP nicotinamide adenine dinucleotide phosphate (Chawla et al. 2009).....	15
Figure 2: The synthesis mechanism of cellulose by <i>Acetobacter xylinum</i> at the cell surface. Linear polymer formation takes place in the pore of the cell surface, while microfibril formation is exogenous (Vitta and Thiruvengadam 2012).	16
Figure 3: FE-SEM and AFM images of bacterial cellulose network structure.....	16
Figure 4: FE-SEM image of <i>Acetobacter xylinum</i>	17
Figure 5: Molecular structure of cellulose.....	19
Figure 6: Hydrogen bonding network structure in cellulose I α	20
Figure 7: Projections of the crystal structures of cellulose I α (left) and I β (right) down the axes (top), perpendicular to the chain axis and in the plane of the hydrogen bonded sheets (middle) and perpendicular to the hydrogen bonded sheets (bottom). The cellulose chains are represented by red skeletal models. The asymmetric unit of each structure is also represented in thicker lines with carbons in yellow. The unit cell of each structure is shown in white (Nishiyama et al. 2003).	21
Figure 8: Potential biomedical applications of bacterial cellulose based materials (Fu et al. 2013).	23
Figure 9: Scheme of the piezoelectric cantilever experimental set up, AFM image of ZnO/bacterial cellulose film and its output voltage (Tsalagkas & Csoka 2013).....	27
Figure 10: A scheme for HIUS treatment using no water bath (NoW, a), cold water bath (CW, b) and ice water bath cooling (IW, c). Ultrasonic probe was placed close to the top (4 cm distance) and to the bottom (1 cm distance) of the container.....	32

Figure 11: Block diagram of obtaining the bacterial cellulose films.....	32
Figure 12: FT-IR spectra in the 4000-400 cm ⁻¹ region corresponding to purified and not-ultrasonicated treated samples.....	40
Figure 13: FT-IR spectra in the 4000-400 cm ⁻¹ region corresponding to water purified and ultrasound treated samples.....	41
Figure 14: FT-IR spectra in the 4000-400 cm ⁻¹ region corresponding to one step purified and ultrasound treated samples.....	41
Figure 15: FT-IR spectra in the 4000-400 cm ⁻¹ region corresponding to two step purified and ultrasound treated samples.....	42
Figure 16: FT-IR spectra in the 4000-400 cm ⁻¹ region corresponding to 0.01 M NaOH purified and ultrasound treated samples.....	42
Figure 17: Comparative FT-IR spectra in the 4000-2600 cm ⁻¹ and 1800-800 cm ⁻¹ regions respectively corresponding to purified only treated samples.	43
Figure 18: Comparative FT-IR spectra in the 4000-2600 cm ⁻¹ and 1800-800 cm ⁻¹ regions respectively corresponding to water purified and ultrasonicated treated samples.....	43
Figure 19: Comparative FT-IR spectra in the 4000-2600 cm ⁻¹ and 1800-800 cm ⁻¹ regions respectively corresponding to one step purified and ultrasonicated treated samples.....	44
Figure 20: Comparative FT-IR spectra in the 4000-2600 cm ⁻¹ and 1800-800 cm ⁻¹ regions respectively corresponding to two step purified and ultrasonicated treated samples.....	44
Figure 21: Comparative FT-IR spectra in the 4000-2600 cm ⁻¹ and 1800-800 cm ⁻¹ regions respectively corresponding to 0.01 M NaOH purified and ultrasonicated treated samples.	45
Figure 22: The deconvoluted spectra of 3600-3000 cm ⁻¹ region, for (a) WP, (b) OSP, (c) TSP and (d) NaP purification treatments of bacterial cellulose.	47
Figure 23: The deconvoluted spectra of 3600-3000 cm ⁻¹ region, for (a) WP_NoW_1cm, (b) WP_CW_1cm, (c) WP_IW_1cm, (d) WP_NoW_4cm, (e)	

WP_CW_4cm and (f) WP_IW_4cm, of water purified cellulose after ultrasonication.....	48
Figure 24: The deconvoluted spectra of 3600-3000 cm ⁻¹ region, for (a) OSP_NoW_1cm, (b) OSP_CW_1cm, (c) OSP_IW_1cm, (d) OSP_NoW_4cm, (e) OSP_CW_4cm and (f) OSP_IW_4cm, of one step purified cellulose after ultrasonication.....	49
Figure 25: The deconvoluted spectra of 3600-3000 cm ⁻¹ region, for (a) TSP_NoW_1cm, (b) TSP_CW_1cm, (c) TSP_IW_1cm, (d) TSP_NoW_4cm, (e) TSP_CW_4cm and (f) TSP_IW_4cm, of two step purified cellulose after ultrasonication.....	50
Figure 26: The deconvoluted spectra of 3600-3000 cm ⁻¹ region, (a) NaP_NoW_1cm, (b) NaP_CW_1cm, (c) NaP_IW_1cm, (d) NaP_NoW_4cm, (e) NaP_CW_4cm and (f) NaP_IW_4cm, of 0.01 M NaOH purified cellulose after ultrasonication.	51
Figure 27: Crystallinity indices (TCI, LOI) and hydrogen bond intensity (HBI) prepared at different not-ultrasound purification treatments.....	55
Figure 28: Crystallinity indices (TCI, LOI) and hydrogen bond intensity (HBI) prepared at different ultrasound conditions, after water purification treatment...	56
Figure 29: Crystallinity indices (TCI, LOI) and hydrogen bond intensity (HBI) prepared at different ultrasound conditions, after one step purification treatment.	58
Figure 30: Crystallinity indices (TCI, LOI) and hydrogen bond intensity (HBI) prepared at different ultrasound conditions, after two step purification treatment.	59
Figure 31: Crystallinity indices (TCI, LOI) and hydrogen bond intensity (HBI) prepared at different ultrasound conditions, after 0.01 M NaOH purification treatment.....	60
Figure 32: X-ray diffraction of bacterial cellulose with different purification methods.....	62
Figure 33: X-ray diffraction of water purified bacterial cellulose with different ultrasound conditions.	63

Figure 34: X-ray diffraction of one step purified bacterial cellulose with different ultrasound conditions.	63
Figure 35: X-ray diffraction of two step purified bacterial cellulose with different ultrasound conditions.	64
Figure 36: X-ray diffraction of 0.01 M NaOH purified bacterial cellulose with different ultrasound conditions.	64
Figure 37: TGA curves of WP, OSP, TSP and NaP treated bacterial cellulose samples under different ultrasound operating conditions.	68
Figure 38: dTGA curves of WP, OSP, TSP and NaP treated bacterial cellulose samples under different ultrasound operating conditions.	69
Figure 39: TGA and dTGA curves of WP treated bacterial cellulose samples under different ultrasound operating conditions.	70
Figure 40: TGA and dTGA curves of OSP treated bacterial cellulose samples under different ultrasound operating conditions.	71
Figure 41: TGA and dTGA curves of TSP treated bacterial cellulose samples under different ultrasound operating conditions.	72
Figure 42: TGA and dTGA curves of NaP treated bacterial cellulose samples under different ultrasound operating conditions.	73
Figure 43: DSC thermograms of WP treated bacterial cellulose samples under different ultrasound operating conditions.	76
Figure 44: DSC thermograms of OSP treated bacterial cellulose samples under different ultrasound operating conditions.	76
Figure 45: DSC thermograms of TSP treated bacterial cellulose samples under different ultrasound operating conditions.	77
Figure 46: DSC thermograms of NaP treated bacterial cellulose samples under different ultrasound operating conditions.	77
Figure 47: FE-SEM micrographs of WP, OSP, TSP and NaP purified bacterial cellulose samples.	79
Figure 48: FE-SEM micrographs (1 μ m and 200 nm) of WP and WP_CW_1cm bacterial cellulose samples.	80

Figure 49: FE-SEM micrographs (1 μ m and 200 nm) of OSP and OSP_CW_4cm bacterial cellulose samples.	80
Figure 50: FE-SEM micrographs (1 μ m and 200 nm) of TSP and TSP_CW_1cm bacterial cellulose samples.	81
Figure 51: FE-SEM micrographs (1 μ m and 200 nm) of NaP and NaP_CW_1cm bacterial cellulose samples.	81
Figure 52: AFM images (5x5 μ m) of the most favourable bacterial cellulose samples prior to (left) and after (right) ultrasonication.	82
Figure 53: AFM images (1x1 μ m) of the most favourable bacterial cellulose samples prior to (left) and after (right) ultrasonication.	83
Figure 54: Bacterial cellulose WP, NaP and NaP_CW_1cm dried films.....	84

List of Tables

Table 1: The energy hydrogen bond and hydrogen bonding distance of intramolecular hydrogen bond of 3-OH...O-5 for studied samples.	52
Table 2: Determined crystallinity indices (TCI and LOI), hydrogen bond intensity (HBI) and mean hydrogen bond intensity (MHBS) for purified, not-ultrasonicated bacterial cellulose samples.	54
Table 3: Infrared crystallinity indices (TCI, LOI), hydrogen bond intensity (HBI) and mean hydrogen bond strength (MHBS) of ultrasonicated bacterial cellulose, after water purification treatment.	56
Table 4: Infrared crystallinity indices (TCI, LOI), hydrogen bond intensity (HBI) and mean hydrogen bond strength (MHBS) of ultrasonicated bacterial cellulose, after one step purification treatment.	57
Table 5: Infrared crystallinity indices (TCI, LOI), hydrogen bond intensity (HBI) and mean hydrogen bond strength (MHBS) of ultrasonicated bacterial cellulose, after two step purification treatment.	59
Table 6: Infrared crystallinity indices (TCI, LOI), hydrogen bond intensity (HBI) and mean hydrogen bond strength of ultrasonicated bacterial cellulose, after 0.01 M NaOH purification treatment.	60
Table 7: XRD peak intensity percent (%) at 2θ angles and Cr.I for purified bacterial cellulose with different ultrasound parameters.	65
Table 8: d-spacings, crystallites sizes, and crystalline interior chain values of treated bacterial cellulose samples.	67
Table 9: Summary of TGA and dTGA data for bacterial cellulose samples after different purification and ultrasound treatments.	74
Table 10: Peak wavenumbers of FTIR absorption bands related to cellulose I and regenerated cellulose II, their interpretation according to the literature (Carrillo et al. 2004, Ciolacu et al. 2011, Colom & Carrillo 2002, Colom et al. 2003, Fan et al. 2012, Gea et al. 2011, Halib et al. 2012, Kondo & Sawatari 1996, Kondo 1998, Liu et al. 2005, Ohet al. 2005, Široký et al. 2010).	105

Table 11: Explanation of abbreviation names, given to the investigated bacterial cellulose specimens.	110
--	-----

1. Introduction and problem statement

1.1. Introduction – bacterial cellulose

Plant based cellulose, even though useful for many applications, is not produced in pure state. The presence of lignin, hemicelluloses and other molecules, even though are important for the cell structure of woods, requires intensive processes until is suitable for medical use. In contrast, bacterial cellulose while identical to plant cellulose in chemical structure is produced without contaminant molecules and morphologically differs from plant cellulose. Bacterial cellulose, also known as microbial cellulose, is a promising natural polymer synthesized by certain bacteria. Bacterial cellulose due to its supramolecular structure and high purity, cellulose content demonstrates unique properties. Microbial cellulose is entirely free of “contaminants” such as lignin, hemicelluloses and pectin typical components in plant cellulose of wood. Thus, bacterial cellulose is a very useful biomaterial, which could be used in many different industrial processes.

1.2. Bacterial cellulose biosynthesis

Bacterial cellulose is produced by species of various genera of bacteria including *Acetobacter* (renamed *Gluconacetobacter*), *Agrobacterium*, *Achromobacter*, *Aereobacter*, *Acanthamoeba*, *Achromobacter*, *Sarcina*, *Rhizobium*, *Alcaligenes*, *Zoogloea* and others. The most widely studied bacteria is strains of *Acetobacter xylinum* or nowadays *Glucoanacetobacter xylinus* due to its high efficient productivity of bacterial cellulose (Chawla et al. 2009, Petersen and Gateholm, 2011).

Synthesis of an extracellular gelatinous film produced from *Acetobacter xylinum* first time was reported in 1866 by A. J. Brown, but intensive studied of producing bacterial cellulose films started in the second half of the 20th century. Biosynthesis of bacterial cellulose is a precise and specifically adjusted multi-step process, involving a large number of both individual enzymes and complexes of catalytic and regulatory proteins. The process and mechanisms includes the (i) synthesis of uridine diphosphoglucose (UDPGlc) which is the cellulose precursor, followed by formation of β -1,4-glucan chain and glucose polymerization, and (ii) assembly and crystallization of cellulose chains into characteristic

ribbon-like structure formed by many individual chains (Bielecki et al. 2005, Chawla et al. 2009) (**Figure 1**).

A detailed description regarding cellulose formation from bacteria is given by Vitta and Thiruvengadam (2012) (**Figure 2**). The synthesis of bacterial cellulose network is extracellular, occurs between the outer and plasma membranes of the bacterial cell and has two distinct stages: (i) linear polymerization of the cellobiose units catalyzed by the enzyme and (ii) cellulose synthase followed by crystallization of the linear chains. During biosynthesis process, several carbon compounds of the nutrition medium are utilized by the bacteria, polymerized into single, linear β -1,4-glucan chains and finally the fibrils secreted outside the cells through a linear row of pores located on their outer membranes in the culture medium, creating this dense network by self-assembling.

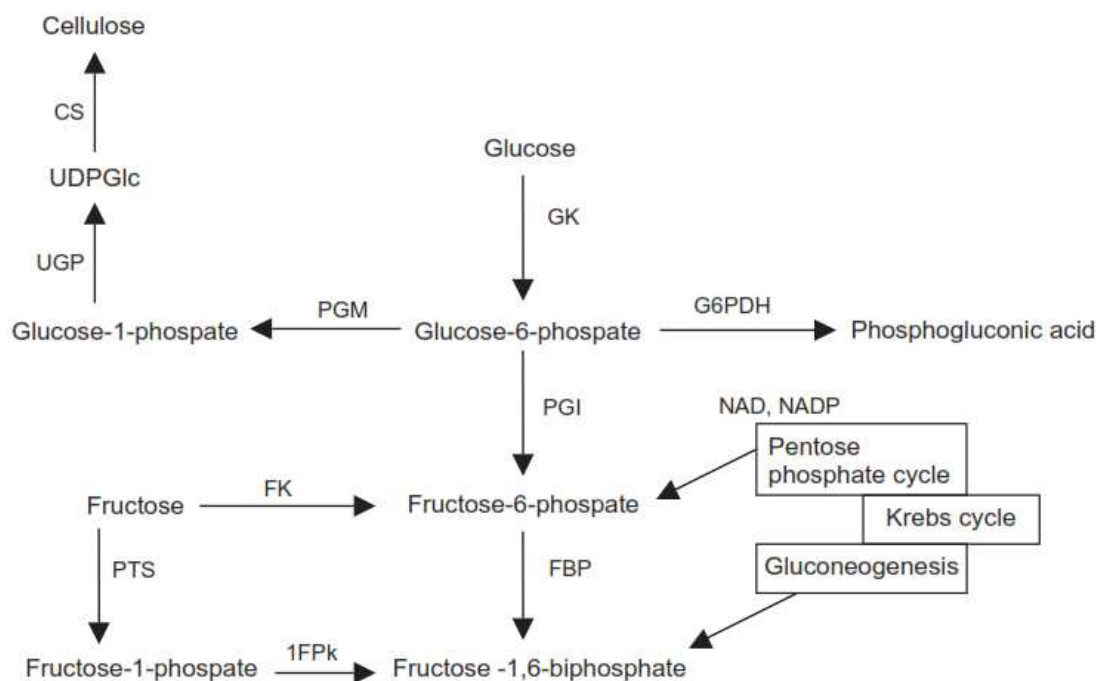


Figure 1: Biochemical process for cellulose synthesis by *A. xylinum*. CS cellulose synthase, GK glucokinase, FBP fructose-1,6-bi-phosphate phosphatase, FK fructocinase, 1FPk fructose-1-phosphate kinase, PGI phosphoglucoisomerase, PGM phosphoglucomutase, PTS system of phosphotransferases, UGP pyrophosphorylase uridine diphosphogluucose, UDPGlc uridine diphosphogluucose, G6PDH glucose-6-phosphate dehydrogenase, NAD nicotinamide adenine dinucleotide, NADP nicotinamide adenine dinucleotide phosphate (Chawla et al. 2009).

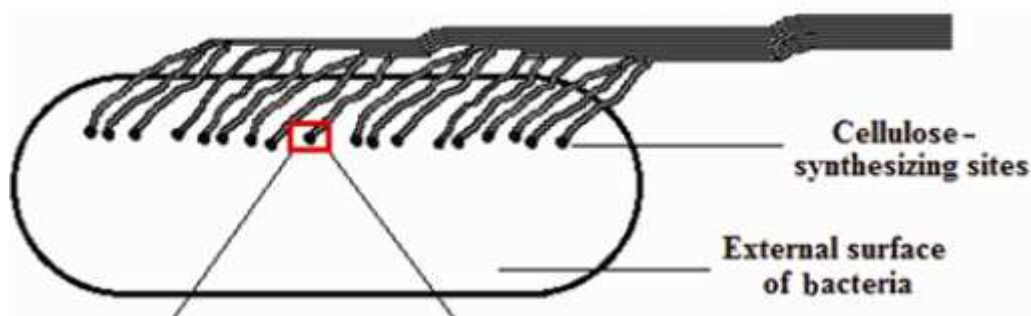


Figure 2: The synthesis mechanism of cellulose by *Acetobacter xylinum* at the cell surface. Linear polymer formation takes place in the pore of the cell surface, while microfibril formation is exogenous (Vitta and Thiruvengadam 2012).

Around 10 to 15 linear β -1,4-glucan chains aggregate to form subfibrils, which have a width of approximately 1.5 nm. Bacterial cellulose subfibrils are crystallized into microfibrils of width 3.5 nm. Following, microfibrils are combined to form bundles, which shaped into ribbons. The aggregates form bands of width \sim 100 nm called fibrillar bands. The thick, gelatinous membrane formed in static culture conditions is characterized by a 3-D structure consisting of an ultrafine network of highly, uniaxially oriented cellulose fibrillar bands, stabilized by the hydrogen bonds existing in cellulose units (Czaja et al 2006, Vitta and Thiruvengadam 2012) (**Figure 3**).

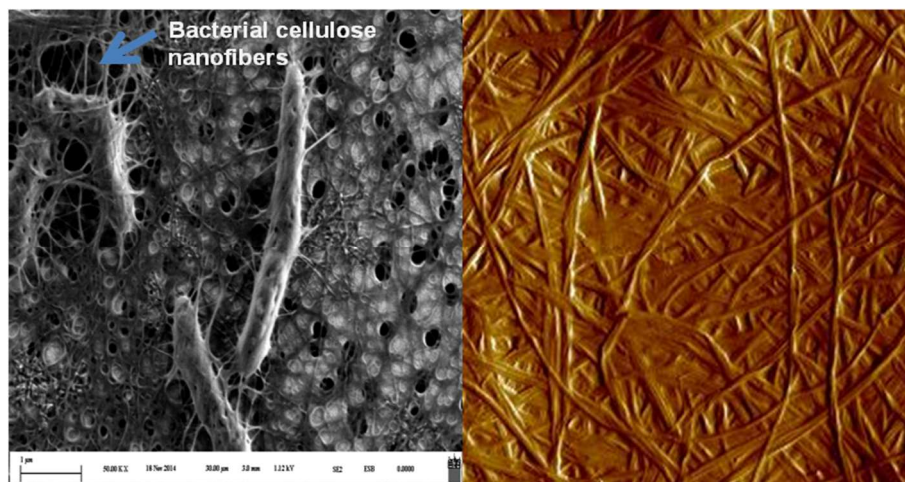


Figure 3: FE-SEM and AFM images of bacterial cellulose network structure

“Bacterial cellulose membranes exhibit uniplanar orientation with the $(1\bar{1}0)$ planes parallel to the fiber surface and an additional axial orientational component that depends on the drying procedure” (Fu et al. 2011).

The main effect of the nanosize of the fibrils is an increase in surface area of the bacterial cellulose network, which is reflected in strong interactions with the surrounding environment. Therefore bacterial cellulose, binds large amounts of water, up to 99 % of its own weight during biosynthesis in the aqueous culture media. From this 99% water present in bacterial cellulose, the majority is bound to cellulose and only 10% behaves like a free bulk water (Gelin et al. 2007).

1.3. *Acetobacter xylinum*

Acetobacter xylinum (**Figure 4**) was first described by Brown in 1886 who identified a jelly like film formed over the surface of a vinegar fermentation broth. It is a simple, aerobic, Gram-negative, prokaryotic, non-photosynthetic bacterium which has an ability to synthesize a large quantity of high quality cellulose organized as twisting ribbons of microfibrillar bundles. (Czaja et al 2006).

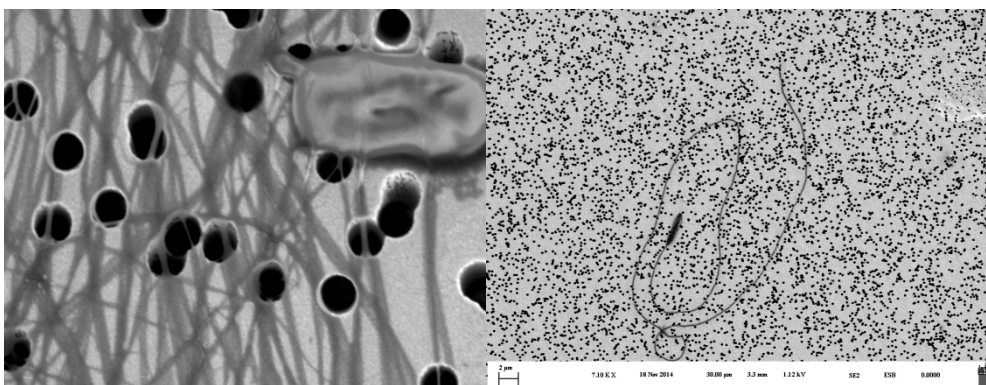


Figure 4: FE-SEM image of *Acetobacter xylinum*.

The amount of bacterial cellulose produced from *Acetobacter spp.* could vary from 1.0 to 4.0 % (w/v) depending on fermentation media and the carbon compounds (Lin et al. 2013). At pH values ranging from 4 to 6, temperature between 28 and 30 °C and duration of

cultivation from 3 to 7 days the production efficiency is usually around 50% (Chawla et al. 2009, Esa et al. 2014).

1.4. Bacterial cellulose fabrication

Many researchers have investigated the production of bacterial cellulose as well as the factors which influence their productivity, crystallinity, molar mass, I_α/I_β (cellulose I_α to cellulose I_β) ratio and other physicochemical effect of the obtained bacterial cellulose pellicles. These structural differences can be of great significance since they determine the properties and hence the final applications of bacterial cellulose.

Many variables influence the total production process and performance of the biomaterial: (i) type and conditions (time of fermentation, additives) of culture methods, (ii) fermentation medium compounds based on carbon and nitrogen sources, (iii) type of bacterial strains, (iv) environmental factors (pH, temperature, dissolved oxygen content, stirrer speed), (v) post-fermentation operations, (vi) type of efficient, large scale fermentation process.

The two main methods of bacterial cellulose cultivation are static and agitated cultures. Macroscopic morphology and properties of bacterial cellulose is highly affected by cultivation conditions (Czaja et al. 2004, Sarkono et al. 2014, Uraki et al. 2007, Watanabe et al. 1998).

Acetobacter xylinum has the ability to grow and produce cellulose on a variety of substrates. The fermentation medium contains carbon, nitrogen and other macro- and micronutrients required for the growth of the organism. The changes in the carbon and/or nitrogen sources affect the growth and the product formation directly or indirectly. The productivity of carbon resources could be different in many studies which may be related to the time of fermentation, the carbon source concentration, the surface/volume ratio or the relative surface area of the fermentation system (Khajavi et al. 2011, Pineda et al. 2010, Sheykhnazari et al. 2011).

Many bacterial strains exhibit differences in the cellulose production process as well as in the structure of the obtained cellulose (Castro et al. 2012, Czaja et al. 2007, McKenna et al. 2009, Mohite & Patil 2014).

Bacterial microorganisms, such as *Acetobacter xylinum* respond rapidly to environmental changes in many aspects such as induction and repression of protein synthesis and changes in cell morphology (Chawla et al. 2009).

Post fermentation operations such as the degree of dehydration, physical squeezing, and treatment with bases affect the efficiency of the final membrane (Czaja et al 2006).

1.5. Bacterial cellulose structure

Cellulose is a natural, linear polymer consisting of ringed glucose molecules made of β -1,4 glucopyranose molecules, which are covalently linked through acetal functions between the OH groups of C1 and C4 carbon atoms. The repeat unit is comprised of two anhydroglucose rings ($C_6H_{10}O_5$)_n bond together in such a way that one molecule is rotated 180 degrees in order to accommodate the bond angles of acetal oxygen bridges. These two adjacent glucose molecules compose the basic repeat cellulose unit called cellobiose (**Figure 5**).

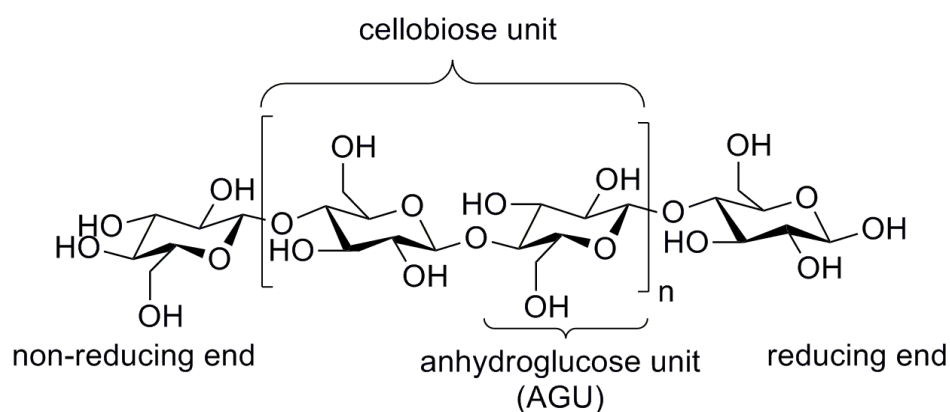


Figure 5: Molecular structure of cellulose

Physical properties of cellulose are influenced by its hydrogen bonding network. The three kinds of hydroxyl groups bond equatorially in anhydroglucose units under different polarities, and the resulting inter- and intramolecular interactions are responsible for the stabilization, crystalline structure and hydrophilic nature of cellulose (**Figure 6**).

Cellulose has different crystalline polymorphs. In native cellulose (cellulose I) found in nature, there are two intramolecular hydrogen bonds, which are between the OH-3...O5', and between the OH-2... O6' for bonding the layers and one intermolecular hydrogen bond, OH-6...O3 for linking the layers laterally, depending on the hydroxymethyl conformation at the C-6 position. (Kondo 2004).

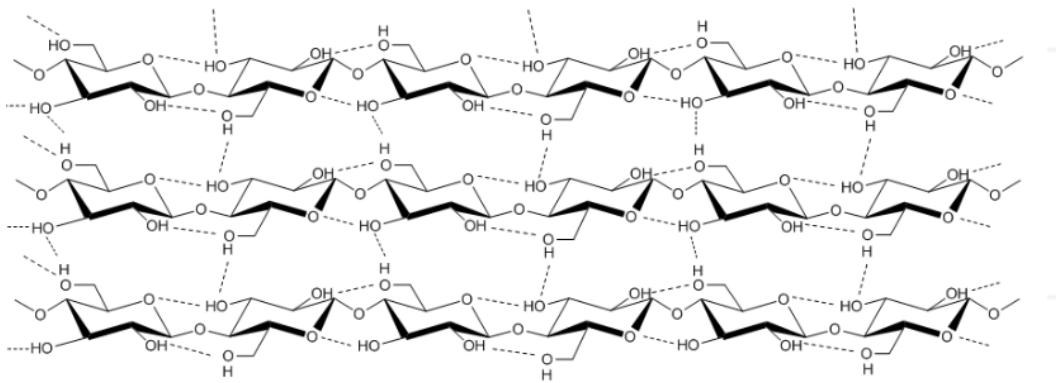


Figure 6: Hydrogen bonding network structure in cellulose I $_{\alpha}$.

Native cellulose I consists of two distinct crystal phases, namely I $_{\alpha}$ and I $_{\beta}$. The I $_{\alpha}$ /I $_{\beta}$ ratio defines cellulose properties and varies within the cellulose microfibrils as well as in different cellulose sources. Algae and bacterial cellulose specimens are rich in I $_{\alpha}$ form, while cotton, wood and ramie fibers are rich in I $_{\beta}$ crystalline allomorph (Habibi et al. 2010).

The crystal structure and hydrogen-bonding system in cellulose I $_{\alpha}$ and I $_{\beta}$ respectively from synchrotron X-ray and neutron fiber diffraction apparatus are shown in **Figure 7** (Nishiyama et al. 2003 and 2002). In both of these structures, cellulose chains are parallel but they differ in their hydrogen bonding patterns, i.e. in the crystalline structure. I $_{\alpha}$ corresponds to a triclinic unit cell ($a = 0.6717$ nm, $b = 0.5962$ nm, $c = 1.040$ nm, $\alpha = 118.08^{\circ}$, $\beta = 114.80^{\circ}$ and $\gamma = 80.37^{\circ}$) containing only one chain per unit cell, while I $_{\beta}$ exists in a monoclinic unit cell having two cellulose chains ($a = 0.7784$ nm, $b = 0.8201$ nm, $c = 1.038$ nm, $\alpha = \beta = 90^{\circ}$ and $\gamma = 96.5^{\circ}$). Furthermore, I $_{\alpha}$ type cellulose is metastable and can be converted irreversibly into the irreversible I $_{\beta}$.

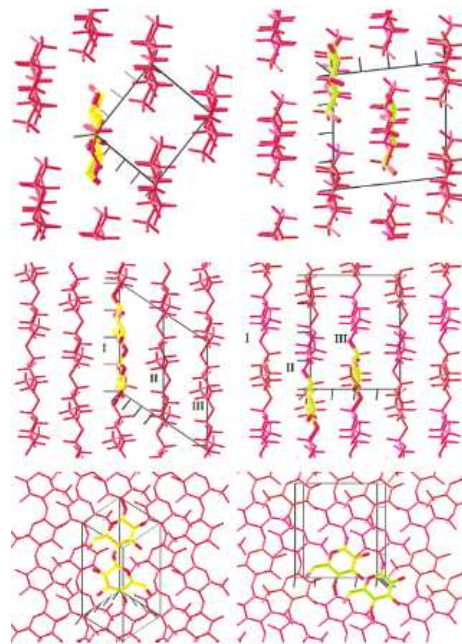


Figure 7: Projections of the crystal structures of cellulose I α (left) and I β (right) down the axes (top), perpendicular to the chain axis and in the plane of the hydrogen bonded sheets (middle) and perpendicular to the hydrogen bonded sheets (bottom). The cellulose chains are represented by red skeletal models. The asymmetric unit of each structure is also represented in thicker lines with carbons in yellow. The unit cell of each structure is shown in white (Nishiyama et al. 2003).

1.6. Bacterial cellulose properties

The chemical structure of bacterial cellulose is like that of plant cellulose, but the degree of polymerization differs. Degree of polymerization is 2,000 to 6,000 for bacterial cellulose, while for plant cellulose is around 13,000 to 14,000 anhydroglucose units. Its nanofibrils have similarities with extracellular matrix components and more particularly with collagen (Bielecki et al. 2005, Khajavi et al. 2011). Bacterial cellulose exhibits higher purity, water-holding capacity, crystallinity and mechanical strength related to plant based cellulose (Sheyknazari et al. 2011).

Bacterial cellulose fibers have high aspect ratio with a diameter of 20-100 nm. The size of bacterial cellulose microfibrils specific surface is 100 times smaller than plant cellulose (3-4 nm thick and 70-80 nm wide). As a result, bacterial cellulose has a large surface area per unit mass that in combination with the hydrophilic nature of cellulose can hold a large

amount of water, up to 200 times of its dry mass (Czaja et al. 2006, Khajavi et al. 2011, Fu et al. 2011).

Bacterial cellulose has a crystallinity of the order of 65-79%. Typically its crystals have square section, there is around 100 cellulose chains per crystals with roughly 40 chains located at the crystal surface (Verlhac and Dedier, 1990). The Young's modulus of a single filament or microfibril of bacterial cellulose as estimated using a Raman spectroscopy technique is 130-140 GPa (Gea et al. 2011).

Further it is a biocompatible, non toxic with no allergenic side effects material. (Lin et al. 2013). Bacterial cellulose is remarkable for its strength and its ability to be engineered structurally and chemically at nano-, micro- and macroscales in any shape or form. Bacterial cellulose hydrogels demonstrate significant characteristics such as (i) the biofabrication of a dimensional stable hydrogel, (ii) control of 3D shape, which could be reproduced of predetermined shape by the type of cultivation and kind of bioreactor and (iii) control of macroporosity by introduction of porogens (Gatenholm and Klemm 2010, Petersen and Gateholm, 2011).

Rodlike species, such as cellulose, can form ordered liquid crystal phases when their concentration reaches a certain critical value depending on the source and on the hydrolysis conditions. Above the critical concentration, suspensions of cellulose crystallite separate into two phases with very clear phase boundaries. The lower anisotropic phase shows optical properties characteristic of chiral nematic liquid crystals (Hirai et al. 2009).

However, the lack of large scale commercialization production, its low volumetric production and high price of bacterial cellulose restricts its utilization in many practical applications.

1.7. Applications of bacterial cellulose

Beside the drawbacks, described above there are several key practical applications, where the price for example can not play a significant role. Moreover, because of its unique physicochemical and mechanical properties, bacterial cellulose can be utilized in various, specific fields. Several publications have focused on its applications or potential

applications. The applications of the bacterial cellulose could be summarized in the following applications.

1.7.1. Biological/ health care applications

Much work has already focused on designing ideal biomedical devices from bacterial cellulose such as artificial skin, artificial blood vessels, artificial cornea, heart valve prosthesis, artificial urethra, artificial bone, artificial cartilage, artificial porcine knee menisci (**Figure 8**)(Fu et al. 2013).

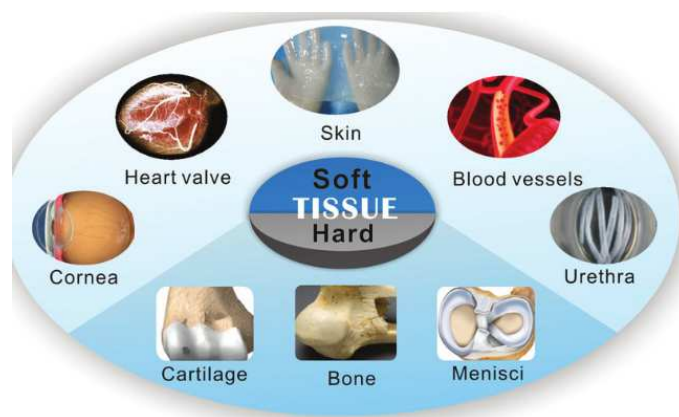


Figure 8: Potential biomedical applications of bacterial cellulose based materials (Fu et al. 2013).

1.7.2. Electronic applications

Another future application is to achieve an electronic (OLED) display using bacterial cellulose membrane (Legnani et al. 2008, Ummartyotin et al. 2012). The main advantages of an electronic paper device are its high paper-like reflectivity, flexibility, contrast and biodegradability. The device has the potential to be extended to various applications, for instance e-book tablets, e-newspapers, dynamic wall papers, rewritable maps and learning tools (Shah and Brown 2005), biosensors or actuators (Baptista et al. 2013, Yang et al 2009). Bacterial cellulose also is a superior material for headphone and loudspeaker membranes

due to the high modulus of elasticity and large internal loss factor (Gatenholm and Klemm 2010).

1.7.3. Polymer reinforcements

The thermal stability and degree of polymerization of nanocrystals are two crucial factors for their use as reinforcing material in the fabrication of polymer nanocomposites.

1.7.4. Nata de coco

Chemically pure cellulose can be used in processed foods as thickening and stabilizing agent. Bacterial cellulose is mainly produced to make nata de coco, originated from Philippines. Nata de coco is a white, gelatinous dietary sweet used in food applications such as desserts and fruit cocktails. It is usually produced in static cultivation of *Acetobacter xylinum* with coconut water used as carbon source. The thick sheets of bacterial cellulose are then cut into cubes, washed and boiled in water before cooking in sugar syrup. Commercial nata de coco is made by large and mid-size companies and small or home industries in Philippines, Indonesia, Thailand and other South East Asian countries (Esa et al. 2014, Phisalaphong & Chiaoprakobkij 2012).

Nata de coco as a source of bacterial cellulose has been intensively examined by a research group in Malaysia. They investigated the physicochemical properties (Halib et al. 2012), solubility behavior (Pandey et al. 2014) and the effect of drying methods (Amin et al. 2014, Pa'e et al. 2014) of nata de coco. Hosakun et al. (2014) utilized bacterial cellulose membranes obtained from nata de coco for CO₂/CH₄ gas separation, and Blaker et al. (2010) produced a nata de coco/poly(lactic acid) (PLA) nanocomposite film to obtain 3D scaffolds.

1.8. Acoustic cavitation as a method used for cellulose fiber isolation

There are several methods existing for cellulose fiber isolation. The most important and widely used ones for producing cellulose nanofibrils are the mechanical, chemical, physical and biological method or combinations of them. The most well known mechanical methods are refining, high pressure homogenization, microfluidization, grinding,

cryocrushing and ultrasonication. Physical methods include microwave and gamma rays irradiation. Chemical isolations usually include acid hydrolysis with strong acids like sulfuric acid (H_2SO_4), alkaline hydrolysis mostly with sodium hydroxide (NaOH), organic solvent treatments, ionic liquid treatments. Enzymatic hydrolysis is considered as a biological method. However, cellulose nanocrystals produced by most of these methods results in reduced crystallinity cellulose or regenerated cellulose II type, or demand large energy amounts (Abdul Khalil et al. 2014, Frone et al. 2011).

Ultrasound generators transform electrical energy into ultrasonic energy, which is a mechanical energy. The effects of high intensity ultrasound depend on many variables such as reaction time characteristics, treatment parameters, ultrasound generator characteristics and size and geometry of treatment vessel, but also on ultrasonication conditions (Raso et al. 1999). The electrical power input into a sonochemical process is related to the energy conversion of an ultrasonic device, thus to the efficiency of sonochemical process (Löning et al. 2001).

According to Zhao et al. (2007) the use of ultrasound, i.e. by acoustic cavitation has been demonstrated to be an efficient tool in cellulose isolation, decomposition, processing and pretreatment in many occasions. Acoustic cavitation is the formation, growth and sudden collapse of microbubbles in liquids, generating high temperature and pressure conditions which can induce chemical and physical transformations. The main chemical effects of cavitation phenomena include free radical formation, due to the decomposition of water.

Wang and Cheng (2009) investigated the effect of six ultrasound parameters, i.e. power, temperature, time, concentration, fibers size and distance of ultrasonic probe to check the efficiency of high intensity ultrasound on cellulose isolation. They concluded that ultrasound could be used to treat cellulosic materials in order to produce small fibrils.

1.9. Piezoelectricity

The famous French brothers Pierre and Jacques Curie in 1880 discovered an unusual characteristic of some crystals. These crystals displayed an electric polarization when mechanical stress was applied (called direct piezoelectric effect) and reverse (called converse piezoelectric effect). This behavior was labeled as piezoelectric effect from the

Greek word “piezein” meaning to press or squeeze (Stephens 1972). The term “piezoelectricity” refers to the production of bound electrical charges in the surfaces of a material or crystals specimens by the imposition of some form of elastic, mechanical or electrical stress (Ballato 1996).

Piezoelectric materials owe their capacities generally to their asymmetrical arrangement of positively and negatively charged atoms in their crystal structure. Piezoelectricity is found in many natural substances, such as bone, wood and ice, due to their polar nature and crystal asymmetry in their structure (Fukada 1995). The oldest scientific work about the piezoelectric effect of wood was a paper from 1940 cited in the book “Piezoelectric Properties of Wood” by the Soviet researcher Valerie A. Bazhenov (Plackner 2009).

In general, any kind of cellulose (native or regenerated) is capable of producing piezoelectricity. Piezoelectric effect of wood or any other cellulose source (bacterial, tunicates, wooden pulp, ramie etc.) exists due to the chemical and crystalline structure of cellulose fibrils. The magnitude of piezoelectric constant depends on the degree of crystallinity, the alignment of its disordered and amorphous regions and the orientation of cellulose crystals (Fukada 2000, Hirai et al. 2011).

Piezoelectricity in cellulose is generated from dipole orientation and the monoclinic and triclinic crystal structure in cellulose chains. According to Fukada (1968) these dipoles are the hydroxyl groups in crystal lattice of cellulose. Csoka et al. (2012) estimated the shear piezoelectric constant of aligned cellulose nanocrystals thin films to be 0.21 nm/V. The piezoelectric constant of regenerated cellulose was measured to be 0.035-0.06 nm/V (Huang 2008). Tsalagkas et al. (2013) investigated the likelihood of zinc oxide (ZnO)/bacterial cellulose films as material for low powering, energy harvesting devices (**Figure 9**). Results showed that the measured piezoelectric constant and energy conversion efficiency could be potentially suitable for such kind of applications. However, further research and improvements are still needed to be accomplished.

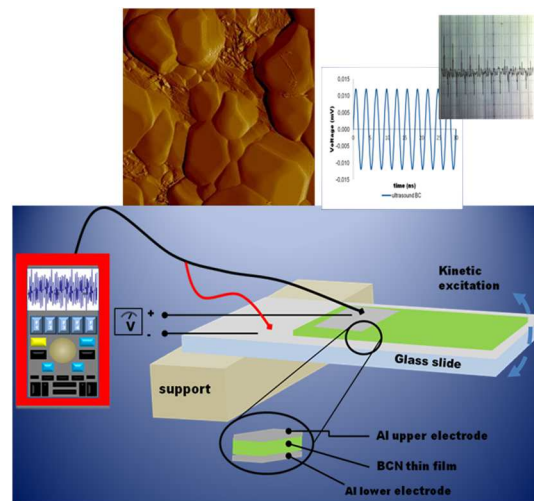


Figure 9: Scheme of the piezoelectric cantilever experimental set up, AFM image of ZnO/bacterial cellulose film and its output voltage (Tsalagkas & Csoka 2013).

1.10. Problem statement

The main purpose of this study was to develop an easy, fast, low cost method for obtaining bacterial cellulose thin films suitable for nanotechnology and energy harvesting applications. To meet these expectations we specified the objectives as follows:

Objective I: Purification of bacterial cellulose obtained from nata de coco

Even though, bacterial cellulose is free from hemicelluloses and lignin contaminants, the ferment broth contains other impurities such as bacterial cellulose debris and culture medium remainings. Thus, the fermented broth needs to be purified, to obtain pure cellulose. The most suitable purification methods for removal of the above mentioned impurities are using distilled water, sodium hydroxide and sodium hypochlorite aqueous solutions, or organic acids like acetic acids (Chawla et al. 2009, Pecoraro et al. 2007).

Highly crystalline cellulose is always in demand as an engineered cellulose to incorporate in production of bio-nanocomposites. The aims of the used purification treatments were to: (i) maintain the native cellulose I form of bacterial cellulose, and (ii) act

as chemical pretreatment and swelling of bacterial cellulose, to enhance the subsequent ultrasound treatment.

Objective II: Isolation of bacterial cellulose microfibrils

To the best of our knowledge there are not many publications related to the influence of ultrasound operating conditions on bacterial cellulose. Tischer et al. (2010) and Wong et al. (2009) investigated only the effect of ultrasound time periods on bacterial cellulose morphology and properties. Our purpose was to investigate the effect of two main high intensity ultrasonication parameters, specifically the effect of temperature and distance of ultrasonic probe on defibrillation and crystallinity of previously purified bacterial cellulose samples. Additionally, it was necessary to select the best set of operating conditions so that maximum cavitation effects could be obtained with minimum possible energy consumption.

Objective III: Preparation of bacterial cellulose films

Piezoelectric effect, defined by the piezoelectric, dielectric and elastic coefficients depends on the piezoelectric properties of the material, the dimensions (especially thickness) of piezoelectric material films, the type and thickness of electrodes, the size and shape of the cantilever and the direction of electrical and mechanical excitation. Piezoelectric performance of cellulose is influenced on the origin of cellulose source, the degree of crystallinity and the orientation and degree of alignment of cellulose nanoparticles.

The ultimate aim of this thesis was to develop a method for producing flexible, thin, homogenous, highly crystalline, thermodynamically more stable and self-sustaining bacterial cellulose films suitable for energy harvesting applications such as piezoelectric strain sensors.

Orientation and alignment of bacterial cellulose nanofibrils is another challenging research to form ordered films for energy harvesting or optical devices. Cellulose nanofibers alignment could be achieved with microfluidic channels, mechanical wet stretching, convective-shear shelf assembly under electric and/or magnetic field

techniques, Langmuir-Shaeffer technique or electrospinning technique. In our study, we would like to examine the possibility of self-sustained, oriented films due to ultrasonication treatment and casting evaporation drying method.

Nevertheless, in accordance with the results of this research, the most favourable ultrasound treated bacterial cellulose suspensions is aimed to be approached to the future for further investigation on the preparation of oriented films, with other orientation methods also.

2. Materials and methods

2.1. Materials

Bacterial cellulose was extracted from a commercially available product, Nata de coco. Nata de coco gel, as a source of bacterial cellulose was purchased in the form of cubes from local importing food company, distributed by PT. Cocomas Indonesia (Cocomas nata de coco gel in syrup). The ingredients of each package are nata de coco, water, sugar, citric acid, sodium benzoate and aroma flavor.

2.2. Experimental details

2.2.1. Purification of Nata de coco

Nata de coco cubes were washed and soaked in distilled water until the pH was neutral (pH 5-7) to remove the citric acid and other components of syrup added for preservation. This time of period could require up to 10-15 days, and is so on called as water purification (WP).

In order to improve purity of bacterial cellulose, same amounts of water purified nata de coco (≈ 1 g.) were further purified by alkaline treatment to remove any remaining bacterial cell debris, microorganisms and other soluble polysaccharides. The one step and two step purification methods were conducted by the procedure reported by Gea et al. (2011). After harvesting, nata de coco cubes were immersed overnight in 2.5 m/m NaOH solution. This process hereafter referred to as one step purification (OSP). Another sample was prepared in the same way and subsequently treated in 2.5 m/m NaOCl solution, further referred as two step purification (TSP). A third sample was prepared by boiling a concentration of 0.5 (w/v%) nata de coco in 0.01 M NaOH at 70 °C for 2 h under continuous stirring, called as 0.01 M NaOH purification treatment (NaP).

Afterwards, nata de coco cubes were rinsed under distilled water several times at room temperature, to remove any solvent, until the pH of the water became neutral.

Once neutral pH was reached bacterial cellulose was mechanically ground in a laboratory blender for a few minutes to be homogenized. Bacterial cellulose suspensions were poured into silicon trays and dried up in the oven at 50 °C.

2.2.2. Ultrasonication of bacterial cellulose films

Bacterial cellulose films after drying at 50 °C were cut. The cut films (0.1 w/v%, immersed in 80 mL distilled water) were redispersed and subjected to further grinding, with a hand blender, prior to ultrasonication. The concentration was estimated as dry weight percent of cellulose films in distilled water. High intensity ultrasonication (HIUS) was directly applied to redispersed bacterial cellulose suspensions. Sonication was achieved at low frequency (20 kHz) using an ultrasonic horn (Tesla 150 WS), having a 18 mm tip diameter dipped in the suspension. Two essential parameters of acoustic cavitation, i.e. temperature (no water-, cold water-, ice water bath) and distance of the ultrasonic probe (4 cm and 1 cm from the bottom of container) were considered to evaluate the effects of ultrasound on bacterial cellulose aqueous suspensions (**Figure 10**). Maximum power (20 W/cm²), ultrasonication time (30 min) and sample concentration (0.1 % w/v, 80 mL distilled water) were maintained constant.

HIUS power was controlled during the ultrasonication process. A time controller was used in the system to adjust treatment time. A mercury laboratory thermometer was used to record temperatures (°C) during the treatments. A metal arm was used to adjust the distance from the tip of the HIUS probe to the beaker bottom.

2.2.3. Preparation of bacterial cellulose films

Thereafter, the liquid supernatant solutions were collected from treated materials and were poured once more, into silicon trays. After this process, the ultrasonicated bacterial cellulose was reconstituted in the form of thin films after casting evaporation drying at 50 °C for second time. Due to drying evaporation method, properties of the bacterial cellulose films were independent of direction.

Figure 11 demonstrates a flow process diagram of purifying and obtaining the ultrasound bacterial cellulose films.

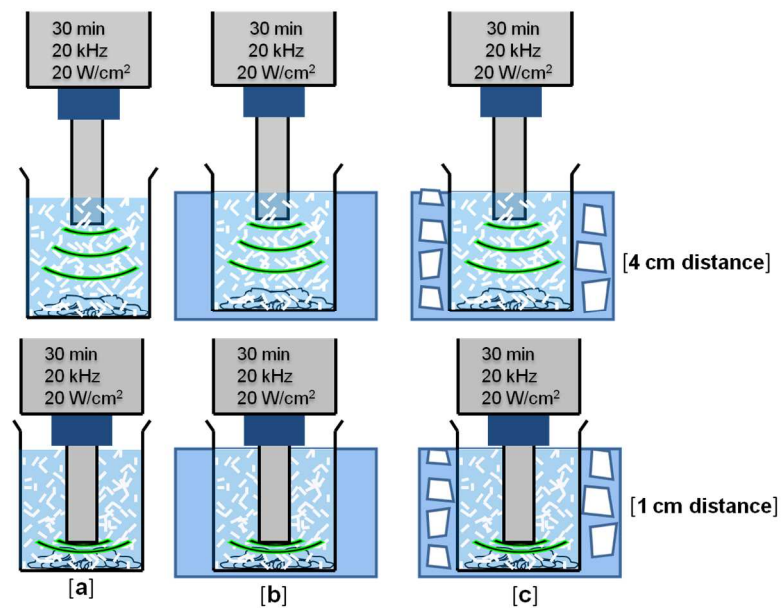


Figure 10: A scheme for HIUS treatment using no water bath (NoW, a), cold water bath (CW, b) and ice water bath cooling (IW, c). Ultrasonic probe was placed close to the top (4 cm distance) and to the bottom (1 cm distance) of the container.

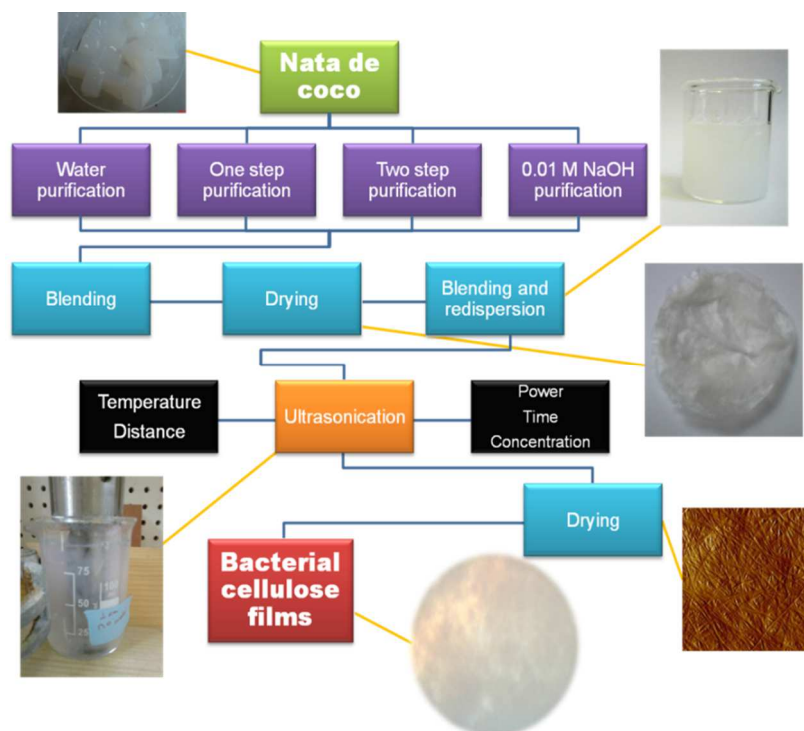


Figure 11: Block diagram of obtaining the bacterial cellulose films.

2.3. Bacterial cellulose films characterization techniques

2.3.1. Structural analysis of bacterial cellulose films

The cellulose supermolecular structure, i.e. i) hydrogen bonding network, ii) crystallinity changes and iii) cellulose I_α and I_β determination of the samples were evaluated by Fourier Transform Infrared Spectroscopy (FTIR) and X-ray powder diffraction (XRD) techniques.

Fourier Transform Infrared Spectroscopy (FTIR)

FTIR spectra of the bacterial cellulose films were obtained using a Jasco FT/IR6300 equipped with a ATR PRO 470-H spectrometer. A total of 50 cumulative scans were taken per sample with a resolution of 4 cm⁻¹, in the wavenumber range of 4000-400 cm⁻¹, in absorbance mode. ATR correction was applied in each measurement. FTIR spectra absorbance of bands between 4000 and 400 cm⁻¹ were analysed using OriginPro 8 software (OriginLab Corporation) and PeakFit v4.12 (Systat software, Inc).

For a good differentiation of the bands the Savitsky-Golay method (second-order polynomial with fifteen data points) was made using OriginPro8. The second derivative of IR spectra intensifies the apparent resolutions and exposes small differences of spectrum, i.e small differences of the samples (Popescu et al. 2009).

The spectra measurements of the 3800-2750 cm⁻¹ were deconvoluted using Gaussian (PeakFit v4.12.) to calculate and compare the integral absorption bands assigned to -OH region.

The most important absorbance bands assigned to crystalline cellulose I and cellulose II, based on previous published references are shown in Appendix (**Table 10**). These assignments will be used in the discussion of the results.

The Lateral Order Index (LOI) and Total Crystallinity Index (TCI), proposed by Nelson and O'Connor (1964a,b) and O'Connor (1958) respectively, were used to study the crystallinity changes of cellulose samples (Carrillo et al. 2004).

These infrared ratios, obtained from the 1420/893 (LOI) and 1375/2900 cm⁻¹ (TCI) absorbance ratios, produce different values which represent spectral differences, due to the different structural conformation (Colom & Carrillo 2002).

The absorbance ratio A_{1420}/A_{893} was defined as an empirical Crystallinity Index (CrI). It should be noted that this method even though is simple and fast provides only relative Cr.I. values, owing to the spectrum always contains contributions from both crystalline and amorphous regions (Terinte et al. 2011). The absorbance at 1420 and 894 cm^{-1} wavenumber are sensitive to the amount of crystalline versus amorphous structure in the cellulose, thus broadening of these bands depicts more disordered structure (Fan et al. 2012). The absorption band at 1430 cm^{-1} wavenumber is known as the “crystallinity band”, indicates that a decrease in its intensity reflects reduction in the degree of crystallinity of the samples, while the FTIR absorption band at 898 cm^{-1} wavenumber, is designed as an “amorphous” absorption band, and an increase in its intensity happens in the amorphous samples, compared to the initial ones (Ciolacu et al. 2011).

As for Total Crystallinity Index (TCI), various reports seem not to show a coherent result (Fan et al. 2012). However, according to Colom & Carrillo (2002) previous studies of substrates with a high crystalline cellulose I content demonstrate that this ratio is useful to follow structural changes during caustic treatments. In combination with Lateral Order Index (LOI), is a good method for reporting crystallinity changes of cellulose treated with sodium hydroxide.

In the structure of cellulose there are three hydroxyl groups that are available forming secondary valence bonds. Thus, the hydrogen bonding network in cellulose is considered as one of the most influential factor on the physical properties and chain structure of cellulose and its derivatives (Kondo 2004). The so-called hydrogen bond intensity (HBI), which compares the ratio of absorption bands at 3336 cm^{-1} and 1336 cm^{-1} , is closely related to the well ordered crystalline phase and the degree of intermolecular regularity. Lower HBI values means fewer available hydroxyl groups to interact by inter- and/or intramolecular hydrogen bonding (Široký et al. 2010, Kondo 2004).

The energy of the hydrogen bonds or hydrogen bonding energy (E_H) for the OH stretching band was calculated using equation (Struszczyk, 1986):

$$E_H = \frac{1}{k} \left[\frac{(v_0 - v)}{v_0} \right] \quad (1)$$

where v_0 is standard wavenumber corresponding to free -OH groups (3650 cm^{-1}), v the wavenumber of the bonded -OH groups and $\frac{1}{k}$ is a constant equal with 2.625×10^2 kJ.

The hydrogen bonding distances (Pimentel & Sederholm, 1956) are obtained by using the Sederholm equation:

$$\Delta\nu \text{ (cm}^{-1}\text{)} = 4.43 * 10^3 (2.84 - R) \quad (2)$$

where $\Delta\nu = \nu_0 - \nu$

ν_0 is monomeric -OH wavenumber (3600 cm^{-1}), ν the stretching wavenumber observed in the infrared spectrum of the sample.

On the other hand, the mean strength of the H-bonds (MHBS) was calculated as the ratio of $A_{\text{OH}}/A_{\text{CH}}$, where A is the absorbance of the stretching vibration of subscript groups (El-Saied et al. 2008).

X-ray powder diffraction (XRD)

The X-ray diffraction patterns were recorded at room temperature in the 5–80° 2θ range using an MPD Pro Panalytical diffractometer equipped with a linear Xcelerator detector. Cu-K_α (1.54056 Å) radiation was used with the 0.016° recording step and the 1000 s per step counting time. The samples have been powdered before the analysis.

X-ray diffractograms were analysed using OriginPro 8 software (OriginLab Corporation) and PeakFit v4.12 (Systat software, Inc).

X-ray diffraction parameters

Crystallinity index (CrI):

X-ray diffraction is a more accurate method to determine the degree of order (i.e. apparent crystallinity or crystallinity index) since considers more contributions of crystalline regions and less of the less ordered fractions of cellulose, in relation to FTIR spectroscopy (Terinte et al. 2011). However, all XRD measurements allow a qualitative or semi-quantitative estimation of crystallinity index. Lack of appropriate cellulose standards, which are necessary for calibration, is the main bottleneck.

The reflection mode geometry is thought to be more suitable for quantitative determination morphological composition, instead of transmission mode. With reflection mode the absorption factor is constant with angle and also there is less risk that the sample

is perturbed by pressing. Even more, large air scattering effect to the background of reflection mode diffractogram was almost negligible (Terinte et al. 2011, Thygessen et al. 2005).

There are several methods reported in the literature to calculate the degree of crystallinity from an X-ray diffractogram such as: 1. Peak height method (Segal method), 2. Ruland-Vonk method (amorphous subtraction method), 3. Hermans-Weidinger method, 4. Jayme-Knolle method and 5. Peak deconvolution method (curve fitting). Crystallinity index varies significantly depending on the measurement method (Terinte et al. 2011, Park et al. 2010). Each of these methods presents several benefits and drawbacks, based on XRD equipment and preparation of the samples and their simplicity, precision and contribution of cellulose and amorphous regions.

In our investigation crystallinity index was determined by i) peak height and ii) peak deconvolution method. XRD peak height method, developed by Segal and coworkers (1959), determines the crystallinity index by the following equation (Eq.3)

$$Cr.I = \frac{I_{200} - I_{am}}{I_{200}} 100 \quad (3)$$

where I_{200} is the peak intensity at the (200) ($2\theta \approx 22.5^\circ$) plane, and I_{am} is the minimum intensity at the valley between (200) and (110) peaks ($2\theta \approx 18^\circ$). The expression requires that the amorphous material diffracts with the same intensity and that the crystalline cellulose does not contribute to the amorphous intensity peak. Peak height is used for relative estimations of crystallinity between cellulose samples and not for estimating the amount of crystalline and amorphous material within a cellulose sample. Due to its simple and rapid way of application, is preferred from many researchers, although compared to all X-ray diffraction approaches, peak height method gave the highest X-ray crystallinity values.

XRD deconvolution method requires software to separate amorphous and crystalline contributions to the diffraction spectrum using a curve fitting process. An important assumption for this analysis is that increased amorphous contribution is the main contributor to peak broadening. For the curve fitting, a few assumptions have to be made, such as the shape and number of peaks. Gaussian, Lorentzian and Voigt functions are commonly used for deconvolution of XRD spectra. Individual crystalline peaks were extracted by a curve-fitting process from the diffraction intensity profiles (Terinte et al. 2011, Park et al. 2010).

For our investigation PeakFit v4.12 software AutoFit Peaks III Deconvolution (Spectroscopy, baseline linear D2) was used to calculate the areas of $1\bar{1}0$ (d_1), 110 (d_2) and 200 (d_3) planes of polymorph cellulose I and a broad area at around 18° to 20.5° assigned to the amorphous contribution. The apparent crystallinity (%) is calculated from the ratio of the area of all crystalline peaks to the total area including non-crystalline fraction following the equation:

$$Cr.I. = \frac{I_{1\bar{1}0} + I_{110} + I_{200}}{I_{1\bar{1}0} + I_{110} + I_{200} + I_{am}} 100 \quad (4)$$

where Cr.I is apparent crystallinity [%], $I_{1\bar{1}0}$ represents the area under the first crystalline peak in the diffraction pattern corresponding to the Miller index $1\bar{1}0$, I_{110} and I_{200} stand for the two areas under the second and deconvoluted crystalline peak corresponding to the Miller index 110 and 200 and I_{am} is the area under the non-crystalline peak of the cellulose diffraction pattern.

The interplanar distances of the crystallites (d-spacings) could be calculated with Bragg's law,

$$\lambda = 2d \sin\theta \quad (5)$$

where λ is the wavelength of the X-rays (and moving electrons, protons, and neutrons), d is the spacing between the crystal planes in the atomic lattice, and θ is the Bragg angle between the incident ray and the scattering planes (Moosavi-Nasab & Yousefi 2010).

The crystallite sizes at d_1 , d_2 and d_3 the three main peaks respectively, were determined using the Scherrer equation (Cheng et al. 2009):

$$Cr.S. = \frac{0.9 \lambda}{H_{hkl} \cos\theta_{hkl}} \quad (6)$$

where $Cr.S.$ is the crystallite size, λ is the wavelength of incident X-rays, H_{hkl} is the full-width at half-maximum (FWHM) and θ_{hkl} is the Bragg angle at the corresponding lattice plane.

2.3.2. Thermal analysis of bacterial cellulose films

Thermal analysis techniques, thermogravimetric analysis (TGA) and differential scanning calorimetry (DSC) were used to measure the thermal stability behavior of bacterial cellulose films. Thermogravimetric (TG) data were acquired between 0 and 500°C using a

Perkin Elmer Diamond thermal analyzer under nitrogen purging gas ($100 \text{ cm}^3\text{min}^{-1}$) at a heating rate of 2 K min^{-1} . Differential scanning calorimetry (DSC) analysis was carried out on a Netsch DSC204 instrument under nitrogen purging gas ($30 \text{ cm}^3\text{min}^{-1}$) at a heating/cooling rate of 2 K min^{-1} . Temperature and enthalpy were calibrated using the melting transition of standard materials (Hg, In, Sn).

2.3.3. Morphological analysis of bacterial cellulose films

The topography and morphology of bacterial cellulose oven dried films were images using Atomic Force Microscopy and Field Emission Scanning Electron Microscopy images.

Atomic force microscopy (AFM)

AFM experiments were performed using a MultiMode atomic force microscopy 8 with a Nanoscope Veeco V controller (Bruker Nano Surfaces, Santa Barbara, CA, USA) instrument. Small cut pieces of oven dried bacterial cellulose films were placed on magnetic slides and the scans were obtained in no tapping mode with a V-shape cantilever model. Prior to the measurements, the tip radius and geometry were calculated. Two repetition of imaging ($5 \times 5 \mu\text{m}$ and $1 \times 1 \mu\text{m}$) were carried out. These experiments were implemented in an environment with constant relative humidity and temperature.

Width measurements of bacterial cellulose microfibrils were calculated from two different images ($1 \mu\text{m} \times 1 \mu\text{m}$). Width was measured by using ImageJ software (ImageJ 1.46, National Institute of Health (NIH), USA) by image analysis.

Field emission scanning electron microscopy (FE SEM)

FE-SEM micrographs were obtained using a Zeiss ULTRA Plus (Oberkochen, Germany) instrument at an acceleration voltages of 1 and 2 kV. The suspensions were filtered through a gilded PC membrane and dried for 1 h at room temp. All samples were coated with a highly conductive film of gold by Bal-Tec SCD 500.

In total, for this study twenty eight bacterial cellulose samples were prepared for investigation. There were applied four purification sets, with no ultrasound irradiation as follows: water purification (WP), one step purification (OSP), two step purification (TSP) and 0.01 M NaOH purification (NaP) process. Each purified sample was further subjected to six different ultrasound treatments depending on the temperature [no water bath (NoW), cold water bath (CW), ice water bath (IW)] and the distance of the ultrasonic probe from the bottom of the container (1 cm and 4 cm). From each sample, there were taken three repetitions, during their characterization measurements.

In some cases, the group classification of bacterial cellulose treated samples will be referred in abbreviation way. The explanations of their given abbreviation names are presented in Appendix (**Table 11**).

3. Results

3.1. Structural analysis

3.1.1. Fourier Transform Infrared (FT-IR) spectroscopy

Fourier Transform infrared (FT-IR) spectroscopy is a successful and useful technique for analyzing the structural, physical and chemical changes taking place in cellulose based polymers consisting of native cellulose (I), regenerated cellulose (II) and/or amorphous cellulose domains (Carrillo et al. 2004). Any alteration of the crystalline organization leads to a transformation of the spectral contour through changes in intensity or even disappearance of the bands characteristic of the crystalline domains and provides us with information on the supermolecular structure of cellulose molecules.

The corroboration of the treatments described previously regarding to purity of native cellulose, as well as the influence of acoustic cavitation, were first evaluated by FT-IR spectroscopy.

A general view of the infrared spectra of the series of bacterial cellulose treatments in the range of 4000-400 cm^{-1} are presented in **Figures 12-16**.

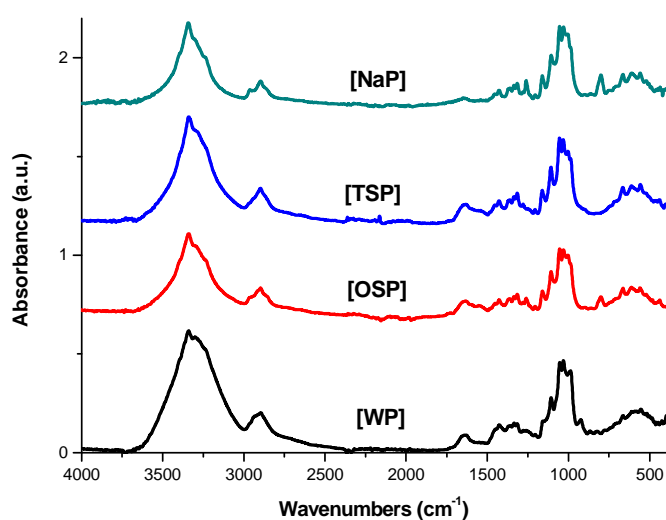


Figure 12: FT-IR spectra in the 4000-400 cm^{-1} region corresponding to purified and not-ultrasonicated treated samples.

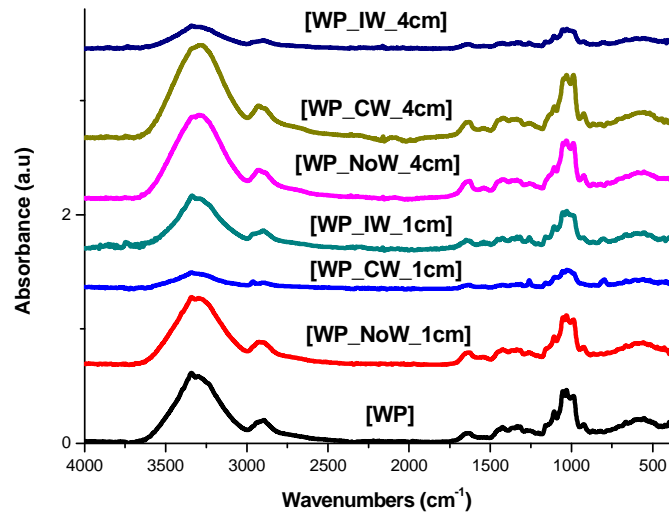


Figure 13: FT-IR spectra in the 4000-400 cm⁻¹ region corresponding to water purified and ultrasound treated samples.

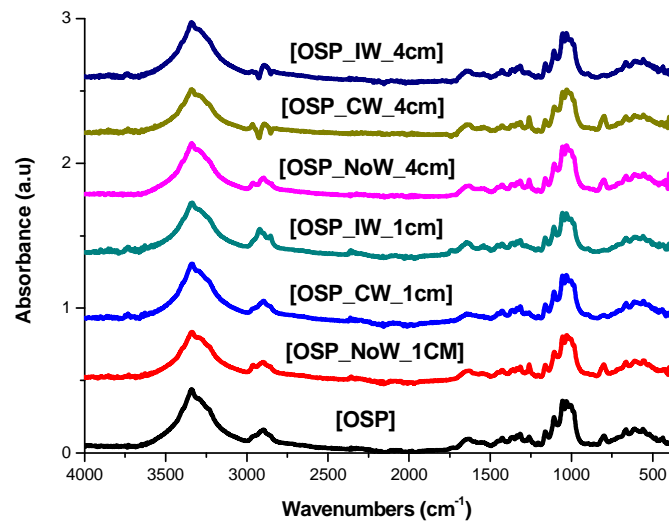


Figure 14: FT-IR spectra in the 4000-400 cm⁻¹ region corresponding to one step purified and ultrasound treated samples.

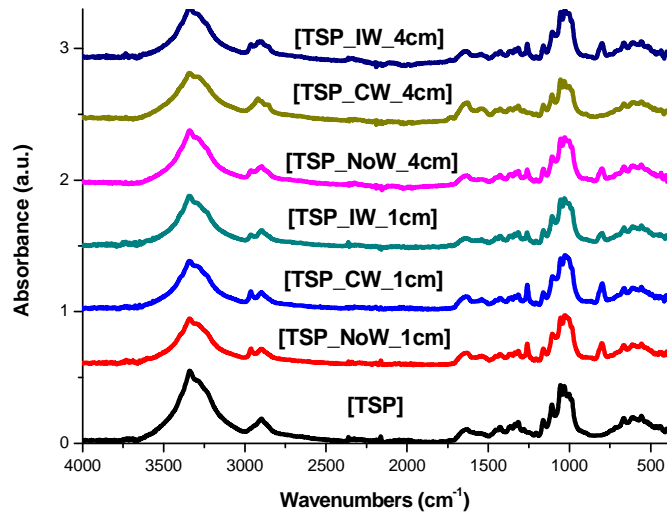


Figure 15: FT-IR spectra in the 4000-400 cm⁻¹ region corresponding to two step purified and ultrasound treated samples.

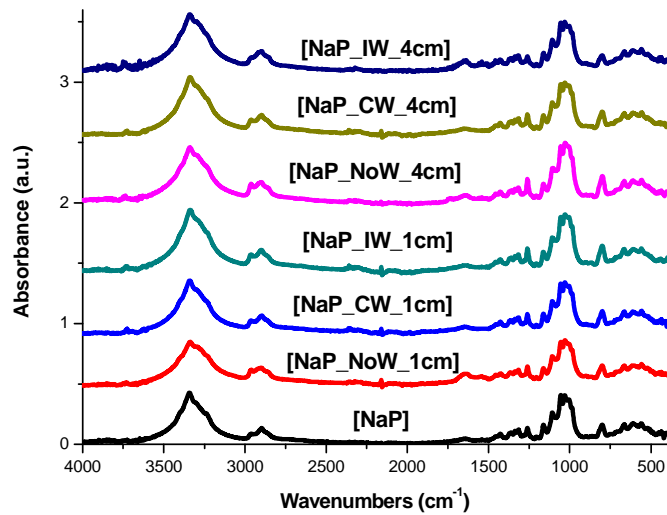


Figure 16: FT-IR spectra in the 4000-400 cm⁻¹ region corresponding to 0.01 M NaOH purified and ultrasound treated samples.

For a more comprehensive and qualitative analysis and investigation of the FT-IR spectra, in order to determine the most significant absorption bands and identify any changes occurred during purification and ultrasound treatments, FT-IR spectra were divided in two regions, 4000-2600 cm^{-1} and 1800-800 cm^{-1} wavenumber (**Figures 17-21**).

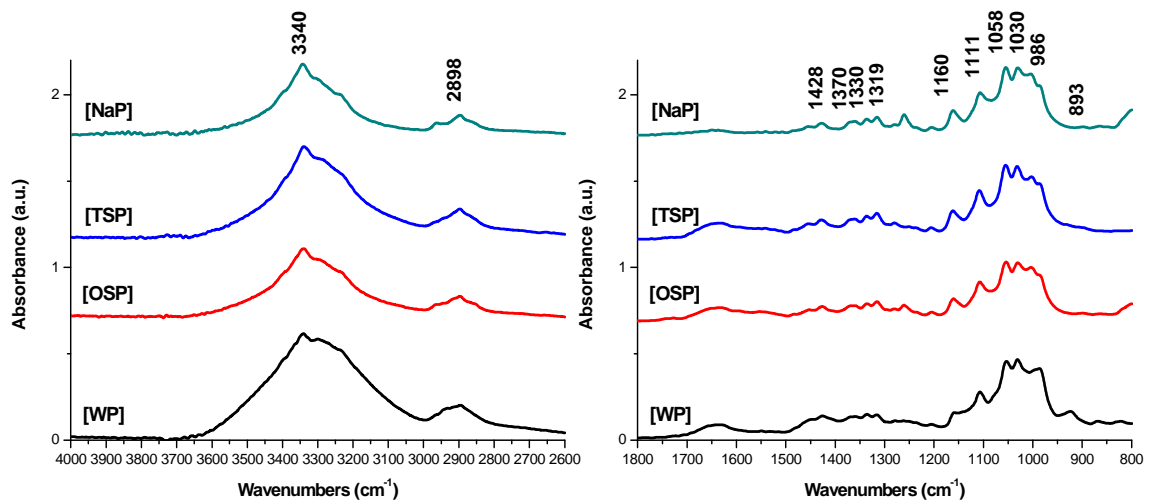


Figure 17: Comparative FT-IR spectra in the 4000-2600 cm^{-1} and 1800-800 cm^{-1} regions respectively corresponding to purified only treated samples.

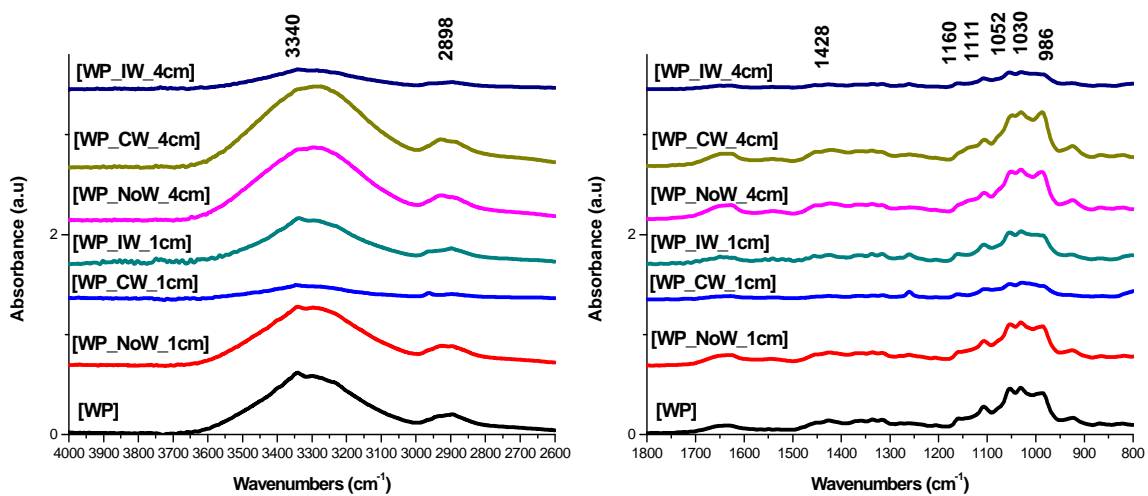


Figure 18: Comparative FT-IR spectra in the 4000-2600 cm^{-1} and 1800-800 cm^{-1} regions respectively corresponding to water purified and ultrasonicated treated samples.

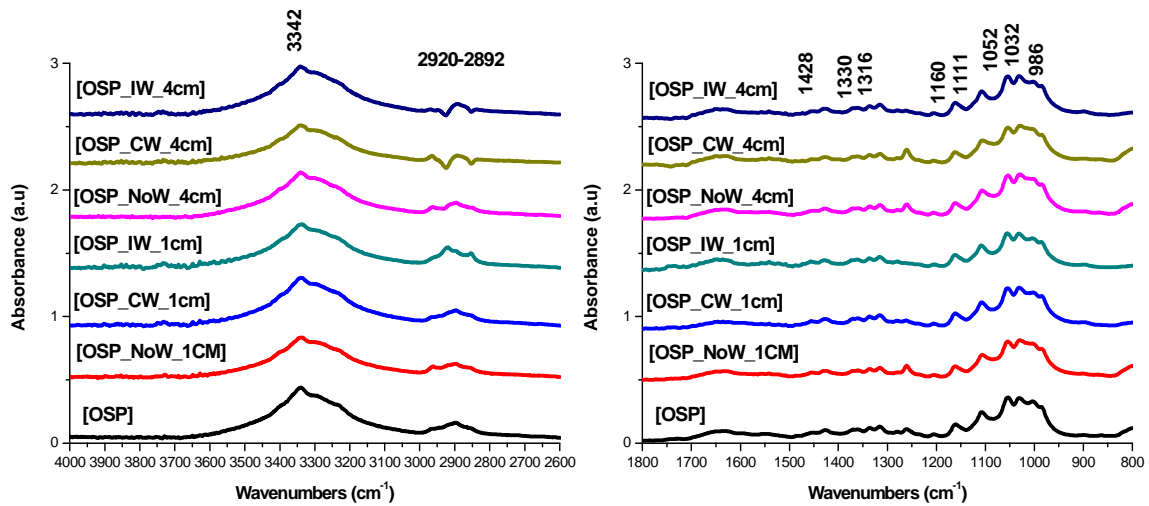


Figure 19: Comparative FT-IR spectra in the 4000-2600 cm^{-1} and 1800-800 cm^{-1} regions respectively corresponding to one step purified and ultrasonicated treated samples.

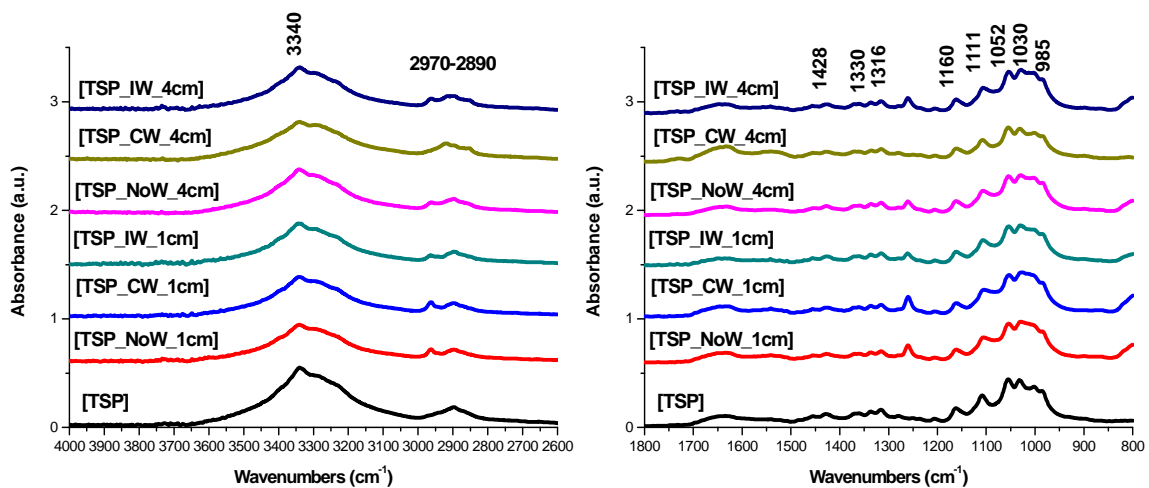


Figure 20: Comparative FT-IR spectra in the 4000-2600 cm^{-1} and 1800-800 cm^{-1} regions respectively corresponding to two step purified and ultrasonicated treated samples.

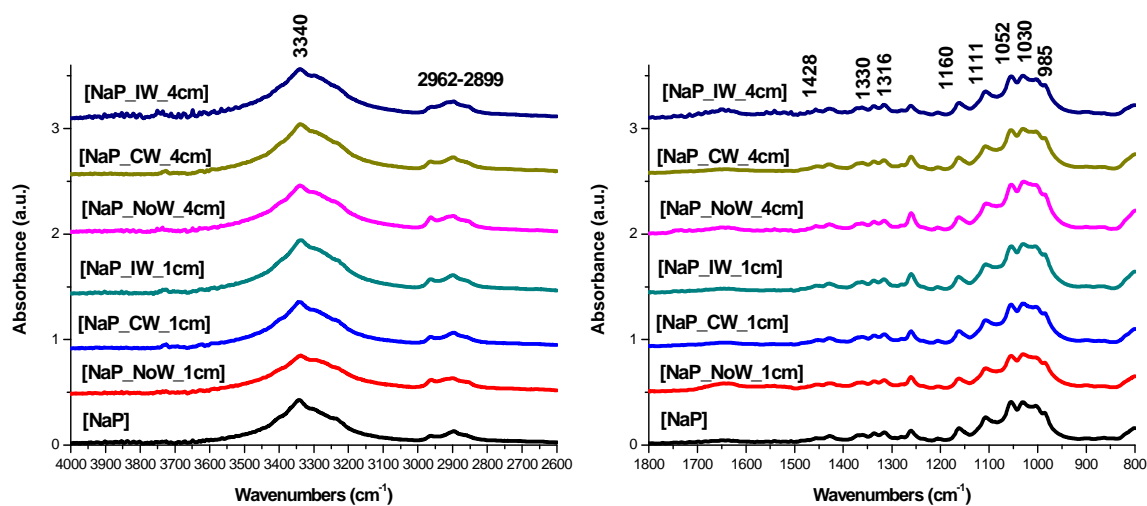


Figure 21: Comparative FT-IR spectra in the 4000-2600 cm^{-1} and 1800-800 cm^{-1} regions respectively corresponding to 0.01 M NaOH purified and ultrasonicated treated samples.

The most representative bands in the 3800-2600 cm^{-1} are those assigned to -OH intramolecular and intermolecular stretching modes (3570-3175 cm^{-1}) and methoxyl C-H stretching modes (2970-2890 cm^{-1}). Within the absorbance range 3600 to 3000 cm^{-1} , a consistent strong and sharp peak (3340 cm^{-1}) typical to cellulose I intramolecular hydrogen bond was observed in all treatments. In purified treated samples the C-H stretching band existed in 2898 cm^{-1} , which is also assigned to cellulose I. However, after ultrasonication the absorbance in this region became broader and alkaline treated samples displayed two peaks.

The “fingerprint” region 1800-800 cm^{-1} is more complicated. This region contains the largest number of spectral differences, which licenses for the identification of any structural changes within cellulose samples. In all FT-IR spectra the following characteristic bands were observed: 1640 cm^{-1} (absorbed water), 1428 cm^{-1} (CH_2 symmetric bending), 1370-1361 cm^{-1} (CH bending), 1330 cm^{-1} (-OH in plane bending), 1319-1316 cm^{-1} (CH_2 wagging at C-6), 1160 cm^{-1} (C-O-C asymmetric stretching), 1111 cm^{-1} (ring asymmetric stretching), , 1058-

1052 cm^{-1} (C-O stretching), 1032-1030 cm^{-1} (stretching C-O) and 986-985 cm^{-1} (C-O valence vibration at C-6).

Many researchers concentrated on the influence of sodium hydroxide concentration on various native celluloses (Higgins et al. 1958), the comparison and/or behavior of cellulose I and II polymorphs or the transition of native cellulose I to cellulose II.

They reported that the most notable changes in cellulose I occur at 1430 cm^{-1} , 1162 cm^{-1} , 1111 cm^{-1} , 990 cm^{-1} and 893 cm^{-1} absorption bands. In these bands the crystalline cellulose I spectrum differs significantly in relation to cellulose II and amorphous cellulose (Carrillo et al. 2004, Široký et al. 2010).

If the content of cellulose II was significant, the band at 1430 cm^{-1} should have been shifted to a lower absorption band at 1420 cm^{-1} . The absence of a characteristic peak around 895-893 cm^{-1} (amorphous cellulose, group C₁ frequency) is an additional evidence correlated to the existence of cellulose I (Carrillo et al. 2004). Even more, there is no evidence of the following absorption bands, 1376 and 1278 cm^{-1} , assigned mainly to crystalline cellulose II and amorphous cellulose (Colom & Carrillo 2002).

This spectra behavior and the presence of 1430 cm^{-1} , 1160 cm^{-1} , 1111 cm^{-1} absorption bands (Carrillo et al. 2004) in all samples indicates that the used ultrasound treatments had no effect in crystalline structure of bacterial cellulose. Even more, as it was expected, the alkaline treatments did not change the structure of pure bacterial cellulose (Gea et al. 2011, Tischer et al. 2010).

The consistent and reproducible shape of spectra curves are a sign of the origin of cellulose (Halib et al., 2012). Our spectra samples, optically seems to be similar to the spectra displayed in their paper. Thus, we believe that there is a strong confirmation that, the used nata de coco material was produced from bacteria species of *Acetobacter xylinum*.

OH region

It is essential to characterize the type of hydrogen bonding pattern exist in cellulose molecules. Inter- and intra- hydroxyl groups of cellulose units are regarded as one of the most dominant parameter on the correlation between structure of amorphous region and

physical properties of cellulose and cellulose derivatives, including crystallinity, reactivity and solubility (Fan et al. 2012, Kondo 1996).

Assuming, that all vibration modes follow a Gaussian distribution in the structure of cellulose there are three hydroxyl groups that are available forming secondary valence bonds. According to Gardner-Blackwell model, hydrogen bonds for cellulose I including two intramolecular bonds, O(2)H...O(6) and O(3)H...O(5) and one intermolecular bond, O(6)H...O(3) Compared with the bands of cellulose I, a new band related to intermolecular hydrogen bond of 2-OH...O-2' and/or intermolecular hydrogen bond of 6-OH...O-2' appears in cellulose II appears (Fan et al. 2012, Oh et al 2005).

From the deconvolution of hydrogen bonding OH stretching as shown in **Figure 22** all samples appear two or three characteristic bands, related to the intermolecular hydrogen bond for 6-OH...O-3' (3271.8 - 3276.8 cm^{-1}), the intramolecular hydrogen bond of 3-OH...O-5 (3335 - 3354.7 cm^{-1}) and to the sum of valence vibration of H- bonded OH groups and the intramolecular hydrogen bond of 2-OH...O-6 (3486.7 - 3576.4 cm^{-1}) respectively.

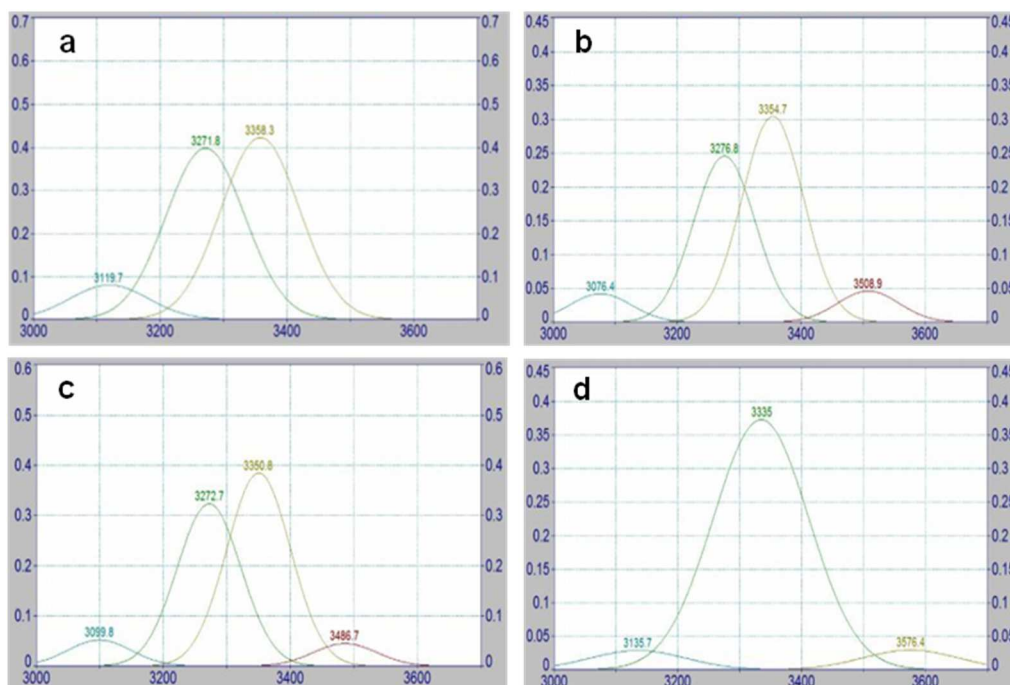


Figure 22: The deconvoluted spectra of 3600-3000 cm^{-1} region, for (a) WP, (b) OSP, (c) TSP and (d) NaP purification treatments of bacterial cellulose.

The resolutions of OH regions, of water purified bacterial cellulose samples under the different ultrasound conditions, are shown in **Figure 23**. In water purified samples, the intramolecular hydrogen bonds for 2-OH...O-6 appear at 3263.2-3265.1 cm^{-1} , the intramolecular hydrogen bond of 3-OH...O-5 at 3281.3-3358.2 cm^{-1} . The characteristic band related to the sum of valence vibration of H-bonded OH groups and the intramolecular hydrogen bond of 2-OH...O-6 (3501.5 cm^{-1}) is demonstrated only in 1 cm ice water ultrasonicated samples.

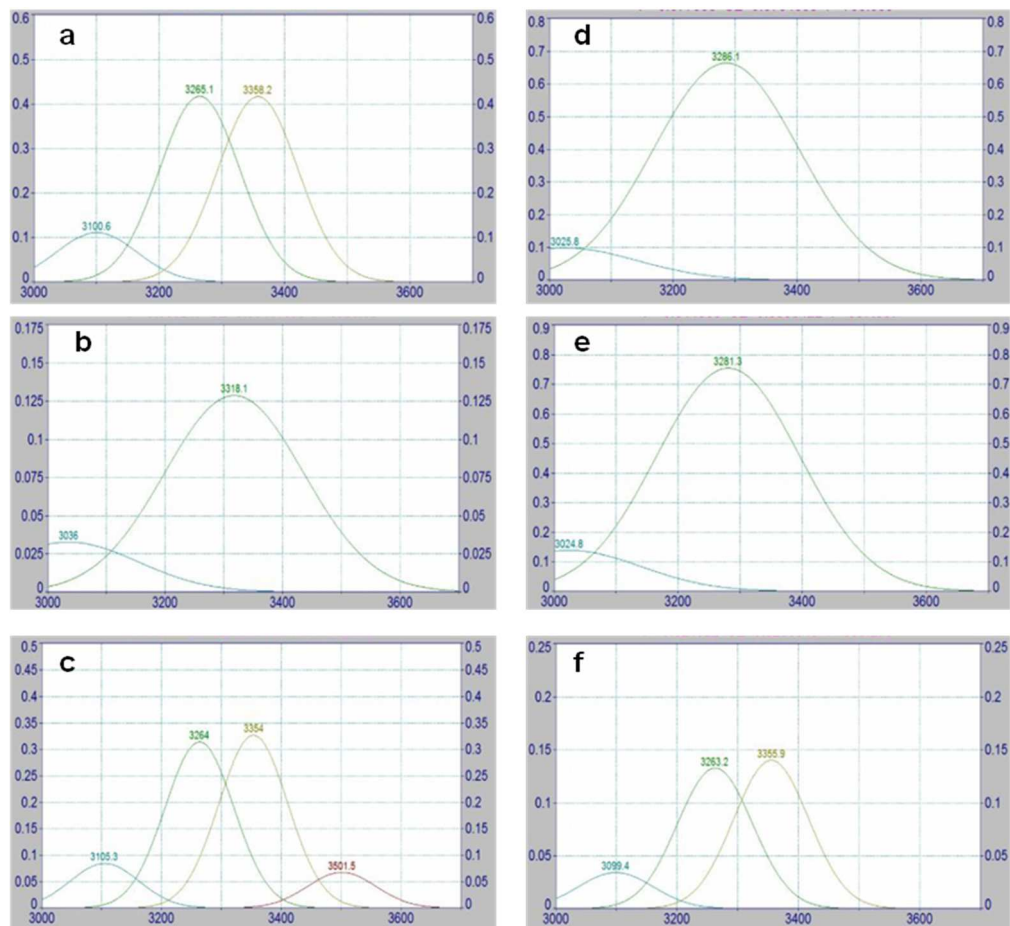


Figure 23: The deconvoluted spectra of 3600-3000 cm^{-1} region, for (a) WP_NoW_1cm, (b) WP_CW_1cm, (c) WP_IW_1cm, (d) WP_NoW_4cm, (e) WP_CW_4cm and (f) WP_IW_4cm, of water purified cellulose after ultrasonication.

Similar behavior is presented in the other purification samples after acoustic cavitation treatment. In one step purified cellulose samples the intramolecular hydrogen bonds for 2-OH...O-6, the intramolecular hydrogen bond of 3-OH...O-5 and the sum of valence vibration of H-bonded OH groups and the intramolecular hydrogen bond of 2-OH...O-6 appear at 3269.9-3281.9 cm^{-1} , 3322.8-3355.2 cm^{-1} and 3503.6-3578.3 cm^{-1} respectively (**Figure 24**).

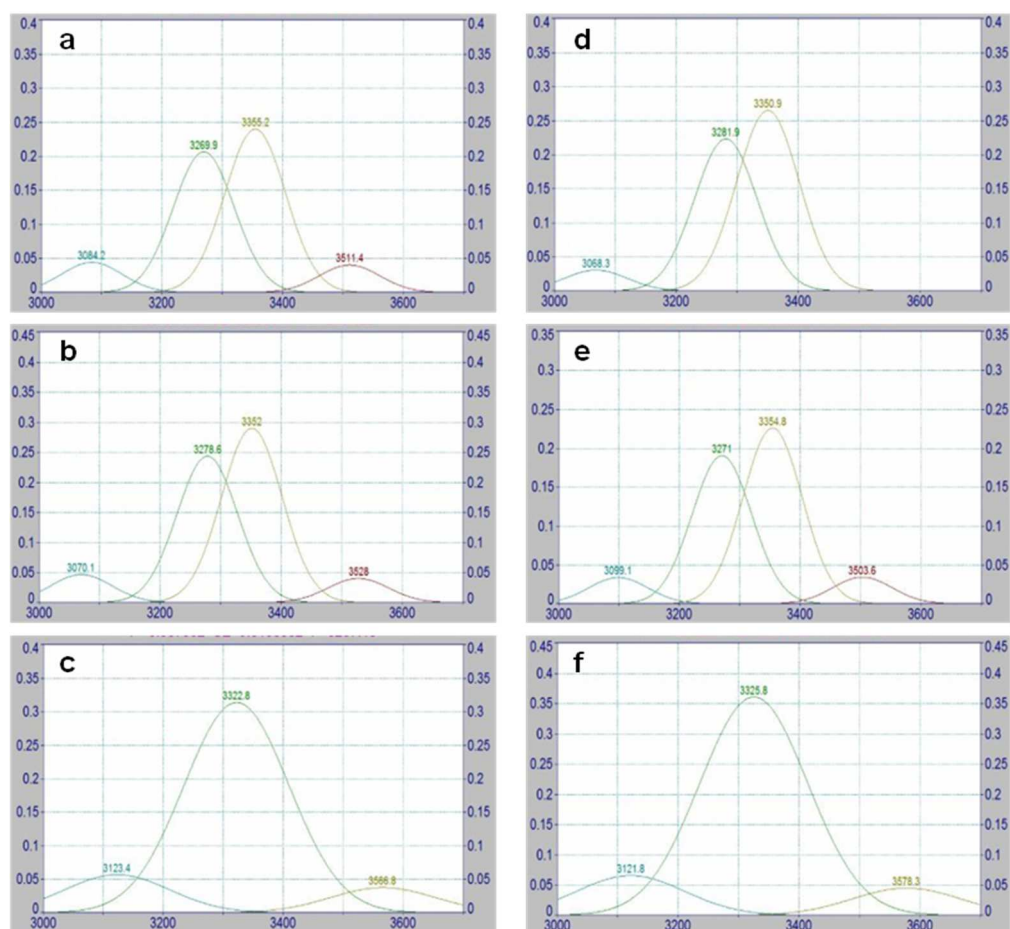


Figure 24: The deconvoluted spectra of 3600-3000 cm^{-1} region, for (a) OSP_NoW_1cm, (b) OSP_CW_1cm, (c) OSP_IW_1cm, (d) OSP_NoW_4cm, (e) OSP_CW_4cm and (f) OSP_IW_4cm, of one step purified cellulose after ultrasonication.

In two step purified cellulose samples (**Figure 25**) the intramolecular hydrogen bonds for 2-OH...O-6, the intramolecular hydrogen bond of 3-OH...O-5 and the sum of valence vibration of H- bonded OH groups and the intramolecular hydrogen bond of 2-OH...O-6 appear at 3264.7-3282.2 cm^{-1} , 3347-3358.3 cm^{-1} and 3490.9-3551 cm^{-1} respectively.

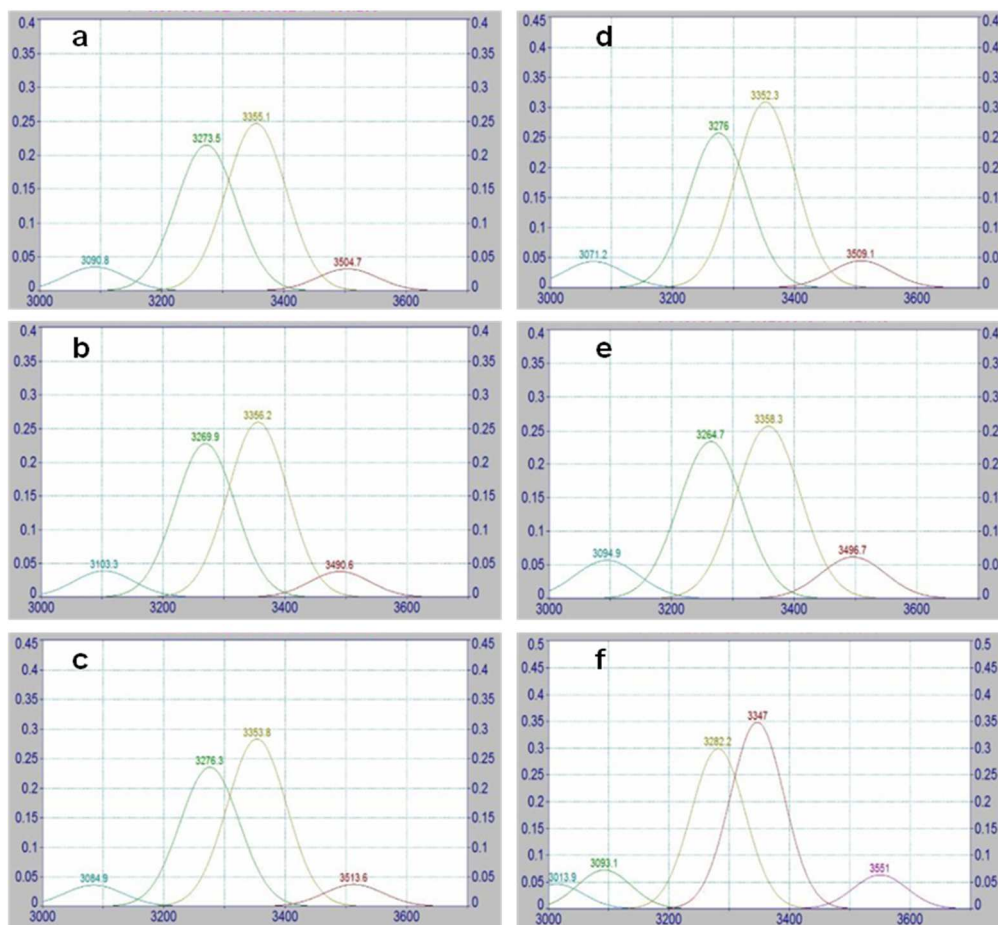


Figure 25: The deconvoluted spectra of 3600-3000 cm^{-1} region, for (a) TSP_NoW_1cm, (b) TSP_CW_1cm, (c) TSP_IW_1cm, (d) TSP_NoW_4cm, (e) TSP_CW_4cm and (f) TSP_IW_4cm, of two step purified cellulose after ultrasonication.

In 0.01 M NaOH purified cellulose samples (**Figure 26**) the intramolecular hydrogen bond of 3-OH...O-5 and the sum of valence vibration of H- bonded OH groups and the intramolecular hydrogen bond of 2-OH...O-6 appear at 3319.7-3331.5 cm^{-1} and 3565.2-3590.3 cm^{-1} respectively. In all 0.01 M NaOH purified samples there is not existence of the characteristic peak related to intramolecular hydrogen bonds for 2-OH...O-6 hydroxyl group.

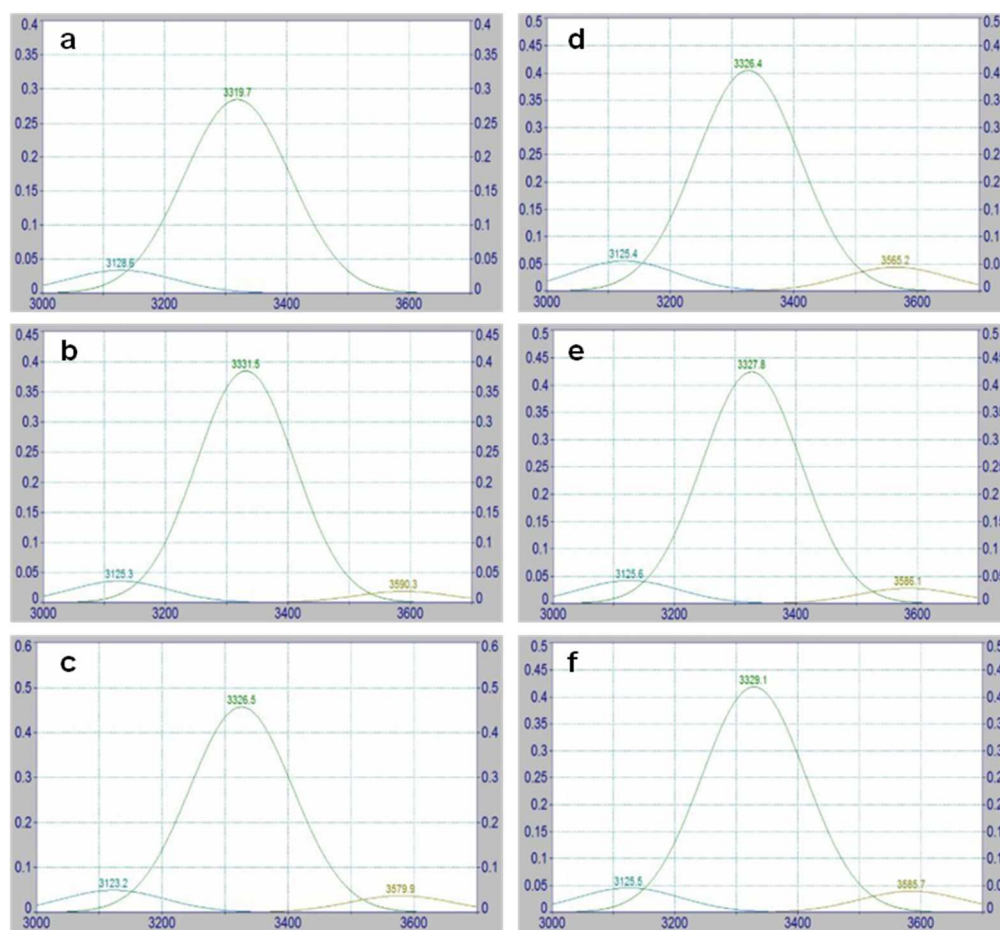


Figure 26: The deconvoluted spectra of 3600-3000 cm^{-1} region, (a) NaP_NoW_1cm, (b) NaP_CW_1cm, (c) NaP_IW_1cm, (d) NaP_NoW_4cm, (e) NaP_CW_4cm and (f) NaP_IW_4cm, of 0.01 M NaOH purified cellulose after ultrasonication.

Table 1: The energy hydrogen bond and hydrogen bonding distance of intramolecular hydrogen bond of 3-OH...O-5 for studied samples.

Purification treatment	Ultrasound conditions	Hydrogen bonding	Hydrogen bonding
		Energy (kJ/g mol)	distance (Å)
Water purification	<i>WP</i>	20.97	2.78
	<i>WP_NoW_1cm</i>	20.98	2.78
	<i>WP_CW_1cm</i>	23.86	2.77
	<i>WP_IW_1cm</i>	21.28	2.78
	<i>WP_NoW_4cm</i>	26.17	2.76
	<i>WP_CW_4cm</i>	26.51	2.76
	<i>WP_IW_4cm</i>	21.15	2.78
One step purification	<i>OSP</i>	21.23	2.78
	<i>OSP_NoW_1cm</i>	21.20	2.78
	<i>OSP_CW_1cm</i>	21.43	2.78
	<i>OSP_IW_1cm</i>	23.53	2.77
	<i>OSP_NoW_4cm</i>	21.51	2.78
	<i>OSP_CW_4cm</i>	21.23	2.78
	<i>OSP_IW_4cm</i>	23.31	2.77
Two step purification	<i>TSP</i>	21.51	2.78
	<i>TSP_NoW_1cm</i>	21.20	2.78
	<i>TSP_CW_1cm</i>	21.12	2.78
	<i>TSP_IW_1cm</i>	21.30	2.78
	<i>TSP_NoW_4cm</i>	21.40	2.78
	<i>TSP_CW_4cm</i>	20.97	2.78
	<i>TSP_IW_4cm</i>	21.79	2.78
0.01 M NaOH purification	<i>NaP</i>	22.65	2.78
	<i>NaP_NoW_1cm</i>	23.75	2.77
	<i>NaP_CW_1cm</i>	22.90	2.77
	<i>NaP_IW_1cm</i>	23.26	2.77
	<i>NaP_NoW_4cm</i>	23.27	2.77
	<i>NaP_CW_4cm</i>	23.17	2.77
	<i>NaP_IW_4cm</i>	23.07	2.77

From the derivative and deconvoluted FT-IR spectra of the samples there is clear evidence, that neither the mentioned alkaline treatments nor acoustic cavitation conditions indicated any sign of transformation of cellulose I to cellulose II. All these characteristic absorption bands are typical of cellulose I. There are not any trademarks, which can betray any transmission of cellulose I to cellulose II (Carrillo et al. 2004, Fan et al. 2012, Oh et al. 2005).

However, these main bands positions and absorbencies of hydroxyl groups are shifted differently or they appear or disappear in some cellulose samples. These results, indicate alterations in the content of cellulose samples and the interactions of inter- and intramolecular hydrogen bonds.

The calculated energy of hydrogen bond, and the hydrogen bonding distance the intramolecular hydrogen bond of 3-OH...O-5 (around 3340 cm^{-1} region) are shown in **Table 1**. The mean values of energy bond and hydrogen bonding distance were found 21.51 (± 1.5) kJ/g mol and 2.83 (± 0.00034) Å respectively. This energy for cellulose ranges from 19 to 21 kJ/g mol (Janardhnan and Sain, 2006).

Crystallinity, HBI and MHBS indices

The crystallinity analysis is based on the use of the crystallinity FT-IR indices. All measured values were different, indicating alterations in the crystalline structure of alkaline and ultrasound treated bacterial cellulose samples.

Carrillo et al. (2004) investigated the crystallinity indexes of different types of regenerated cellulose II. According to the co-authors, lyocell fibers demonstrated higher TCI and lower LOI indices against viscose and modal fibers, thus exhibited higher crystallinity. Široký et al. (2010) observed that microcrystalline cellulose, which is more crystalline than lyocell showed significantly higher TCI and LOI values and lower HBI values. LOI values represent the ordered regions perpendicular to the chain direction, which is greatly influenced by chemical processing of cellulose.

Hydrogen bond intensity (HBI) comparing the ratio of absorption bands at 3336 cm^{-1} and 1336 cm^{-1} , is closely related to the well ordered crystalline phase and the degree of

intermolecular regularity. Lower HBI values imply that there are fewer available hydroxyl groups, to interact by inter- and/or intramolecular hydrogen bonding (Široký et al. 2010).

It is apparent that crystalline indices, i.e. crystal structure changes of the samples depend on the origin and type of cellulose, as well as the chemical treatments cellulose might have been subjected.

The results and comparison of total crystallinity index (TCI), lateral order index (LOI) and hydrogen bond intensity (HBI) of water and sodium hydroxide purification treatments of bacterial cellulose are shown in **Table 2** and **Figure 27**. It was observed that there were not changes among TCI values of water-, one step- and two step purification methods. However, TCI was increased after 0.01 M NaOH treatment. In all purification treatments HBI values were decreased. However, LOI values were higher in alkali treated samples compared to only water purified bacterial cellulose samples. MHBS in 0.01 M NaOH purified bacterial cellulose was the strongest, and in one step purification the weakest.

The results obtained indicated the complexity of cellulose as material. However, 0.01 M NaOH purified bacterial cellulose (higher TCI and LOI), as in microcrystalline cellulose, could presented a higher crystallinity than the other alkali purification treatments and pure form of bacterial cellulose.

Table 2: Determined crystallinity indices (TCI and LOI), hydrogen bond intensity (HBI) and mean hydrogen bond intensity (MHBS) for purified, not-ultrasonicated bacterial cellulose samples.

Purification treatments	TCI A_{1372}/A_{2900}	LOI A_{1430}/A_{898}	HBI A_{3308}/A_{1330}	MHBS A_{3308}/A_{2900}
WP (1)	0.675	0.85	3.98	2.97
OSP (2)	0.68	1.54	3.53	2.65
TSP (3)	0.68	1.56	3.87	3.001
NaP (4)	0.73	1.32	3.8	3.20

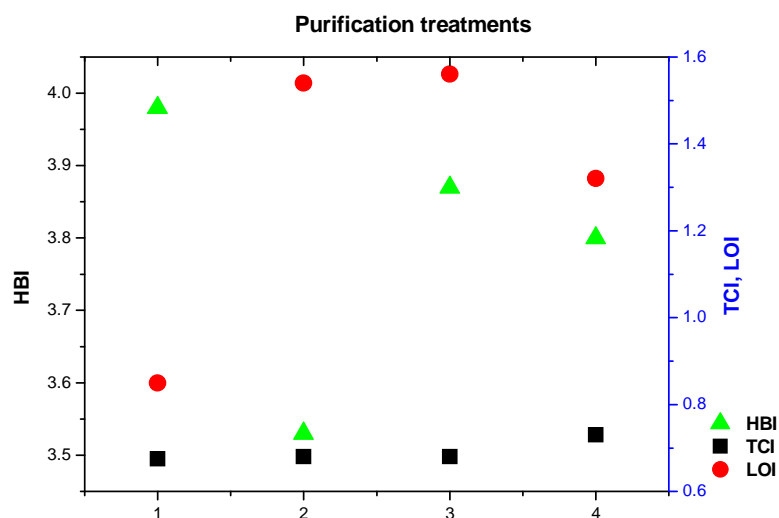


Figure 27: Crystallinity indices (TCI, LOI) and hydrogen bond intensity (HBI) prepared at different not-ultrasound purification treatments.

The results of the infrared crystallinity ratios and hydrogen bond intensity of water purified cellulose, as a function of different ultrasound treatments, are shown in **Table 3** and **Figure 28**, respectively. From the tabulated values it can be noted that the LOI showed not distinct changes in the samples except for “1 cm ice water bath ultrasonicated treatment”, which was increased. TCI values were decreased in most treated samples or were almost identical to no ultrasound sample. HBI values were increased only in “4 cm no water and 4 cm cold water bath” cellulose samples. The maximum MHBS value was obtained in “1 cm no water bath”, while the lowest were obtained in “1 and 4 cm cold water bath” process.

Table 3: Infrared crystallinity indices (TCI, LOI), hydrogen bond intensity (HBI) and mean hydrogen bond strength (MHBS) of ultrasonicated bacterial cellulose, after water purification treatment.

Water purif.- ultrasound	TCI	LOI	HBI	MHBS
	A_{1372}/A_{2900}	A_{1430}/A_{898}	A_{3308}/A_{1330}	A_{3308}/A_{2900}
WP (1)	0.675	0.85	3.98	2.97
WP_NoW_1cm (2)	0.63	0.86	3.75	3.93
WP_CW_1cm (3)	0.68	0.84	3.15	2.43
WP_IW_1cm (4)	0.62	0.90	3.87	2.70
WP_NoW_4cm (5)	0.64	0.84	4.22	2.82
WP_CW_4cm (6)	0.63	0.84	4.14	2.43
WP_IW_4cm (7)	0.67	0.83	3.51	2.65

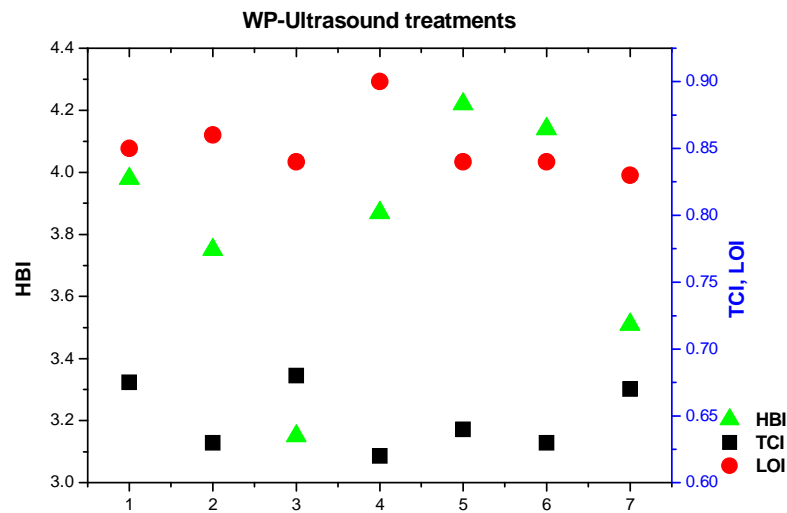


Figure 28: Crystallinity indices (TCI, LOI) and hydrogen bond intensity (HBI) prepared at different ultrasound conditions, after water purification treatment.

The results of the infrared crystallinity ratios and hydrogen bond intensity of one step purified cellulose, as a function of different ultrasound treatments, are shown in **Table 4** and **Figure 29**. LOI values were significantly decreased in all ultrasonicated samples compared to one step purified cellulose. HBI values displayed similar behavior, with exception of “4 cm ice water bath”. TCI values of 1 cm distance of ultrasonic probe manner were decreased, while in contrary, TCI values of 4 cm were increased, especially in cold and ice water bath treatment. It was observed that maxima MHBS value occurred in 4 cm ice water and the minima in 1 cm ice water process.

Table 4: Infrared crystallinity indices (TCI, LOI), hydrogen bond intensity (HBI) and mean hydrogen bond strength (MHBS) of ultrasonicated bacterial cellulose, after one step purification treatment.

One step purif.- ultrasound	TCI A_{1372}/A_{2900}	LOI A_{1430}/A_{898}	HBI A_{3308}/A_{1330}	MHBS A_{3308}/A_{2900}
OSP (1)	0.68	1.54	3.53	2.65
OSP_NoW_1cm (2)	0.66	1.29	3.33	2.37
OSP_CW_1cm (3)	0.65	1.28	3.38	2.43
OSP_IW_1cm (4)	0.53	1.47	3.24	1.88
OSP_NoW_4cm (5)	0.69	1.33	3.54	2.75
OSP_CW_4cm (6)	0.93	1.16	3.27	3.4
OSP_IW_4cm (7)	0.77	1.31	3.72	3.87

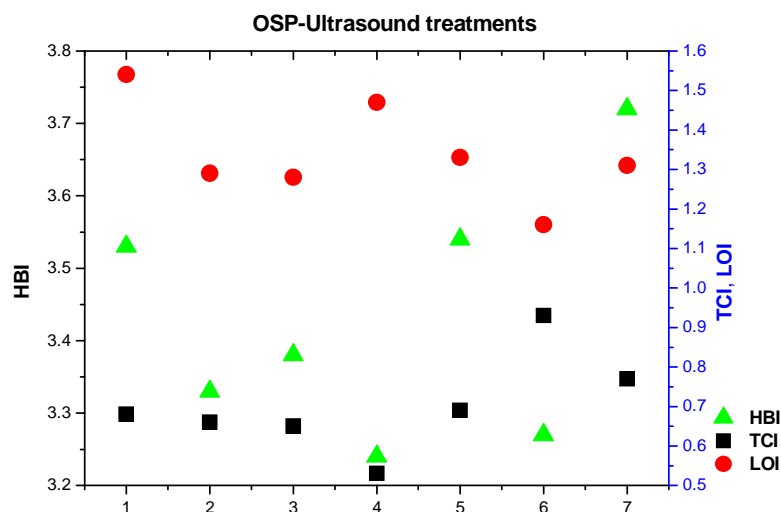


Figure 29: Crystallinity indices (TCI, LOI) and hydrogen bond intensity (HBI) prepared at different ultrasound conditions, after one step purification treatment.

The results of the infrared crystallinity ratios and hydrogen bond intensity of two step purified cellulose, as a function of different ultrasound treatments, are shown in **Table 5** and **Figure 30**. In two step purified bacterial cellulose samples, LOI and HBI values were decreased after acoustic cavitation was applied. TCI values of two step purified bacterial cellulose exhibited reverse results after ultrasonication in comparison with one step purification process.

TCI values were increased in 1 cm distance and not in 4 cm distance placement of ultrasonic probe, as in previous method. The strongest MHBS was observed after “1 cm cold water bath” ultrasonication, whilst the weakest in “4 cm cold water bath” treatment.

The results of the infrared crystallinity ratios and hydrogen bond intensity of 0.01 M NaOH purified cellulose, as a function of different ultrasound treatments, are shown in **Table 6** and **Figure 31**. In general, LOI and HBI values in most cases were also decreased, with a few exceptions. TCI was significantly decreased in all 4 cm treated samples and “1 cm ice water bath” ultrasonicated bacterial cellulose. Although, TCI was increased in “1 cm no water and 1 cm cold water bath” processes. In 0.01 M NaOH purification, not ultrasonicated bacterial cellulose samples exhibited the maximum MHBS value, while the minimum value was showed after “1 cm no water bath” ultrasound conditions.

Table 5: Infrared crystallinity indices (TCI, LOI), hydrogen bond intensity (HBI) and mean hydrogen bond strength (MHBS) of ultrasonicated bacterial cellulose, after two step purification treatment.

Two step purif.- ultrasound	TCI	LOI	HBI	MHBS
	A_{1372}/A_{2900}	A_{1430}/A_{898}	A_{3308}/A_{1330}	A_{3308}/A_{2900}
TSP (1)	0.68	1.56	3.87	3.00
TSP_NoW_1cm (2)	0.69	1.34	3.58	2.86
TSP_CW_1cm (3)	0.70	1.37	3.59	3.97
TSP_IW_1cm (4)	0.72	1.3	3.38	2.75
TSP_NoW_4cm (5)	0.66	1.27	3.37	2.50
TSP_CW_4cm (6)	0.62	1.47	3.03	2.00
TSP_IW_4cm (7)	0.63	1.37	3.38	2.33

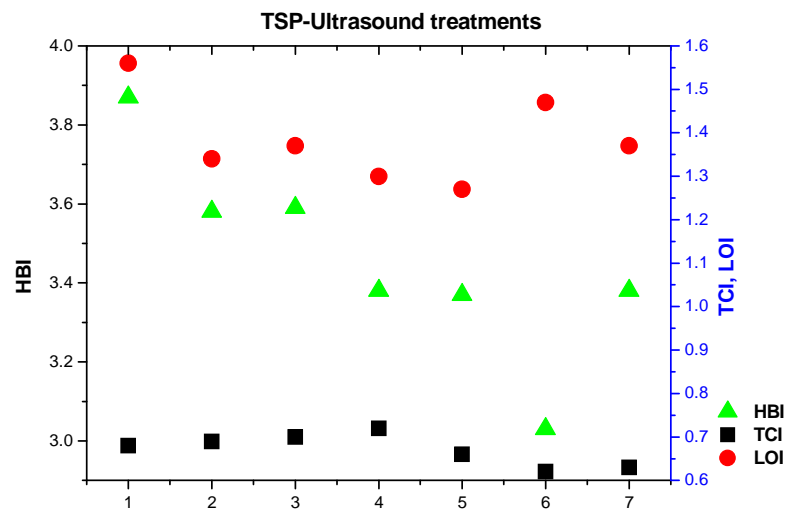


Figure 30: Crystallinity indices (TCI, LOI) and hydrogen bond intensity (HBI) prepared at different ultrasound conditions, after two step purification treatment.

Table 6: Infrared crystallinity indices (TCI, LOI), hydrogen bond intensity (HBI) and mean hydrogen bond strength of ultrasonicated bacterial cellulose, after 0.01 M NaOH purification treatment.

0.01 M NaOH purif.- ultrasound	TCI	LOI	HBI	MHBS
	A_{1372}/A_{2900}	A_{1430}/A_{898}	A_{3308}/A_{1330}	A_{3308}/A_{2900}
NaP (1)	0.73	1.32	3.80	3.20
NaP_NoW_1cm (2)	0.76	1.22	2.81	2.32
NaP_CW_1cm (3)	0.75	1.21	3.35	2.8
NaP_IW_1cm (4)	0.69	1.23	3.38	2.56
NaP_NoW_4cm (5)	0.62	1.30	3.64	2.54
NaP_CW_4cm (6)	0.63	1.30	3.89	2.83
NaP_IW_4cm (7)	0.66	1.40	3.72	2.78

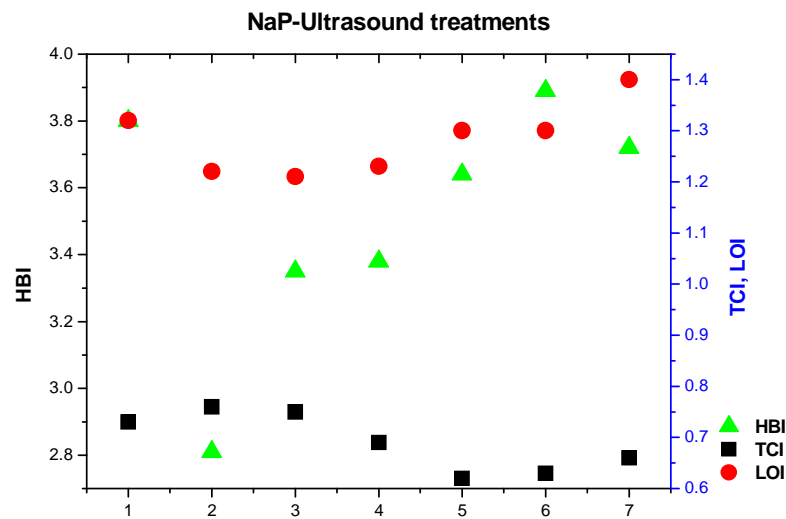


Figure 31: Crystallinity indices (TCI, LOI) and hydrogen bond intensity (HBI) prepared at different ultrasound conditions, after 0.01 M NaOH purification treatment.

The values of crystallinity indices and hydrogen bond intensity were affected by the ultrasound parameters. Power of ultrasound and temperature influenced differently TCI, LOI and HBI in each purification method. Based on the results, we consider the best processes to produce bacterial cellulose films with higher crystallinity order and thus possibly improved properties, the treatments which resulted in the following order combinations: lower LOI, higher TCI and lower HBI values, respectively. Like in case of regenerated cellulose and not microcrystalline cellulose, as we employed earlier in purified only samples.

In total, we selected the 14 best treatments for further characterizations with X-ray diffraction (XRD), field emission scanning microscopy (FE-SEM), atomic force microscopy (AFM), thermogravimetric analysis (TGA) and differential scanning calorimetry (DSC) techniques. These optimum procedures in each purification method were the following:

Water purification: (i) WP_NoW_1cm, (ii) WP_CW_1cm and (iii) WP_IC_4cm 4.

One step purification: (i) OSP, (ii) OSP_CW_1cm, (iii) OSP_NoW_4cm and (iv) OSP_CW_4cm.

Two step purification: (i) TSP, (ii) TSP_CW_1 cm, (iii) TSP_IW_1 cm.

0.01M NaOH purification: (i) NaP, (ii) NaP_NoW_1 cm, (iii) NaP_CW_1 cm and (iv) NaP_CW_4 cm.

3.1.2.X-ray diffraction analysis (XRD)

The X-ray diffraction patterns of bacterial cellulose obtained from nata de coco, treated with water and alkali purification are presented in **Figure 32**. Their X-ray patterns, even of these with sodium hydroxide treatments, show a pattern similar to the native cellulose. The sharper diffraction peak at $2\theta = 22.7^\circ$, in 0.01 M NaOH purified sample at 70 °C for 2 h under continuous stirring, demonstrates region of higher crystallinity. These results confirm the results obtained after FT-IR measurements.

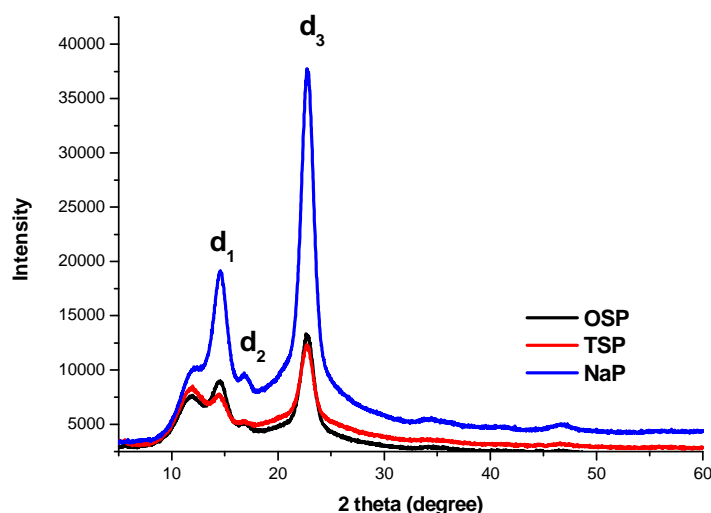


Figure 32: X-ray diffraction of bacterial cellulose with different purification methods.

There are three main characteristic peaks of cellulose I in X-ray diffractions, and these are located at approximately $2\theta = 14^\circ$, 16° and 22° corresponding to $1\bar{1}0$ (d_1 spacing), 110 (d_2 spacing) and 200 (d_3 spacing) crystallographic planes respectively. The typical diffractogram peaks of cellulose II polymorph related to $1\bar{1}0$ (d_1 spacing), 110 (d_2 spacing) and 200 (d_3 spacing) crystallographic planes are located at $2\theta = 11^\circ$, 20° and 21° respectively. The diffractogram peak located at around $2\theta = 35^\circ$, corresponds to 040 crystallographic plane (Gupta et al. 2013, Jiao & Xiong 2014).

The X-ray diffractograms patterns of water, one step- and two step purification treatments are displayed in **Figures 33-36** respectively. The diffractograms show no change in peak intensities located at the crystallographic plane reflections, indicating no transformation of cellulose I in cellulose II polymorph at different ultrasound conditions.

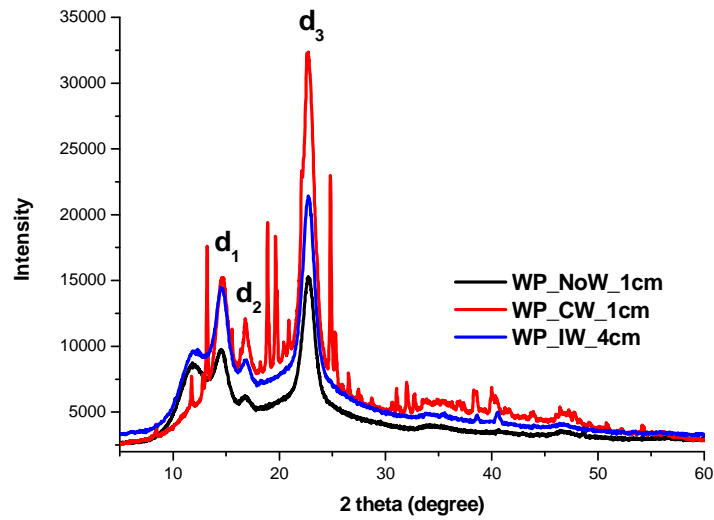


Figure 33: X-ray diffraction of water purified bacterial cellulose with different ultrasound conditions.

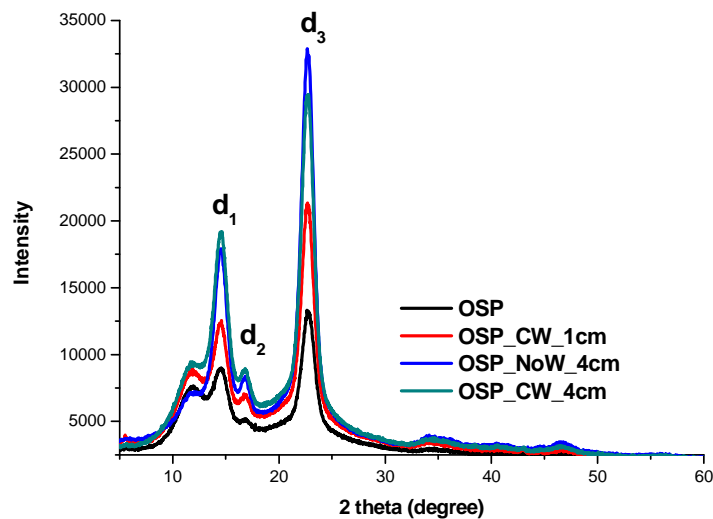


Figure 34: X-ray diffraction of one step purified bacterial cellulose with different ultrasound conditions.

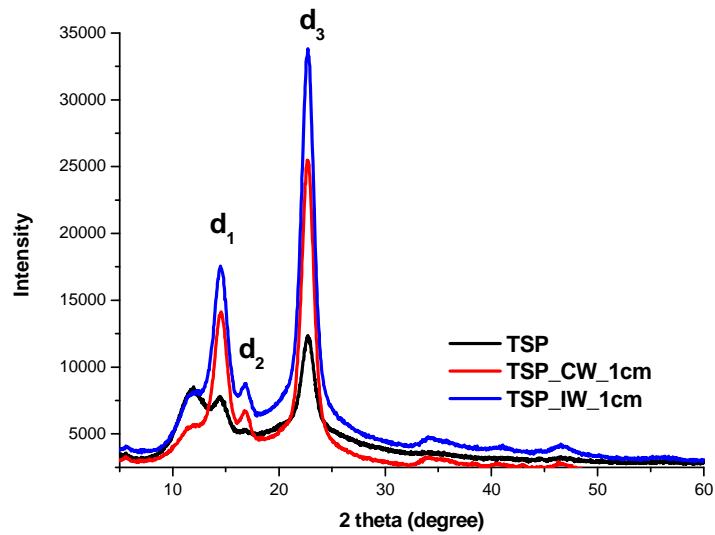


Figure 35: X-ray diffraction of two step purified bacterial cellulose with different ultrasound conditions.

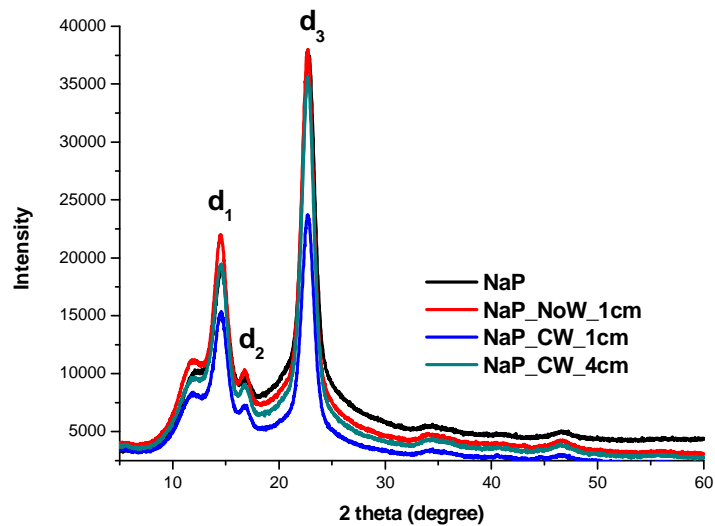


Figure 36: X-ray diffraction of 0.01 M NaOH purified bacterial cellulose with different ultrasound conditions.

Peak intensities at three 2θ angles for the best selected bacterial cellulose samples, as well as their crystallinity index (Cr.I) of peak height and peak deconvolution methods, are given in **Table 7**.

Table 7: XRD peak intensity percent (%) at 2θ angles and Cr.I for purified bacterial cellulose with different ultrasound parameters.

Purification treatments	Ultrasound conditions	2θ degree			Peak intensity (%)			Cr. I	Cr. I
		d1	d2	d3	d1	d2	d3	(peak height)	(peak deconv.)
Water purification	<i>WP_NoW_1cm</i>	14.56	16.81	22.74	31.30	19.96	48.75	64.47	79.94
	<i>WP_CW_1cm</i>	14.66	16.79	22.72	25.45	20.33	54.22	75.06	75.67
	<i>WP_IW_4cm</i>	14.58	16.79	22.76	32.29	19.90	47.82	65.98	79.55
One step purification	<i>OSP</i>	14.54	16.70	22.70	33.07	18.40	48.54	66.89	83.06
	<i>OSP_CW_1cm</i>	14.61	16.86	22.72	30.27	17.38	52.35	74.17	84.96
	<i>OSP_NoW_4cm</i>	14.51	16.76	22.70	30.46	13.91	55.63	82.45	89.57
	<i>OSP_CW_4cm cold</i>	14.53	16.79	22.74	33.35	15.41	51.24	78.79	86.29
Two step purification	<i>TSP</i>	14.46	16.64	22.70	30.51	20.93	48.56	58.87	77.96
	<i>TSP_CW_1cm</i>	14.55	16.76	22.70	30.61	14.33	55.05	81.84	89.10
	<i>TSP_IW_1cm</i>	14.48	16.73	22.73	29.25	14.37	56.38	80.53	87.15
0.01 M NaOH purification	<i>NaP</i>	14.68	16.87	22.77	28.61	14.46	56.93	77.78	83.55
	<i>NaP_NoW_1cm</i>	14.51	16.70	22.69	31.41	14.59	54.01	80.46	87.02
	<i>NaP_CW_1cm</i>	14.54	16.72	22.72	33.07	15.75	51.18	77.62	87.42
	<i>NaP_CW_4cm</i>	14.53	16.70	22.70	30.33	13.92	55.74	81.70	88.00

The peak intensity % at $2\theta = 14.46-14.68^\circ$ ($1\bar{1}0$, d1 spacing) of total peak intensity remained almost constant in all treated cellulose samples, around 30%. The peak intensity % at $2\theta = 16.64-16.87^\circ$ (110, d2 spacing) varied from 13.92% to 20.93% and was decreasing when the crystallinity of cellulose was increasing. The peak intensity % at $2\theta = 22.69-22.76^\circ$ (200, d3 spacing) which is the most dominant was varying from 47.82 to 56.93 %. In contrary

with the second 2θ angle, peak intensities of $2\theta = 22.7^\circ$ were increasing when crystallinity values of cellulose samples, were also enhanced.

The minimum degree of crystallinity (58.87 %) was obtained in two step purification treatment. The degree of crystallinity in one step purification was found to be 66.89 %. This result indicates that the treatment with NaOCl had a decrystallizing effect on bacterial cellulose samples. This outcome could be in contrast with FT-IR results. Based on FT-IR, we might expected better or similar crystallinity since LOI values were increased, eventhough TCI values were almost identical.

Nevertheless, the 0.01 M NaOH treatment, presented the maximum crystallinity index value (77.78 %) compared to the other purification treatments. This alkaline method, instead of decreasing crystallinity, in contrary augmented the crystalline domains of bacterial cellulose.

Likewise, treatments with acoustic cavitation demonstrated a beneficial effect in the crystalline structure of cellulose samples. Crystallinity was raised in one step and two step purification treated samples after ultrasonication. In the already high percentage crystallinity of 0.01 M NaOH purified samples, crystallinity was further slightly enhanced. The ultrasound energy, which was transferred through searing and cavitation to the glucan chains, resulted in promoting the conversion of amorphous material into crystalline material (Tischer et al. 2010).

The d-spacing values and crystallite sizes of the three characteristic planes, and the proportion of crystallite interior chains of bacterial cellulose samples, calculated from X-ray diffractograms are listed in **Table 8**.

The changes in the d-spacings represent a different proportion of I_α and I_β cellulose allomorphs. d-spacing values are in accordance with Amin et al. (2014) who investigated the properties of acid and mechanical treated, spray dried bacterial cellulose obtained from nata de coco. Mean values of d_1 , d_2 and d_3 spacings were 0.608 (± 0.002), 0.528 (± 0.002) and 0.39 (± 0.0004) nm respectively.

The crystallite sizes in $1\bar{1}0$ (d_1 spacing), 110 (d_2 spacing) and 200 (d_3 spacing) lattice planes the mean values were 5.456 (± 0.427), 5.572 (± 0.293) and 5.67 (± 0.332) nm respectively. The mean value proportion of crystalline interior chains was 0.637 (± 0.018) nm.

Table 8: d-spacings, crystallites sizes, and crystalline interior chain values of treated bacterial cellulose samples.

Purification treatments	Ultrasound conditions	d spacings (nm)			Cr. size (nm)			Cr. Interior
		d1	d2	d3	d1	d2	d3	Chain (nm)
Water purification	<i>WP_NoW_1cm</i>	0.60	0.52	0.39	5.81	5.83	5.88	0.65
	<i>WP_CW_1cm</i>	0.60	0.52	0.39	7.66	7.68	7.75	0.72
	<i>WP_IW_4cm</i>	0.60	0.52	0.39	5.56	5.57	5.60	0.63
One step purification	<i>OSP</i>	0.60	0.53	0.39	5.74	5.75	5.81	0.64
	<i>OSP_CW_1cm</i>	0.60	0.52	0.39	5.60	5.61	5.67	0.63
	<i>OSP_NoW_4cm</i>	0.60	0.52	0.39	5.55	5.93	6.41	0.67
	<i>OSP_CW_4cm cold</i>	0.60	0.52	0.39	5.45	5.48	5.53	0.63
Two step purification	<i>TSP</i>	0.61	0.53	0.39	5.25	5.26	5.31	0.61
	<i>TSP_CW_1cm</i>	0.60	0.52	0.39	5.39	5.80	6.31	0.67
	<i>TSP_IW_1cm</i>	0.61	0.53	0.39	4.36	4.86	5.51	0.62
0.01 M NaOH purification	<i>NaP</i>	0.60	0.52	0.39	5.45	5.47	5.52	0.62
	<i>NaP_NoW_1cm</i>	0.60	0.53	0.39	4.88	5.43	6.17	0.66
	<i>NaP_CW_1cm</i>	0.60	0.52	0.39	4.71	5.19	5.81	0.64
	<i>NaP_CW_4cm</i>	0.60	0.53	0.39	5.55	5.57	5.62	0.63

3.2. Thermal analysis

3.2.1. Thermo Gravimetric Analysis

The results of thermogravimetric analysis (TGA) and derivative thermogravimetric (DTGA) to study the effect of purification treatment and ultrasound conditions on the purified cellulose samples are shown in **Figures 37 and 38**, respectively. To examine the thermal degradation phenomenon, the onset temperature was taken at 10% weight loss. The thermal decomposition temperature of bacterial cellulose samples, known as the maximum degradation weight loss rate (T_{dmax}) was determined from dTGA curves.

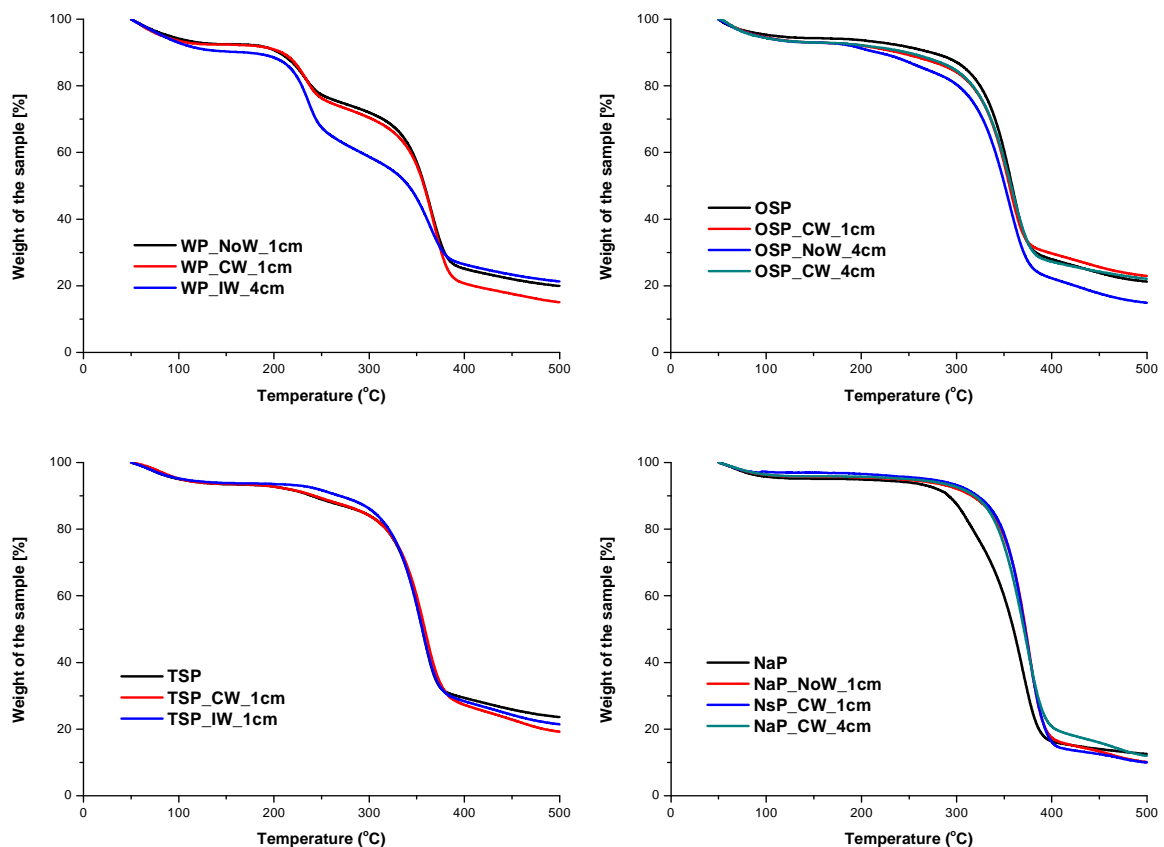


Figure 37: TGA curves of WP, OSP, TSP and NaP treated bacterial cellulose samples under different ultrasound operating conditions.

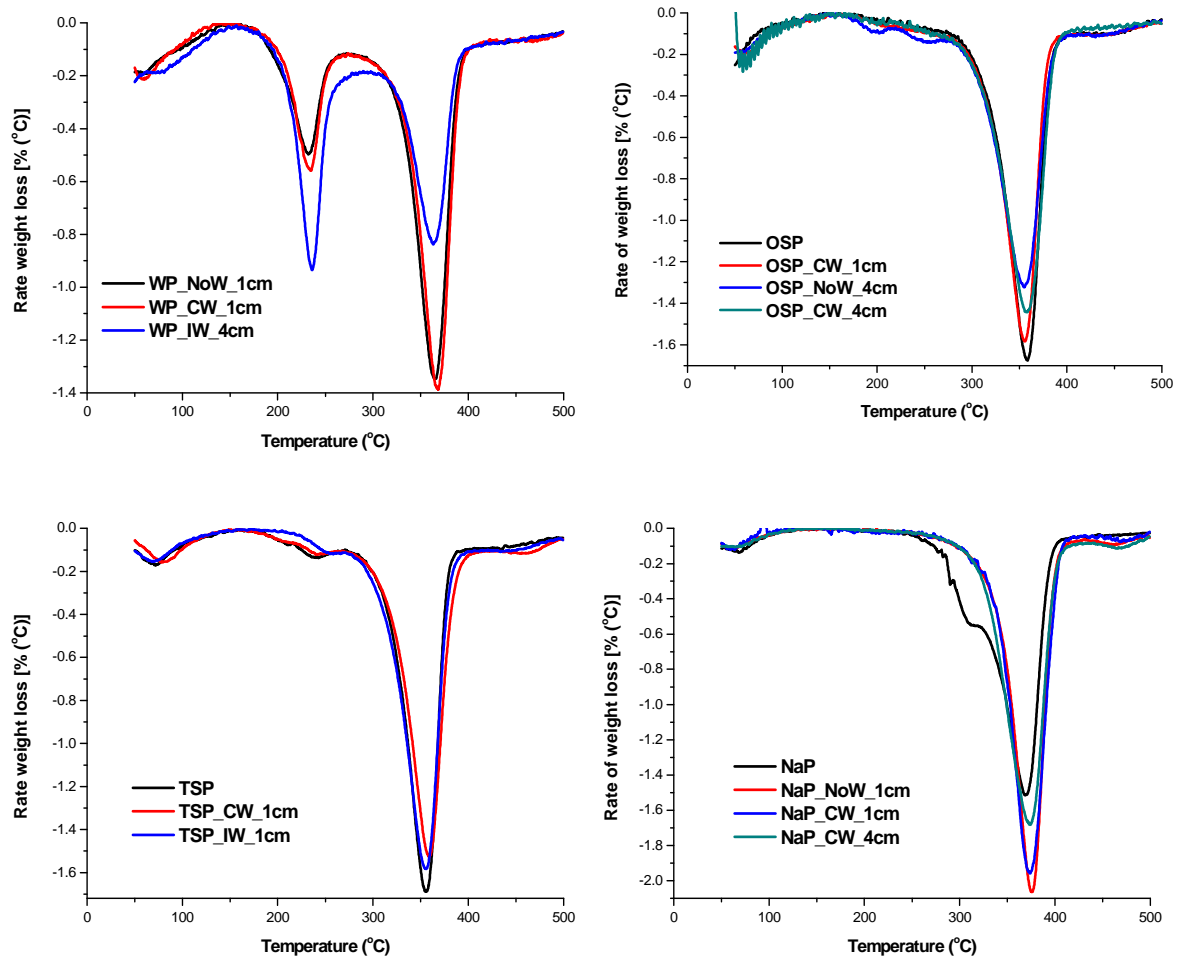


Figure 38: dTGA curves of WP, OSP, TSP and NaP treated bacterial cellulose samples under different ultrasound operating conditions.

The thermogravimetric analysis (TGA) and derivative thermogravimetric (dTGA) curves of each individual bacterial cellulose sample are illustrated in **Figures 39-42**, respectively.

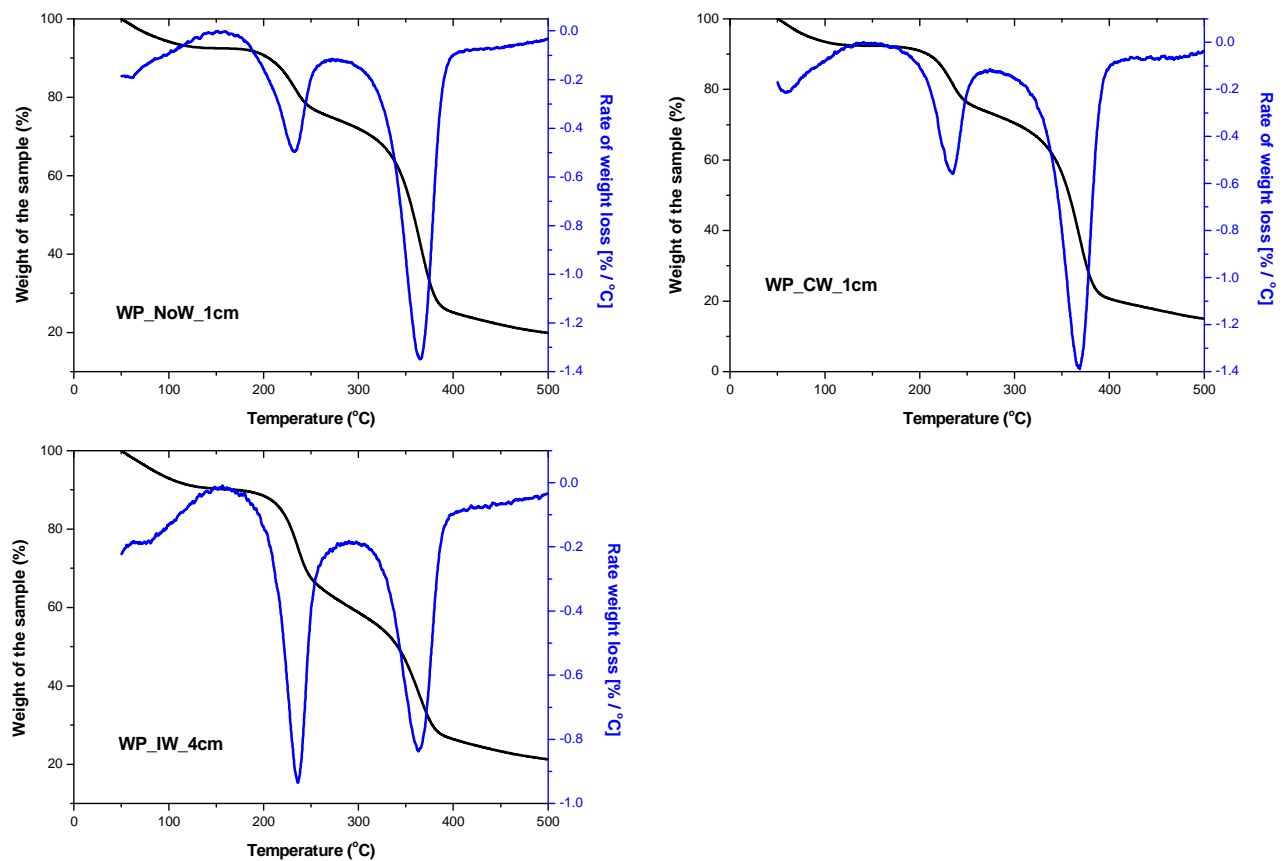


Figure 39: TGA and dTGA curves of WP treated bacterial cellulose samples under different ultrasound operating conditions.

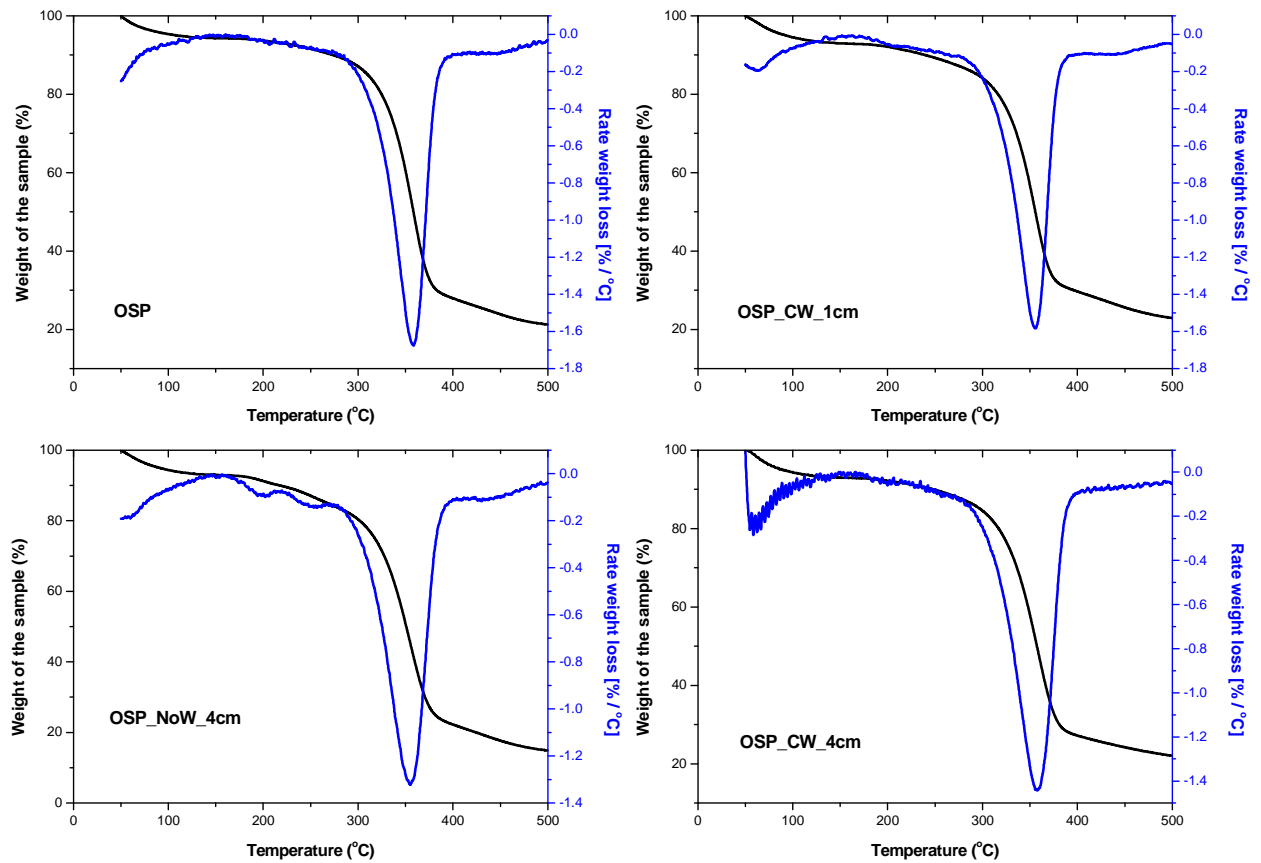


Figure 40: TGA and dTGA curves of OSP treated bacterial cellulose samples under different ultrasound operating conditions.

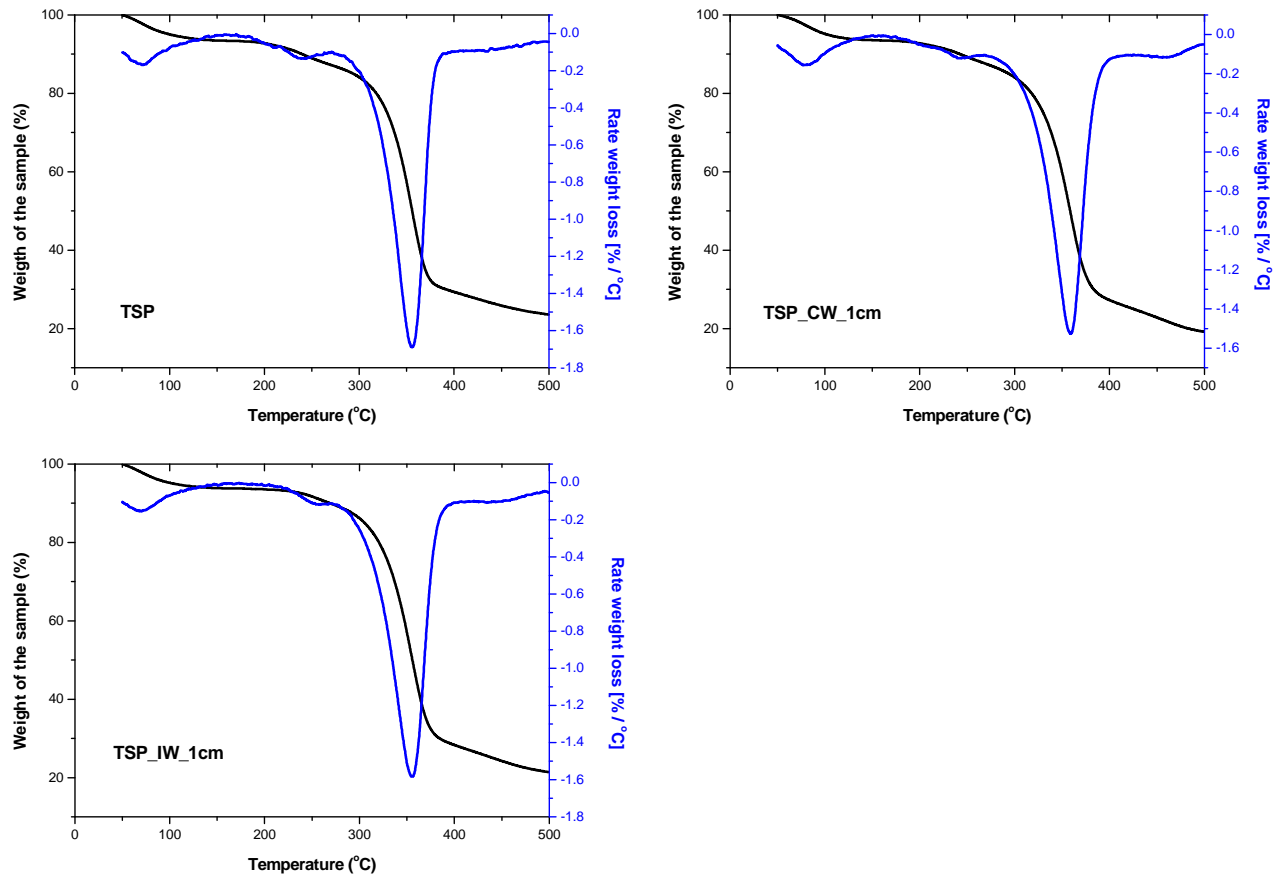


Figure 41: TGA and dTGA curves of TSP treated bacterial cellulose samples under different ultrasound operating conditions.

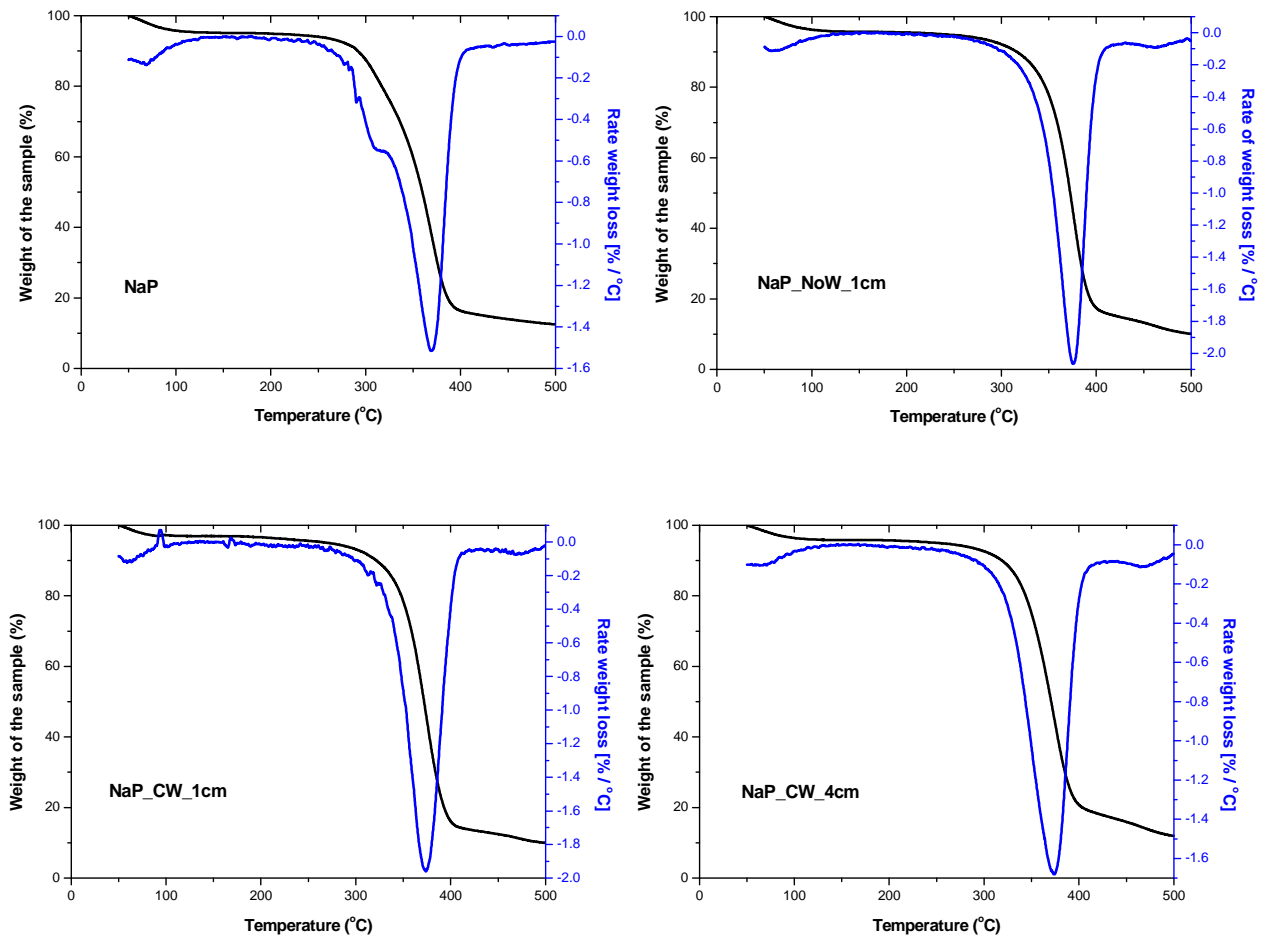


Figure 42: TGA and dTGA curves of NaP treated bacterial cellulose samples under different ultrasound operating conditions.

The onset temperature of the thermal degradation (T_d) with the associated maximum cellulose decomposition temperature (T_{dmax}) as well as the solid residue mass at 500 °C of the cellulose samples are compared in **Table 9**.

Table 9: Summary of TGA and dTGA data for bacterial cellulose samples after different purification and ultrasound treatments.

Purification treatments	Ultrasound conditions	T_d (°C)	T_{dmax} (°C)	Solid residue (%)
Water purification	<i>WP_NoW_1cm</i>	185	365	19.91
	<i>WP_CW_1cm</i>	192	368	15.02
	<i>WP_IW_4cm</i>	186	364	21.27
One step purification	<i>OSP</i>	241	359	21.26
	<i>OSP_CW_1cm</i>	195	356	22.9
	<i>OSP_NoW_4cm</i>	196	355	14.86
	<i>OSP_CW_4cm cold</i>	198	357	22.05
Two step purification	<i>TSP</i>	208	356	23.58
	<i>TSP_CW_1cm</i>	217	359	19.19
	<i>TSP_IW_1cm</i>	244	356	21.4
0.01 M NaOH purification	<i>NaP</i>	285	368	12.49
	<i>NaP_NoW_1cm</i>	309	376	10.07
	<i>NaP_CW_1cm</i>	316	374	9.988
	<i>NaP_CW_4cm</i>	312	374	11.94

Thermal degradation behavior of bacterial cellulose includes depolymerisation, dehydration and decomposition of glycosic units accompanied with the formation of a charred residue (George et al. 2011). The water purified cellulose samples displayed two peaks, as native bacterial cellulose, first one around 235 °C and the second around 365 °C.

The first peak is attributed to the thermal degradation of proteinous impurities present in native cellulose, while the second is indicative of the degradation of cellulose. In the case

of chemically treated samples, only one sharp distinguished peak was noticed between 355-376 °C correlated to cellulose decomposition temperature, suggesting an effective removal of protein impurities and other ingredients by the alkali treatment. In one and two step purification treatments there were observed small peaks and shouldered areas around 200 to 250 °C, indicating still the existence of bacterial impurities. A small peak occurring around 100 °C, depicts weight loss due to moisture evaporation.

The onset temperature T_d of thermal degradation (temperatures at 10% weight loss) for one step, two step and 0.01 M NaOH samples were 241 °C, 208 °C and 285 °C, respectively. George et al. (2005) report that native bacterial membranes started degradation at 150 °C and 15-20% weight loss was ranging between 250-285 °C. Carrillo et al. (2014) report that higher onset temperatures indicate improved thermal stability. Since thermal degradation behavior is affected by crystallinity, probably higher onset could demonstrate higher crystallinity. These results are also confirmed from X-ray diffractograms. 0.01 M NaOH purified samples exhibited the highest crystallinity degree, in comparison with one step and two step purification.

T_{dmax} temperatures presented similar results like T_d . The mean T_{dmax} temperatures were around 365 °C for water purified samples, 357 °C for one step and two step treated bacterial cellulose and 374 °C for 0.01 M NaOH purified cellulose. Further, solid residue mass loss at 500 °C was significantly lower in 0.01 M NaOH samples compared to the other treatments. In addition, it was shown from dTGA curves that acoustic cavitation had an impact on the degradation rate of cellulose. The longer peak valley height differences indicate faster degradation rates.

3.2.2. Differential scanning calorimetry

DSC thermograms of bacterial cellulose membranes obtained of the different bacterial cellulose samples are shown in **Figures 43-46**.

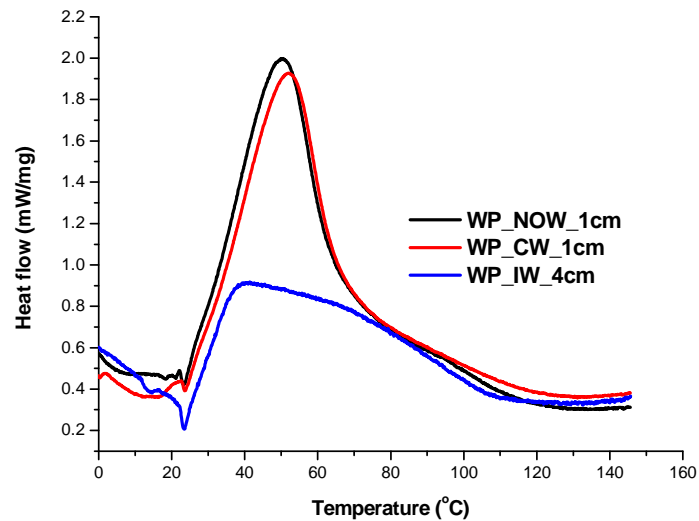


Figure 43: DSC thermograms of WP treated bacterial cellulose samples under different ultrasound operating conditions.

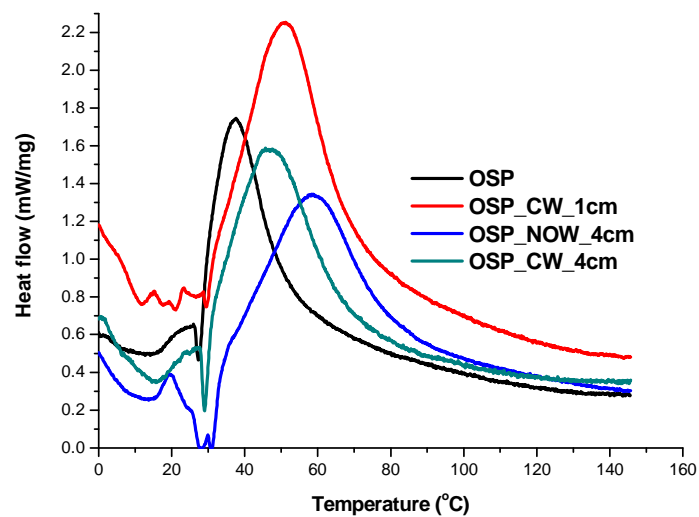


Figure 44: DSC thermograms of OSP treated bacterial cellulose samples under different ultrasound operating conditions.

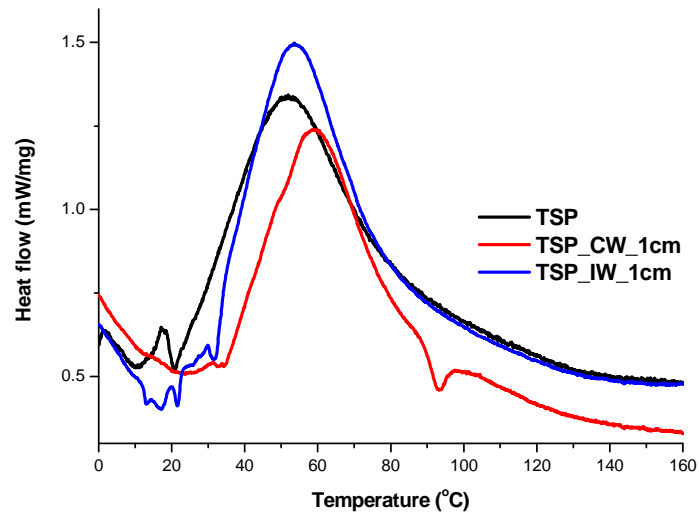


Figure 45: DSC thermograms of TSP treated bacterial cellulose samples under different ultrasound operating conditions.

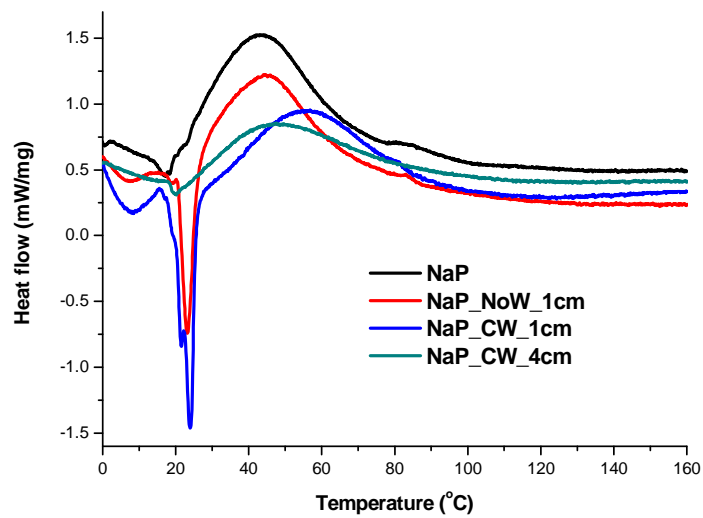


Figure 46: DSC thermograms of NaP treated bacterial cellulose samples under different ultrasound operating conditions.

The thermal behavior presented in all samples is related to monotropic solid to solid transition, which is exothermic and frequently observed in organic compounds, like cellulose. This phenomenon might be observed because of the low heating rate (2 K min^{-1}) and indicates the slow transition of amorphous to the stable crystalline phase and the rearrangement of amorphous regions. With heating rates above 5 K min^{-1} this transition is “overflowed” and is not visible or depicted as a slight exothermic shift. Differences in peak temperatures, are affiliated with mobility of amorphous cellulose, while higher peaks indicate thermodynamically more stable cellulose samples. The glass transition temperature (T_g) of highly crystalline macromolecules like cellulose is difficult to detect properly using this technique because of the broad heat flow curves for which step deviation from the base line is comparatively less.

3.3. Morphological

The formation steps and ribbon shaped microfibrils of bacterial cellulose was first describe by Mühlethaler in 1949. The fibrous network of bacterial cellulose is made of three dimensional well arranged nanofibres, resulting in formation of hydrogel sheet with high surface area and porosity (Esa et al. 2014).

Drying method is crucial to structure, performance and application of nata de coco films. Pa'e et al. (2014) investigated the effect of different methods on the crystallinity, swelling ability and tensile properties of nata de coco. SEM morphology analysis showed that the surface texture for oven drying, tray drying and freeze drying were found slightly different. Surface of oven dried bacterial cellulose films were constituted of numerous randomly oriented and overlapped fibrils, producing an aggregated web structure. According to the authors this result was in agreement with a previous study reported by Nadia et al. (2012).

The structure of redispersed, dried films of the four purification treatments, just before ultrasonication are shown in **Figure 47**. This type of network structure attributed to native bacterial cellulose is presented in all purified samples.

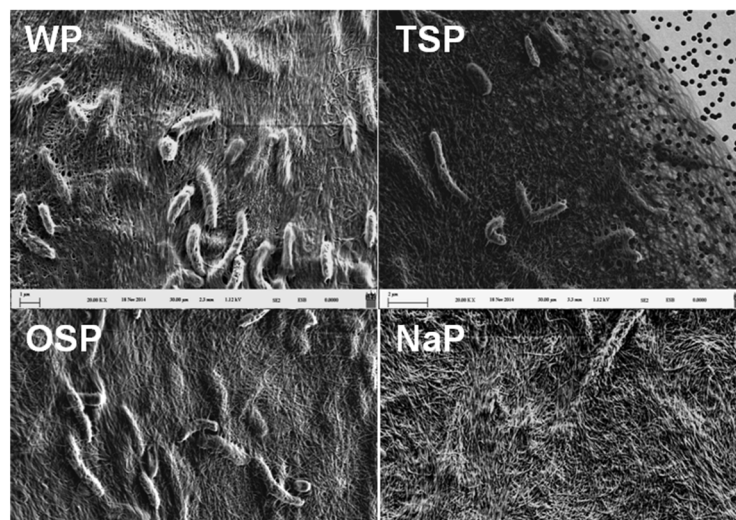


Figure 47: FE-SEM micrographs of WP, OSP, TSP and NaP purified bacterial cellulose samples.

Water purified samples are identical to native bacterial cellulose. Washing and soaking was only adequate to remove the syrups contained in the packaging. Bacterial cell debris and impurities were slightly removed after 2.5 m/m NaOH (OSP) immersed overnight treatment. The successively treatment with 2.5 m/m NaOCl (TSP) caused the removal of more impurities. Bacterial cellulose of 0.01 M NaOH at 70°C for 2 h, under continuous stirring (NaP), occurred the optimum results. On their surface were almost no bacterial skeletons and remained only cellulose fibrils.

However, alkali purifications treatments were suitable to remove bacterial impurities, but not appropriate to form suitable films for nanocellulose applications. In ultrasonicated bacterial cellulose samples, further size reduction was observed in the width of cellulose microfibrils. Even more, acoustic cavitation assisted the separation of aggregates fibrils, since after ultrasonication the size and the number of aggregation was decreased (**Figures 48-51**).

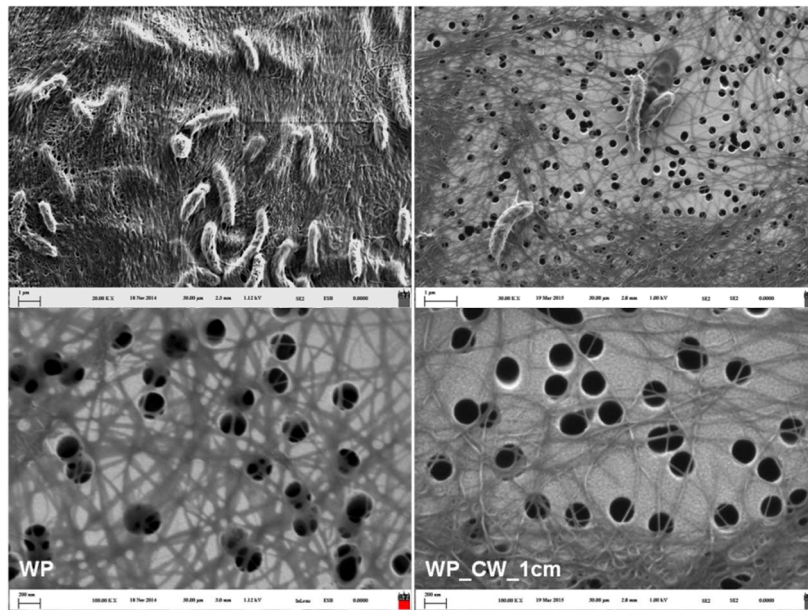


Figure 48: FE-SEM micrographs (1 μm and 200 nm) of WP and WP_CW_1cm bacterial cellulose samples.

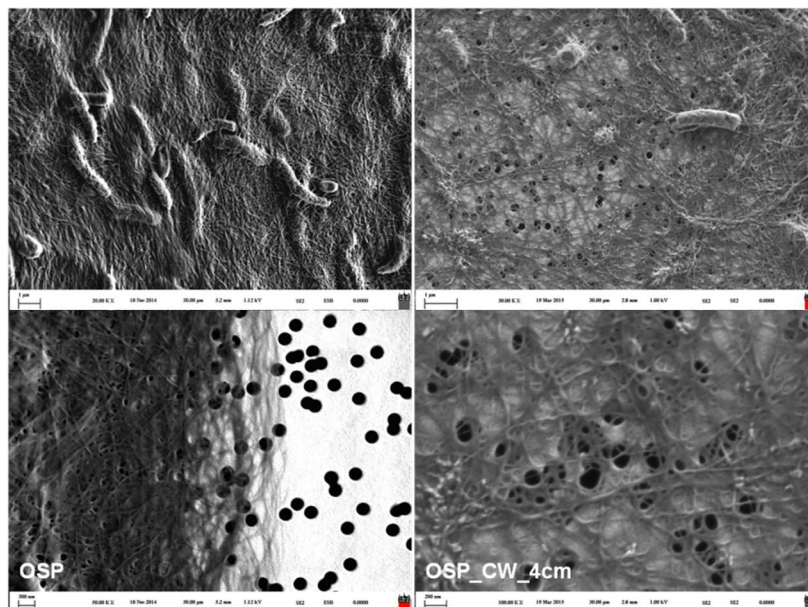


Figure 49: FE-SEM micrographs (1 μm and 200 nm) of OSP and OSP_CW_4cm bacterial cellulose samples.

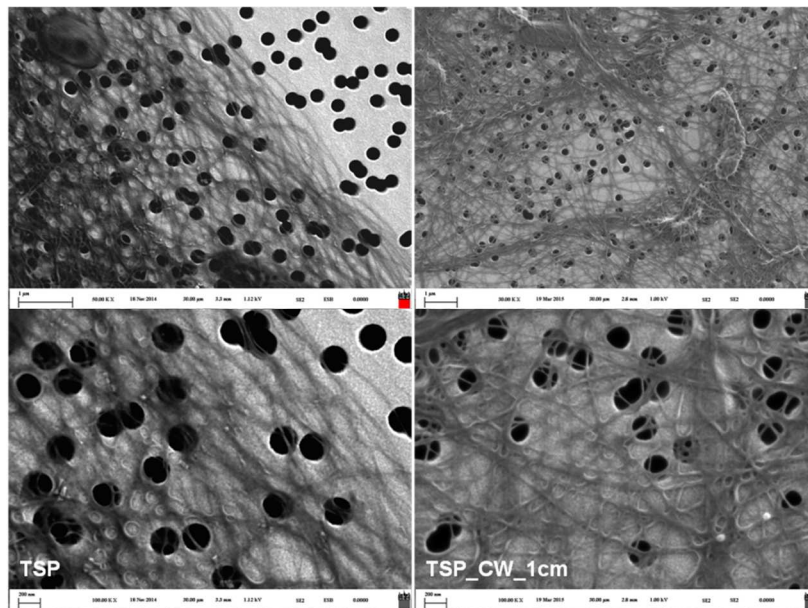


Figure 50: FE-SEM micrographs (1 μm and 200 nm) of TSP and TSP_CW_1cm bacterial cellulose samples.

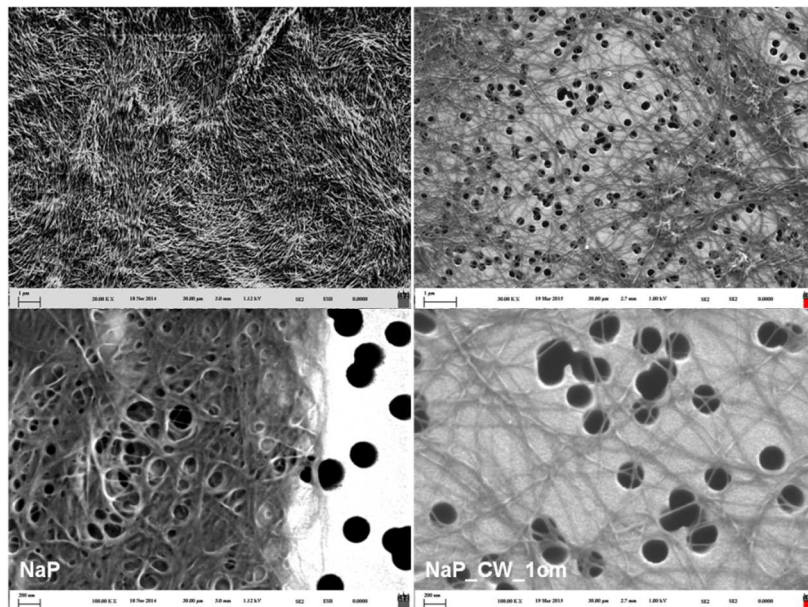


Figure 51: FE-SEM micrographs (1 μm and 200 nm) of NaP and NaP_CW_1cm bacterial cellulose samples.

The ultrafine microfibril network structure of bacterial cellulose of the different purification treatments prior and after ultrasonication by AFM imaging can be seen in **Figures 52 and 53**. The dense and aggregated structure of the randomly oriented distribution of the cellulose microfibrils on the surface of dried films is more evident by AFM microscopy.

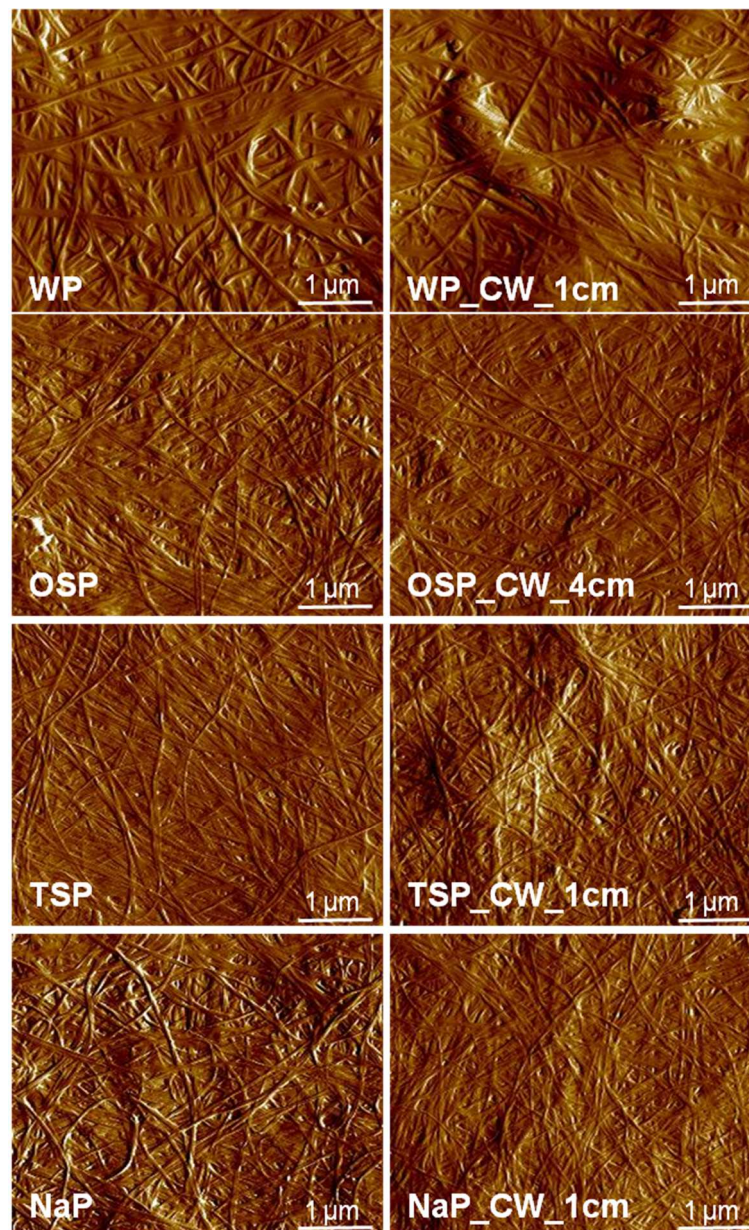


Figure 52: AFM images (5x5 μm) of the most favourable bacterial cellulose samples prior to (left) and after (right) ultrasonication.

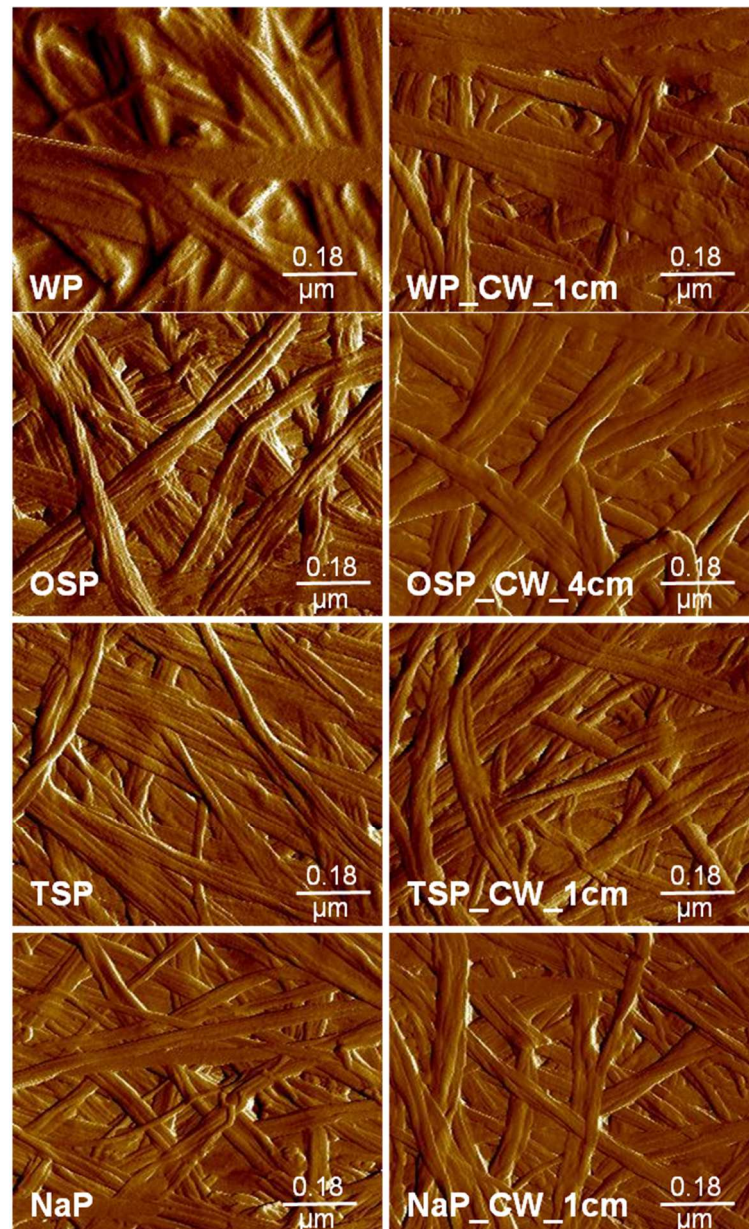


Figure 53: AFM images ($1 \times 1 \mu\text{m}$) of the most favourable bacterial cellulose samples prior to (left) and after (right) ultrasonication.

The surface changes in width of bacterial cellulose, were determined by Image J software. The mean width of the ribbons before ultrasonication, in the untreated bacterial cellulose was determined to be $39.95 (\pm 9.5)$ nm. In the 0.01 M NaOH treated $31.44 (\pm 9.2)$ nm, in one step purified $36.11 (\pm 7.6)$ nm and in two step purified $32.84 (\pm 10.8)$ nm. In 0.01

M NaOH and two step purified bacterial cellulose were apparently a reduction in the width. The estimated width of the measured microfibrils is in accordance with literature (Habibi et al. 2010).

Structural, thermal and morphological characterizations of ultrasound treated samples showed that ultrasound had no significant effect in the supramolecular level of bacterial cellulose. Yet, macroscopically tray dried films were significantly different after ultrasonication (**Figure 54**). Ultrasonic treatment changed the microfibrillar arrangement, leading to new films with a different nanostructure organization. Acoustic cavitation collaborated in the formation of thin self-sustaining dried films.



Figure 54: Bacterial cellulose WP, NaP and NaP_CW_1cm dried films.

4. Discussion

Structural (FT-IR and XRD), thermal (TGA and DSC) and morphological (FE-SEM, AFM) measurements justified that purification and ultrasound treatments resulted in a new purified and more crystalline bacterial cellulose films without significantly altering the native cellulose I polymorph of bacterial cellulose obtained from nata de coco. However, there were significant changes in the hydrogen bonding network that indicates changes in the physical properties of cellulose such as solubility, reactivity and crystallinity. Even more, there were observed small variations among the crystallite sizes of samples. Removal of bacterial cellulose impurities and ultrasonication resulted in the formation of a direct or closer contact between the cellulose fibrils and in the formation of strong intra- and inter-fibrillar hydrogen bonds.

Total crystallinity index (TCI), lateral order index (LOI) and hydrogen bond intensity (HBI) were significantly altered after purification and ultrasound treatments. Initially, it was considered as the most favourable processes to produce bacterial cellulose films with higher crystallinity order and improved properties, the treatments which resulted in the following order combinations: lower LOI, higher TCI and lower HBI values. Based on this combination the following samples should be considered as the best process of each purification treatment: a) WP_CW_1cm, b) OSP_CW_4cm, c) TSP_IW_1cm and d) NaP_NoW_1cm.

However, since there were no significant changes in the crystallinity index of cold treated samples, we would prefer to avoid the two extreme conditions (NoW and IW) and use milder conditions, i.e. cold bath as preferred temperature in all ultrasonication treatments.

The mean values of energy hydrogen bond was calculated to be 21.51 (± 1.5) kJ/g mol. This interfibrillar hydrogen bonding energy is necessary to be overcome in order to achieve the separation of microfibrils into individual fibrils.

Effect of purification treatments

Results showed that alkali treatment played an important role in removing most of the non-cellulosic materials, bacterial cell and other impurities to obtaining pure cellulose. The most effective purification treatment was the one using 0.01 M NaOH. In one step and two step purification treatments bacterial debris were still predominant in cellulose network. This observation can be explained for several reasons. Boiling in sodium hydroxide solution is a common method for sterilization and has been used in a number of studies to treat bacterial cellulose prior to mechanical testing. Warm conditions allow better alkali penetration into the fibers than the ambient temperatures. Additionally, it is well known that proteins and nucleic acids can be hydrolyzed with alkaline solutions at warm temperatures.

Alkaline treatments can cause cellulose to swell and even can dissolve cellulose above 8-10% (m/v) concentrations. Further, cellulose due to its nature is hydrophilic and swells in the presence of water. In our research, it is assumed that the used purification treatments caused a homogeneous, weak to very low swelling on bacterial cellulose samples. This type of swelling could result in an inter-crystalline swelling and the formation of new interactions between water and cellulose molecules or sodium hydroxide and cellulose, respectively. Sodium hydroxide aqueous solutions cellulose formed a Na⁺/water and cellulose system, which chemically forms stable hydrogen bonded network structures. Because of this interaction between cellulose and Na⁺ alkali treatment one step and two step purification it seems had a decrystallising effect on cellulose and resulted in reduced crystallinity. However, those changes preserved the native structure of cellulose I, while simultaneously facilitated isolation of microfibrils during ultrasound. In contrast, the degree of crystallinity using 0.01 M NaOH purification at 70 °C for 2 h was increased. This could be explained, by partial decomposition of amorphous regions.

Effect of ultrasonication

Our results suggests that ultrasonication could be very useful for isolating cellulose microfibrils and fabricating homogeneous nanocellulose films. High intensity ultrasound when was treated with purified bacterial cellulose solutions had a significant impact on morphology of bacterial cellulose nanofibrils and supramolecular properties of cellulose. Nevertheless, ultrasonication did not modified the native crystalline structure of bacterial cellulose. Ultrasound was transferred through shear forces due to cavitation to the glucan chains, enhancing the decomposition of amorphous domains in cellulose. However, longer treatment time could result in cellulose degradation.

Cellulose and ultrasound, from their individual perspectives, seems to be simple, but are quite complex. Ultrasound is influenced by many operating parameters and even slight changes could attribute to significant variations in ultrasound efficiency. Our results indicate that ultrasonication is a very powerful technique for isolating cellulose fibrils from a dense, highly anisotropic structure, without damaging it.

Some parameters, such as geometry of ultrasonic horn, operating frequency and intensity of irradiation or ultrasound energy distribution are not easy to change or to control. On the contrary, the other parameters could be investigated in order to obtain the optimum ultrasound operating conditions.

For this research, a frequency of 20 kHz was considered as the optimum ultrasound frequency. The intensity of ultrasound is proportional to the amplitude of vibration (Santos et al. 2009) and it was kept constant. Furthermore, 20 kHz was found to be effective for extraction of plant contents (Shirsath et al. 2012). Water is the most favourable solvent due to its low cost and it also displays good cavitation effect under ultrasound irradiation. To avoid stability problems, it was decided to use cylindrically shaped containers instead of conically shapes ones where ultrasound energy distribution is better.

It was found that as the exposure time to cavitation increased, crystallinity of the cellulose decreased and faster degradation was observed (Pinjari & Pandit 2010). Moreover, ultrasonic power influences the number of cavitation bubbles formed, their lifetime and the generated cavitation intensity. In this study the operating time and power were 30 min and around 25 W/cm² respectively. Considering the reaction for a cavitation process, bulk

operating conditions such as distance of ultrasonic probe and temperature are crucial factors, which often interact with each other.

Acoustic cavitation phenomenon due to ultrasound leads to an increase of solvent temperature. High temperatures are preferable to disrupt strong interaction forces such as Van der Waals, hydrogen bonds and dipole attraction between the solute molecules and solute-matrix. In contrast, cavitation is performed better at lower temperatures, in which the ultrasonic power is constant (Santos et al. 2009).

Water bath treatments influenced the starting temperature which also affected ultrasound. In the absence of a water bath, colloids obtained rapidly high temperatures into the colloid biphasic system. In the case of an ice water bath, bacterial cellulose samples had the lowest starting temperature. Although the cavitation was more efficient, duration of 30 min was not enough to increase mass transfer in order to disrupt the strong hydrogen bonds existent in cellulose molecules. Taking into account these parameters, bacterial cellulose performed higher crystallinity in mild conditions, such as in a cold water bath.

Ultrasound intensity and the pressure field are not uniformly distributed in the reactor (Klíma et al. 2007). Ultrasonic intensity rapidly decreases mostly axially, but also radially from the ultrasonic probe. Minimizing dead zone areas below ultrasonic probe and the wall of the container, a maximum contact angle between the sample and the cavitation zones was achieved at 1 cm distance. Based on the experimental results, 1 cm distance attended better results compared to 4 cm distance from the bottom of the reactor container. It was observed that ultrasound irradiation generated a local turbulence and liquid micro-circulation in that biphasic system at 1 cm distance of horn tip to bottom, which helped in the liberation of the fibrils as well.

Ultrasonication treatment in biphasic systems produced a colloidal solution and amplified the reduction of aggregates, due to drying and simultaneously improved the separation of microfibrils. This deaggregation phenomena was confirmed by the AFM and FE-SEM images.

Main conclusions of this research work

The main conclusions of this doctoral work can be summarized as follows:

1. The most favourable settings of ultrasonic treatment and NaOH concentration found to be mild enough to preserve the initial crystalline structure (cellulose I) of bacterial cellulose, but simultaneously suitable to remove bacterial cellulose contaminations, achieve high purity, increase the crystallinity, facilitate separation of bacterial cellulose nanofibrils and thus enabling the film formation.
2. It can be stated, from FE-SEM and AFM images that the mild alkaline pretreated bacterial cellulose increased the swelling of amorphous regions compare to the control sample and enhanced the penetration of ultrasound mass transfer forces to bacterial cellulose samples.
3. It can be reported that compare to the control bacterial cellulose, the pretreated and sonicated samples showed variations in the total crystallinity index, lateral order index and hydrogen bond intensity values, which indicates changes in the physical properties and hydrophilic nature of bacterial cellulose films.
4. The selection of the most favourable parameters of ultrasound-treated bacterial cellulose thin film formation were based on the following measured criteria: low lateral order index > high total crystallinity index > low hydrogen bond intensity.
5. It can be stated that ultrasonication increased the overall crystallinity of the bacterial cellulose samples during the treatments based on the XRD analysis, which is a requirement for energy harvesting applications of cellulose based thin films.
6. It has been shown that d-spacing values (the planar distances of crystallites) did not change during the ultrasonication, but crystallite sizes of cellulose I α and I β allomorphs existing in bacterial cellulose were altered.
7. It has been found that thermal onset temperature of degradation was increased when proteinoous bacterial bodies were removed during the purification treatments and the thermal decomposition of cellulose occurred at higher temperatures. The DSC measurement proved that part of amorphous cellulose regions were rearranged to crystalline ordered regions around 50°C.

Acknowledgements

This study was carried out in the Institute of Wood Based Products, Simonyi Karoly Faculty of Engineering, Wood Sciences and Applied Arts at University of West Hungary during 2012-2015. The work was performed as partial fulfillment of the requirements for the degree of doctor of philosophy. All the funding was offered through the Balassi Institute and the Hungarian Scholarship Board Office.

I am grateful to my supervisor associate professor Dr. Csóka Levente for his guidance and insights throughout the research and the ability to know and work with such a wonderful material like bacterial cellulose. I would also like to thank Ms. Dr. Vincze Kristina and the rest members of the Hungarian Scholarship Board, for giving me the opportunity to study and live in Hungary, with their financial support all these years. Further, I would like to thank all the professors I have been privileged to cooperate with or to take courses throughout my Ph.D. studies. It is difficult to think of a word strong enough to describe the gratitude I feel for them.

I would like to express my deepest appreciation to Professors Rastislav Lagaňa, Molnár Gábor, Ida Poljanšek and Primož Oven for their assistance and contribution to the characterization measurements of bacterial cellulose samples.

My sincerely thanks go to my family and friends for their support during my life. Finally, I would like to dedicate this work to my grandparents Nikolaos and Angeliki Kontogianni.

List of my selected publications

1. Dimitrios Tsalagkas, Rastislav Lagaňa, Ida Poljanšek, Primož Oven, Levente Csoka. Morphological, structural and thermal properties of ultrasound-assisted bacterial cellulose films formation. (submitted).
2. Koutsianitis Dimitrios, Mitani Constantina, Giagli Kyriaki, Tsalagkas Dimitrios, Halász Katalin, Kolonics Ottó, Gallis Christos, Csóka Levente. (2015). Properties of ultrasound extracted bicomponent lignocellulose thin films. *Ultrasonics Sonochemistry*, 23, 148-155, doi:10.1016/j.ultsonch.2014.10.014.
3. Németh R., Tsalagkas D., Bak M. (2015). Effect of soil contact on the modulus of elasticity of beeswax-impregnated wood. *Bioresources*, 10 (1), 1574-1586.
4. Dimitrios Tsalagkas, Rastislav Lagaňa, Levente Csóka. (2014). Morphological and structural changes of ultrasound treated bacterial cellulose. Proceedings of the 57th International Convention of Society of Wood of Science and Technology. 23-27 June 2014, Technical University in Zvolen, Slovakia, Part 1, 161-169.
5. Divos, F., Tsalagkas, D & Koutsianitis D. 2013. Wood density determination of trees by microwave impulse radar. Proceedings of the 18th International Symposium on Nondestructive testing and evaluation of wood, 24-27 September 2013, Madison Wi, USA, 143-149.
6. D. Tsalagkas, G. Grozdits, O. J. Rojas, L. Csoka. (2013). ZnO-Bacterial cellulose nanocrystal composite and its potential as energy harvesting material. Proceedings of TAPPI International Conference on Nanotechnology for Renewable Materials, Stockholm, Sweden, 25-27 June 2013, ISBN: 978-1-59510-225-6.
7. Tsalagkas, D. & Csóka L. (2013). BCNs films and its potential as energy harvesting material. Proceedings of the International Scientific Conference for PhD Students “Science for Sustainability”, 19-20 March 2013, Győr, Hungary, 81-86.

8. Tsalagkas, D. & Vasileiou, V. (2010). Effects of curing time on bending strength of the finger joined Black pine and Macedonian fir lumber. Proceedings of the First Serbian Forestry Congress “Future with Forests”, Belgrade, Serbia, 11-13 November, 2010, 1375-1383.
9. Miklos, H., Divos, F., Tsalagkas, D. (2009). Comparison between different dynamic shear modulus determination techniques on *Robinia Pseudoacacia* specimens. Proceedings of the 16th International Symposium on Nondestructive testing and evaluation of wood, 12-14 October 2009, Beijing, China, 308.

5. References

Abdul Khalil, HPS., Davoudpour, Y., Nazrul Islam, Md., Mustapha, A., Sudesh, K., Dungani, R. & Jawaid, M. (2014). Production and modification of nanofibrillated cellulose using various mechanical processes: A review. *Carbohydrate Polymers*, 99, 649-665, doi:10.01016/j.carbpol.2013.08.069.

Amin, MCIM., Abadi, AG. & Katas, H. (2014). Purification, characterization and comparative studies of spray-dried bacterial cellulose microparticles. *Carbohydrate Polymers*, 99, 180-189, doi: 10.01016/j.carbpol.2013.08.041.

Baptista, A., Ferreira, I & Borges, J. (2013). Chapter 4. Cellulose-based bioelectronic devices. *Cellulose-Medical, Pharmaceutical and Electronic Applications*, InTech, 67-82, doi: 10.5772/56721

Ballato, A. (1996). Piezoelectricity: history and new thrusts. *Ultrasonics Symposium, Proceedings, IEEE (Volume 1)*, 575-583, doi:10.0109/ULTSYM.1996.584046.

Bielecki, SE., Krystynowicz, AE., Turkiewicz, M. & Kalinowska HE. (2005). Bacterial cellulose. *Biopolymers Online*. 5. Polysaccharides from Prokaryotes, Wiley Online Library, doi: 10.01002/3527600035.bpol5003.

Blaker, JJ., Lee, K-Y., Mantalaris, A. & Bismarck, A. (2010). Ice-microsphere templating to produce highly porous nanocomposite PLA matrix scaffolds with pores selectively lined by bacterial cellulose nano-whiskers. *Composites Science and Technology*, 70 (13), 1879-1888, doi:10.01016/j.compscitech.2010.05.028.

Castro. C., Zuluaga, R., Álvarez, C., Putaux, J., Caro, G., Rojas, OJ., Mondragon, I. & Gañán, P. (2012). Bacterial cellulose produced by a new acid-resistant strain of *Gluconacetobacter* genus. *Carbohydrate Polymers*, 89, 4, 1033-1037, doi:10.01016/j.carbpol.2012.03.045.

Carrillo, F., Colom, X., Sunol, J. J. & Saurina, J. (2004). Structural FTIR analysis and thermal characterization of lyocell and viscose-type fibres. *European Polymer Journal*, 40, 2229-2234, doi:10.01016/j.eurpolymj.2004.05.003.

Chawla, PR., Bajai, IB., Survase, SA. & Singhal, RS. (2009). Microbial cellulose: Fermentative production and applications. *Food Technology and Biotechnology*, 47 (2), 107-124.

Cheng, KC., Catchmark, J.M. & Demirci, A. (2009). Enhanced production of bacterial cellulose by using a biofilm reactor and its material property analysis. *Journal of Biological Engineering*, 3 (12), doi:10.01186/1754-1611-3-12.

Ciolacu, D. Ciolacu, F. & Popa, I. V. (2011). Amorphous cellulose-structure and characterization. *Cellulose Chem. Technol.*, 45 (1-2), 13-21.

Colom, X. & Carrillo, F. (2002). Crystallinity changes in lyocell and viscose-type fibres by caustic treatment. *European Polymer Journal*, 38, 2225-2230, doi:10.01016/S0014-3057(02)00132-5.

Colom, X., Carrillo, F., Nogués, F. & Garriga, P. (2003). Structural analysis of photodegraded wood by means of FTIR spectroscopy. *Polymer degradation and stability*, 80, 543-549, doi:10.01016/S0141-3910(03)00051-X.

Csoka, L., Hoeger, IC., Rojas, OJ., Peszlen, I., Pawlak, JJ. & Peralta, PN. (2012). Piezoelectric effect of cellulose nanocrystals thin films. *ACS Macro Lett.*, 1 (7), 867-870, doi: 10.01021/mz300234a.

Czaja, KW., Young, JD., Kaweski, MR. & Malcom Brown Jr R. (2007). The future prospects of microbial cellulose in biomedical applications. *Biomacromolecules*, 8 (1), 1-12, doi: 10.01021/bm060620d.

Czaja, W., Krystynowicz, A., Bielecki S. & Malcom Brown Jr, R. (2006). Microbial cellulose - the natural power to heal wounds. *Biomaterials*, 27, 145-151, doi:10.01016/j.biomaterials.2005.07.035.

Czaja, KW., Romanovicz, D. & Malcom Brown, Jr R. (2004). Structural investigations of microbial cellulose produced in stationary and agitated culture. *Cellulose*, 11 (3-4), 403-411, doi: 10.01023/B:CELL.0000046412.11983.61.

El-Saied, H., El-Diwany, A.I., Basta, A.H., Atwa, N.A & El-Ghwas, D.E. (2008). Production and characterization of economical bacterial cellulose. *BioResources*, 3 (4), 1196-1217.

Esa, F., Tasirin, SM., Abd Rahman, N. (2014). Overview of bacterial cellulose production and application. *Agriculture and Agricultural Science Procedia*, 2, 113-119, doi:10.01016/j.aaspro.2014.11.017.

Fan, M., Dai, D. & Huang, B. (2012). Chapter 3. Fourier transform infrared spectroscopy for natural fibres. *Fourier Transform-Materials Analysis, InTech*, 45-68, doi: 10.5772/35482.

Frone, AN., Panaitescu, DM. & Donescu, D. (2011). Some aspects concerning the isolation of cellulose micro- and nano-fibers. *U.P.B. Sci. Bull., Series B.*, 73 (2), 133-152.

Fu, L., Zhang, Y. & Yang, G. (2013). Present status and applications of bacterial cellulose-based materials for skin tissue repair. *Carbohydrate Polymers*, 92 (2), 1432-1442, doi: 10.01016/j.carbpol.2012.10.071.

Fu, L., Zhang, Y., Zhang, J. & Yang, G. (2011). Chapter 13. Bacterial cellulose for skin repair materials, *Biomedical Engineering-Frontiers and Challenges, InTech*, 249-274, doi:10.5772/24323.

- Fukada, E. (1995). Piezoelectricity of biopolymers. *Biorheology*, 32 (6), 593-609.
- Fukada, E. (1968). Piezoelectricity as a fundamental property of wood. *Wood Science and Technology*, 2 (4), 299-307, doi: 10.01007/BF00350276.
- Habibi, Y. Lucia. LA., Rojas, OJ. (2010). Cellulose nanocrystals: Chemistry, self assembly and applications. *Chemical Reviews*, 110 (6), 3479-3500, doi: 10.1021/cr900339w.
- Hirai, N., Sobue, N. & Date, M. (2011). New piezoelectric moduli of wood: d_{31} and d_{32} . *Journal of Wood Science*, 57 (1),1-6, doi: 10.01007/s10086-010-1133-2.
- Hirai, A., Inui, O., Horii, F. & Tsuji, M. (2009). Phase separation behavior in aqueous suspensions of bacterial cellulose nanocrystals prepared by sulfuric acid treatment. *Langmuir*, 25 (1), 497-502, doi: 10.01021/la802947m.
- Hosakun, Y., Wongkasemjit, S. & Chaisuwan, T. (2013). Preparation of bacterial cellulose membranes from nata de coco for CO₂/CH₄ separation. *World Academy of Science, Engineering and Technology, International Science Index, Chemical and Molecular Engineering*, 1 (2), 77.
- Huang. C. (2008). Flexoelectric nanobiopolymers (FEPs) exhibiting higher mechanical strength (7.5 GPa), modulus (250 GPa) and energy transfer efficiency (75%). *WW-EAP Newsletter*, 10 (2), 5-7.
- Gatenholm, P. & Klemm, D. (2010). Bacterial nanocellulose as a renewable material for biomedical applications. *MRS Bulletin*, 35 (03), 208-213, doi: <http://dx.doi.org/10.01557/mrs2010.653>.

Gea, S., Reynolds, C.T., Roohpour, N., Wirjosentono, B., Soykeabkaew, N., Bilotti, E. & Peijs, T. (2011). Investigation into the structural, morphological, mechanical and thermal behavior of bacterial cellulose after a two-step purification process. *Bioresource Technology*, 102 (19), 9105-9110, doi: 10.01016/j.biortech.2011.04.077.

Gelin, K., Bodin, A., Gatenholm, P., Mihranyan, A., Edwards, K. & Strømme, M. (2007). Characterization of water in bacterial cellulose using dielectric spectroscopy and electron microscopy. *Polymer*, 48 (26), 7623-7631, doi:10.01016/j.polymer.2007.10.039.

George, J., Ramana, K.V., Bawa, A.S. & Siddaramaiah. (2011). Bacterial cellulose nanocrystals exhibiting high thermal stability and their polymer nanocomposite. *International Journal of Biological Macromolecules*, 48 (1), 50-57, doi:10.01016/j.ijbiomac.2010.09.013.

Gupta, P.K., Uniyal, V. & Naithani, S. (2013). Polymorphic transformation of cellulose I to cellulose II by alkali pretreatment and urea as an additive. *Carbohydrate Polymers*, 94 (2), 843-849, doi: 10.01016/j.carbpol.2013.02.012.

Habibi, Y., Lucia, L.A. & Rojas, O.J. 2010. Cellulose nanocrystals: chemistry, self-assembly and applications. *Chem. Rev.*, 110 (6), doi: 10.01021/cr900339w.

Halib, N., Amin, M.C.I.M. & Ahmad, I. 2012. Physicochemical properties and characterization of nata de coco from local food industries as a source of cellulose. *Sains Malaysiana*, 41 (2), 205-211.

Higgins, H.G., Goldsmith, V., McKenzie, A.W. (1958). The reactivity of cellulose. 3. Acid hydrolysis of eucalypt alpha-cellulose in the intermediate molecular weight range. *J. Polym. Sci.*, 32 (124), 57-74, doi: 10.01002/pol.1958.1203212405.

Janardhnan, S. & Sain, M.M. (2006). Isolation of cellulose microfibrils- an enzymatic approach. *Bioresources*, 1 (2), 176-188.

Jiao, C. & Xiong, J. (2014). Accessibility and morphology of cellulose fibres treated with sodium hydroxide. *Bioresources*, 9 (4), 6504-6513.

Khajavi, R., Esfahani JE. & Sattari M. (2011). Crystalline structure of microbial cellulose compared with native and regenerated cellulose. *International Journal of Polymeric materials*, 60, (14), 1178-1192, doi: 10.01080/00914037.2010551372.

Klíma, J., Frias-Ferrer, A., González-García, J., Ludvík, J., Sáez, J. & Iniesta, J. (2007). Optimization of 20 kHz sonoreactor geometry on the basis of numerical simulation of local ultrasonic intensity and qualitative comparison with experimental results. *Ultrasonics Sonochemistry*, 14 (1), 19-28, doi:10.1016/j.ultsonch.2006.01.001.

Kondo, T. & Sawatari, C. (1996). A fourier transform infra-red spectroscopic analysis of the character of hydrogen bonds in amorphous cellulose. *Polymer*, 31 (3), 393-399, doi:10.01016/0032-3861(96)82908-9.

Kondo, T. (2004). Chapter 3. Hydrogen bonds in cellulose and cellulose derivatives. *Polysaccharides: Structural diversity and functional versatility*. 1st edition, Marcel Dekker, Inc., 69-98.

Legnani, C., Vilani, C. Calil, VL., Barud, HS., Quirino, WG., Achete, CA., Ribeiro, SJL. & Cremona, M. (2008). *Thin Solid Films*, 517, 1016-1020, doi:10.01016/j.tsf.2008.06.011.

Lin, SP., Calvar, IL., Catchmark, JM., Liu, J., Demirci, A. & Cheng, K. (2013). Biosynthesis, production and applications of bacterial cellulose. *Cellulose*, 20 (5), 2191-2219, 10.01007/s10570-013-9994-3.

Liu, R., Yu, H. & Huang, Y. (2005). Structure and morphology of cellulose in wheat straw. *Cellulose*, 12 (1), 25-34, doi: 10.01007/s10570-004-0955-8.

Löning, J., Horst, C. & Hoffmann, U. (2002). Investigations on the energy conversion in sonochemical processes. *Ultrasonics Sonochemistry*, 9 (3), 169-179, doi:10.01016/S1350-4177(01)00113-4.

McKenna, BA., Mikkelsen, D., Wehr, JB., Gidley, MJ. & Menzies, NW. (2009). Mechanical and structural properties of native and alkali-treated bacterial cellulose produced by *Gluconacetobacter xylinus* strain ATCC 53524. *Cellulose*, 16, 1047-1055, doi:10.01007/s10570-009-9340-y.

Mohite, BV. & Patil, SV. (2014). Physical, structural, mechanical and thermal characterization of bacterial cellulose by *G. hansenii* NCIM 2529. *Carbohydrate Polymers*, 106, 132-141, doi:10.01016/j.carbpol.2014.02.012.

Moosavi-Nasab, M. & Yousefi, A.R. (2010). Investigation of physicochemical properties of the bacterial cellulose produced by *Gluconacetobacter xylinus* from date syrup. *World Academy of Science, Engineering and Technology*, 44, 1258-1263, doi=10.01.1.294.4291.

Mühlethaler, K. (1949). The structure of bacterial cellulose. *Biochimica et biophysica acta*, 3, 527-535, doi:10.01016/0006-3002(49)90126-2.

Nelson, M. L. & O'Conor R. T. (1964a). Relation of certain infrared bands to cellulose crystallinity and crystal lattice type. Part I. spectra of lattice types I, II, III and amorphous cellulose. *J. Appl. Polym. Sci.*, 8 (3), 1311-1323, doi: 10.01002/app.1964.070080322.

Nelson, M. L. & O'Conor R. T. (1964b). Relation of certain infrared bands to cellulose crystallinity and crystal lattice type. Part II. a new infrared ratio for estimation of crystallinity in celluloses I and II. *J. Appl. Polym. Sci.*, 8 (3), 1325-1341, doi: 10.01002/app.1964.070080322.

Nishiyama, Y., Sugiyama, J., Chanzy, H. & Langan, P. (2003). Crystal structure and hydrogen bonding system in cellulose I_α from synchrotron X-ray and neutron fiber diffraction. *J. Am. Chem. Soc.*, 125 (47), 14300-14306, doi: 10.1021/ja037055w.

Nishiyama, Y., Langan, P. & Chanzy, H. (2002). Crystal structure and hydrogen bonding system in cellulose I_β from synchrotron X-ray and neutron fiber diffraction. *J. Am. Chem. Soc.*, 124 (31), 9074-9082, doi: 10.1021/ja0257319.

O'Connor, RT., DuPré, EF. & Mitcham, D. (1958). Applications of infrared absorption spectroscopy to investigations of cotton and modified cottons. Part I: physical and crystalline modifications and oxidation. *Textile Research Journal*, 28 (5), 382-392, doi: 10.01177/004051755802800503.

Oh, SY., Yoo, DI., Shin, Y., Kim, HW., Kim, HY., Chung, YS., Park, WH. & Youk, JH. (2005). Crystalline structure analysis of cellulose treated with sodium hydroxide and carbon dioxide by means of X-ray diffraction and FTIR spectroscopy. *Carbohydrate research*, 340 (15), 2376-2391, doi:10.01016/j.carres.2005.08.007.

Pa'e, N., Hamid, NIA., Khairuddin, N., Zahan, KA., Seng, KF., Siddique, BM & Muhamad, I. (2014). Effect of different drying methods on the morphology, crystallinity, swelling ability and tensile properties of nata de coco. *Sains Malaysiana*, 43 (5), 767-773.

Park, S., Baker, JO., Himmel, ME., Parilla, PA. & Johnson, DK. (2010). Cellulose crystallinity index: measurement techniques and their impact on interpreting cellulase performance. *Biotechnology for Biofuels*, 3 (10), doi:10.01186/1754-6834-3-10.

Pecoraro, É., Manzani, D., Messaddeq., Y & Ribeiro, SJL. (2007). Chapter 17-Bacterial cellulose from *Gluconacetobacter xylinus*: Preparation, Properties and Applications. *Monomers, Polymers and Composites from Renewable Resources*, Elsevier, 369-383.

Petersen, N. & Gatenholm, P. (2011). Bacterial cellulose-based materials and medical devices: current state and perspectives. *Appl. Microbiol. Biotechnol.*, 91 (5), 1277-1286, doi: 10.01007/s00253-011-3432-y.

Phisalaphong, M. & Chiaoprakobkij N. (2012). 7. Applications and Products-Nata de Coco. Bacterial Nanocellulose. A sophisticated multifunctional material. CRC Press (Taylor & Francis Group), 143-157, ISBN: 978-1-4398-6992-5.

Pineda, LDC., Mesa, LAC. & Habert, AC. (2010). Effect of culture and purification conditions on physicochemical and transports properties in bacterial cellulose membranes. www.aidic.it/ibic2010/webpapers/71CarrenoPineda.pdf

Pinjari, DV. & Pandit, AB. (2010). Cavitation milling of natural cellulose to nanofibrils. *Ultrasonics Sonochemistry*, 17 (5), 845-852, doi: 10.1016/j.ultsonch.2010.03.005.

Pimentel, GC. & Sederholm CH. (1956). Correlation and stretching frequencies and hydrogen bond distances in crystals. *J. Chem. Phys.*, 24, 639-641, <http://dx.doi.org/10.01063/1.1742588>.

Plackner J. 2009. The converse piezoelectric effect in wood and cellulose materials. Master Thesis, Institute of Wood Science and Technology, Department of Materials Sciences and Process Engineering, University of Natural Resources and Applied Life Sciences, BOKU-Vienna.

Popescu, CM., Singurel, G., Popescu, MC., Vasile, C., Argyropoulos, S. D. & Willför, S. (2009). Vibrational spectroscopy and X-ray diffraction methods to establish the differences between hardwood and softwood. *Carbohydrate Polymers*, 77 (4), 851-857, doi:10.01016/j.carbpol.2009.03.011.

Raso, J., Mañas, P. Pagán, R. & Sala, FJ. 1999. Influence of different factors on the output power transferred into medium by ultrasound. *Ultrasonics Sonochemistry*, 5 (4), 157-162, doi:10.01016/S1350-4177(98)00042-X.

Santos, H.M., Lodeiro, C. & Capelo-Martinez, J-L. (2009). The power of ultrasound. *Ultrasound in Chemistry: Analytical Applications*, Wiley-VCH Verlag GmbH & Co, 1-16.

Sarkono, Moeljopawiro, S., Setiaji, B. & Sembiring, L. (2014). Physico-chemical properties of bacterial cellulose produced by newly strain *Gluconacetobacter xylinus* ANG-29 in static and shaking fermentations. *Biosci. Biotech. Res. Asia*, 11 (3), 1259-1265, doi:http://dx.doi.org/10.013005/bbra/1514.

Segal, L., Creely, J.J., Martin Jr, A. E. & Conrad, C. M. (1959). An empirical method for estimating the degree of crystallinity of native cellulose using the X-ray diffractometer. *Text. Res. J.*, 29 (10), 786-794, doi: 10.01177/004051755902901003.

Shah, J. & Brown, RM Jr. (2005). Towards electronic paper displays made from microbial cellulose. *Appl. Micorbiol Biotechnol.*, 66, 352-355, doi:10.01007/s00253-004-1756-6.

Shirsath, S.R., Sonawane, S.H. & Gogate, P.R. (2012). Intensification of extraction of natural products using ultrasonic irradiations- A review of current status. *Chemical Engineering and Processing*, 53, 10-23, doi: 10.1016/j.cep.2012.01.003

Sheykhnazari, S., Tabarsa, T., Ashori, A., Shakeri, A. & Golalipour, M. (2011). Bacterial synthesized cellulose nanofibers; Effects of growth times and culture mediums on the structural characteristics. *Carbohydrate Polymers*, 86 (3), 1187-1191, doi:10.01016/j.carbpol.2011.06.011.

Široký, J., Blackburn, S. R., Bechtold, T., Taylor, J. & White, P. (2010). Attenuated total reflectance Fourier-transform Infrared spectroscopy analysis of crystallinity changes in

lyocell following continuous treatment with sodium hydroxide. *Cellulose*, 17 (1), 103-115, doi:10.01007/s10570-009-9378-x.

Stephens, R. (1972). Piezoelectricity and the growth of ultrasonics. *Journal de Physique Colloques*, 33 (C6), 4-9, doi:10.01051/jphyscol:1972602.

Struszczyk, H. (1986). Modification of lignins. III. Reaction of lignosulfonates with chlorophosphazanes. *Journal of Macromolecular Science A*, 23 (8), 973-992, doi:10.01080/00222338608081105.

Terinte, N., Ibbett, R. & Schuster, C. K. (2011). Overview on native cellulose and microcrystalline cellulose I structure studied by X-ray diffraction (WAXD): Comparison between measurement techniques. *Lenzinger Berichte*, 89, 118-131.

Thygesen, A. Oddershede, J., Lilholt, H. (2005). On the determination of crystallinity and cellulose content in plant fibres. *Cellulose*, 12 (6), 563-576, doi: 10.01007/s10570-005-9001-8.

Tischer, PCSF., Sierakowski, MR., Westfahl Jr., H. & Tischer, CA. (2010). Nanostructural reorganization of bacterial cellulose by ultrasonic treatments. *Biomacromolecules*, 11 (5), 1217-1224, doi: 10.01021/bm901383a.

Tsalagkas, D., Grozdits, G., Rojas, OJ., Csoka, L. (2013). ZnO-Bacterial cellulose nanocrystal composite and its potential as energy harvesting material. *Tappi Intern. Nanoconference, Nanotechnology for Renewable Materials*, Stockholm, Sweden.

Ummartyotin, S. Juntaro, J., Sain, M. & Manuspiya, H. (2012). Development of transparent bacterial cellulose nanocomposite film as substrate for flexible organic light emitting diode (OLED) display. *Industrial Crops and Products*, 35, 92-97, doi:10.01016/j.indcrop.2011.06.025.

Uraki, Y., Nemoto, J., Otsuka, H., Tamai, Y., Sugiyama, J., Kishimoto, T., Ubukata, M., Yabu, H., Tanaka, M. & Shimonura M. (2007). Honeycomb-like architecture produced by living bacteria, *Glyconacetobacter xylinus*. *Carbohydrate Polymers*, 69 (1), 1-6, doi:10.01016/j.carbpol.2006.08.021.

Verlhac, C. & Dedier, J. (1990). Availability of surface hydroxyl groups in valonia and bacterial cellulose. *Journal of Polymer Science: Part A: Polymer Chemistry*, 28, 1171-1177.

Vitta, S. & Thiruvengadam, V. 2012. Multifunctional bacterial cellulose and nanoparticle-embedded composites. *Current Science*, 102 (10), 1398-1405.

Wada, M., Okano, T. & Sugiyama, J. (2001). Allomorphs of native cellulose I evaluated by two equatorial d-spacings. *Journal of Wood Science*, 47 (2), 124-128.

Wang, S. & Cheng, Q. (2009). A novel process to isolate fibrils from cellulose fibers by high intensity ultrasonication, Part 1: Process optimization. *Journal of Applied Polymer Science*, 113 (2), 1270-1275, doi: 10.01002/app.30072.

Watanabe, K., Tabuchi, M., Morinaga, Y. & Yoshinag F. (1998). Structural features and properties of bacterial cellulose produced in agitated culture. *Cellulose*, 5 (3), 187-200, doi: 10.01023/A:1009272904582.

Wong, S-S., Kasapis, S. & Tan, YM. (2009). Bacterial and plant cellulose modification using ultrasound irradiation. *Carbohydrate Polymers*, 77, 280-287.

Yang, C., Kim, J-H., Kim, J-H., Kim, J. & Kim, HS. (2009). Piezoelectricity of wet drawn cellulose electro-active paper. *Sensors and Actuators A*, 154, 117-122.

Zhao, HP., Feng, Xi. & Gao, H. (2007). Ultrasonic technique for extracting nanofibers from nature materials. *Appl. Phys. Lett.*, 90, 073112.

Appendix

Table 10: Peak wavenumbers of FTIR absorption bands related to cellulose I and regenerated cellulose II, their interpretation according to the literature (Carrillo et al. 2004, Ciolacu et al. 2011, Colom & Carrillo 2002, Colom et al. 2003, Fan et al. 2012, Gea et al. 2011, Halib et al. 2012, Kondo & Sawatari 1996, Kondo 1998, Liu et al. 2005, Ohet al. 2005, Široký et al. 2010).

Wavenumber (cm ⁻¹)	Assignment	Component
3570-3450	valence vibration of H-bonded OH groups	Cell I
3488	OH stretching intramolecular hydrogen bonds/ Vibration of intramolecular hydrogen bond/ OH inter H-bond	Cell II
3486	OH Intra H-bond	Cell II
3440- 3447	OH stretching intramolecular hydrogen bonds	Cell II
3435	OH stretching	Amorphous Cell
3455-3410	O(2)H...O(6) intramolecular hydrogen bond	Cell I
3460-3405		
3420	OH stretching	Amorphous Cell
3412	OH intra H-bond O(2)-O(6)-inter	Cell I
3405	OH stretching intramolecular hydrogen bonds	Cell I
3375-3345	O(3)H...O(5) intramolecular OH bond)	Cell I
3374	OH Intra H-bond	Cell II
3372	OH Intra H-bond inter-O(3)H-O(5)	Cell I
3352	OH stretching (hydrogen bonded)	Cell I
3350	OH stretching intramolecular hydrogen bonds	Cell I and II
3346	OH stretching vibration	Cell I
3310-3230	Inter H-bond O(6)H-O(3)	Cell I
3315	OH Intra H-bond	Cell II
3309	OH Inter H-bond	Cell II
3309	OH Inter H-bond	Cell I
3308	OH Inter H-bond	Cell II
3305	OH Inter H-bond	Cell I and II
3270	Cellulose I β	Cell I

3240	Cellulose I α	Cell I
3180-3170	O-H stretching	-
3175	OH stretching intramolecular hydrogen bonds	Cell II
3000-2842	C-H stretch	Cell II
2970	CH stretching	Cell I and Cell II
2955	CH stretching	Cell II
2945	CH stretching	Cell I
2924-2926	CH stretching	Amorphous Cell
2901	CH stretching	Cell I
2900	CH stretching	Cell I and Cell II
2899	CH stretching	Cell I
2892	CH stretching	Cell II
2892	CH stretching	Amorphous Cell
2853	CH ₂ assymmetric stretching	Cell I and Cell II
1685-1655	C=O stretch	-
1641	Absorbed H ₂ O	Cell I
1641	Absorbed H ₂ O	Amorphous Cell
1640	Absorbed water H ₂ O	Cellulose
1636	Absorbed water	-
1635	OH of water absorbed from Cellulose	Cell 1 and Cell II
1594 and 1558	C=O stretch	-
1470	OH in plane bending	Cell II
1455	OH in plane bending	Cell I
1435	H-O-C bending	-
1433-1440	CH ₂ bending	Cell I
1431	CH ₂ symmetric bending at C-6	Cell I
1430	β (O-H(..)) of C-O-H alcohol groups	-

1430-1416	CH ₂ scissoring at C(6)	Cell II
1426	CH ₂ bending	Cellulose
1420	CH ₂ symmetric bending	Cell I and Cell II
1420	CH ₂ symmetric bending	Amorphous Cell
1419-1420	CH ₂ symmetric bending	Cell II
1376	CH bending	Cell II
1375	CH bending	Cell I and Cell II
1374	CH bending	Amorphous Cell
1373	CH bending	Cell I
1370	CH bending	Cellulose
1364	Symmetric C-H bending	-
1338-1335	O-H in plain deformation	-
1336	C-OH in plane bending	Cellulose II
1336	OH in plane bending	Cell I
1335	OH in plane bending	Cell II
1335	OH in plane bending	Cellulose
1335	β (O-H(..)) of C-O-H alcohol groups	-
1319	CH ₂ bending (wagging) at C-6	Cell I
1317	CH ₂ bending (wagging) at C-6	Cell II
1316	CH ₂ wagging	Cell I (1317), Cell II (1315)
1315	β (O-H(..)) of C-O-H alcohol groups	-
1282-1277	C-H deformation	-
1282-1300	CH bending	Cell I
1280	O-H in-plane bending	-
1278	C-H bending	Cell II
1236	COH bending in plane at C-6	Cell I
1235-1225	O-H in plain deformation at C(6)	-
1235	C-OH in plane bending	Cell II
1230	C-H bending	-

1228	COH bending in plane at C-6	Cell II
1227	C-OH in plane bending	Cell II
1205-1200	O-H in plain deformation	-
1205	Symmetring stretching C-O-C glycoside	-
1205	OH in plane bending	Cell I
1202	COH in plane bending at C-6	Cell I
1200	COH in plane bending at C-6 or OH in plane bending	Cell II
1170	C-O vibration mainly from C(3)...O(3)H	Amorphous Cell
1165	COC stretching at β -glucosidic linkage or C-O stretching and OH bending	Cell I
1163-1158	Asym. bridge C-O-C stretching	Cellulose
1162-1125	C-O-C asymmetric from β -glycoside link	Cell II
1162	COC stretching at β -glucosidic linkage or C-O-C asymmetric stretching	Cell II
1159	Nonsymmetric bridge C-O-C	Amorphous Cell
1146-1160	C-O-C asymmetric stretching	Cell I
1120-1115	Ring stretch, CC and CO stretching	-
1111	Ring C-C asymmetric stretching	Cell I
1110	Ring asymmetric valence	-
1108	Nonsymmetric in phase ring	Amorphous Cell
1070	Skeletal vibrations involving C-O stretching	Amorphous Cell
1060-1015	C-O vibration mainly from C(3)...O(3)H	Cell II
1059	C-O stretching	Cell I
1055	C-O stretching	Cell I and Cell II
1040	C-O bending	Amorphous Cell
1035	Stretching C-O	Cell I and Cell II
1035-1030	Stretching C-O	-
1032	CO stretching at C-6	Cell I
1019	CO stretching at C-6	Cell II

1007	Ring asymmetric stretching	Cell II
996-985	C-O valence vibration at C(6)	-
993	CO stretching at C-6	Cell II
983	CO stretching at C-6	Cell I
906	CH ₂ bending	Amorphous Cell
900	Antisymmetric out of plane ring stretch	Amorphous Cell
899	Antisymmetric out of phase ring stretching	Amorphous Cell
899	CH ₂ bending	Cell I
898	Asym. out of phase ring stretching	Cellulose
897	COC stretching at β -glycosidic linkage, COC stretching, CCO stretching, and CCH stretching at C-5 and C-6	Cell I
896-892	C-O-C valence vibration of β -glycosidic link or deformation at C(1)	Cell II
895	Group C ₁ frequency	Cell I
894	COC stretching at β -glycosidic linkage, COC stretching, CCO stretching, and CCH stretching at C-5 and C-6	Cell II
893	Group C ₁ frequency	Cell II
893	COC symmetric stretching in plane	Cell II
670-668	O-H out of plane bending	-
669	OH out of phase bending	Amorphous Cell

Table 11: Explanation of abbreviation names, given to the investigated bacterial cellulose specimens.

Abbreviation name	Explanation
WP	Water purification no ultrasound
WP_NoW_1 cm	Water purification no water bath 1 cm distance
WP_CW_1 cm	Water purification cold water bath 1 cm distance
WP_IW_1 cm	Water purification ice water bath 1 cm distance
WP_NoW_4 cm	Water purification no water bath 4 cm distance
WP_CW_4 cm	Water purification cold water bath 4 cm distance
WP_IW_4 cm	Water purification ice water bath 4 cm distance
OSP	One step purification no ultrasound
OSP_NoW_1 cm	One step purification no water bath 1 cm distance
OSP_CW_1 cm	One step purification cold water bath 1 cm distance
OSP_IW_1 cm	One step purification ice water bath 1 cm distance
OSP_NoW_4 cm	One step purification no water bath 4 cm distance
OSP_CW_4 cm	One step purification cold water bath 4 cm distance
OSP_IW_4 cm	One step purification ice water bath 4 cm distance
TSP	Two step purification no ultrasound
TSP_NoW_1 cm	Two step purification no water bath 1 cm distance
TSP_CW_1 cm	Two step purification cold water bath 1 cm distance
TSP_IW_1 cm	Two step purification ice water bath 1 cm distance
TSP_NoW_4 cm	Two step purification no water bath 4 cm distance
TSP_CW_4 cm	Two step purification cold water bath 4 cm distance
TSP_IW_4 cm	Two step purification ice water bath 4 cm distance
NaP	0.01 M NaOH purification no ultrasound
NaP_NoW_1 cm	0.01 M NaOH purification no water bath 1 cm distance
NaP_CW_1 cm	0.01 M NaOH purification cold water bath 1 cm distance
NaP_IW_1 cm	0.01 M NaOH purification ice water bath 1 cm distance
NaP_NoW_4 cm	0.01 M NaOH purification no water bath 4 cm distance
NaP_CW_4 cm	0.01 M NaOH purification cold water bath 4 cm distance
NaP_IW_4 cm	0.01 M NaOH purification ice water bath 4 cm distance